NITA-REPORT-80-35

Propagation Effects on an Intervisibility Measurement System Operating in the SHF Band

E.J. Haakinson

E.J. Violette

G.A. Hufford

U.S. DEPARTMENT OF COMMERCE
Philip M. Klutznick, Secretary

Henry Geller, Assistant Secretary
for Communications and Information

February 1980

TABLE OF CONTENTS

TABLE OF CONTENTS (Continued)

LIST OF FIGURES

LIST OF FIGURES (Continued)

LIST OF FIGURES (Continued)

LIST OF FIGURES (Continued)

LIST OF TABLES

LIST OF TABLES (Continued

PROPAGATION EFFECTS ON AN INTERVISIBILITY MEASUREMENT SYSTEM OPERATING IN THE SHF BAND

E.J. Haakinson*
E.J. Violette*
G.A. Hufford*

A study was conducted to determine the limiting propagation effects on the performance of a microwave system that could be used to detect the optical visibility between two vehicles, separated by up to 10 km, in irregular, obstructed terrain. The study had four objectives: 1) to demonstrate what effects signal variability has on the intervisibility decision process, 2) to identify the possible sources of the signal variability and to estimate the magnitude of each source's contribution to the total variability, 3) to obtain propagation loss data, over various types of terrain and obstructed paths, which could be used to predict received signal variability due to propagation over similar paths, and 4) to use the measured data to predict the performance of a simulated intervisibility measurement system.

A measurement system, operating at 9.6 GHz and 28.8 GHz, was prepared and sent to Ft. Hunter Liggett, CA, where propagation path loss was measured over several selected paths of varying lengths, varying path geometries, and varying amounts of vegetation and rock outcroppings.

The study shows that a microwave intervisibility system is less perfect than a purely optical one, due to the variability of the received microwave radio signal. However, the performance of the microwave intervisibility system can be predicted based upon the magnitude of the signal's variability. With a limited set of propagation measurements in the area where the microwave intervisibility system is to operate, an estimate of the "optimum" microwave signal threshold and the signal variability can be made; this allows a prediction of the system's performance.

Key Words: Intervisibility measurement systems; propagation measurements; SHF

*The authors are with the Institute for Telecommunication Sciences, National Telecommunications and Information Administration, U.S. Department of Commerce, Boulder, Colorado 80303

1. INTRODUCTION

1.1 Assumptions on General Intervisibility Detection System Requirements and Operation

The U.S. Army Combat Developments Experimentation Command (CDEC) conducts mock battles at Ft. Hunter Liggett, CA, to determine the performance of tactical equipment and/or strategies. During the mock battles, the location of equipment and personnel is recorded for later analysis. The CDEC's current data collection system allows a central processor to determine the position on the battlefield of those players instrumented to communicate with the range measurement system. The instrumented players include infantrymen, tanks, helicopters, fighter aircraft, etc. Although the present system can determine the distance between any two players, it was not designed to determine whether any two players are optically visible to one another.

In order to detect intervisibility between players, the CDEC has been studying the feasibility of several intervisibility detection systems. One proposed system uses microwave signals between two mobile end points (players) to estimate whether or not the two points are optically visible to each other. In the proposed system, the receiver (one end point) measures the strength of the received radio signal from the transmitter (the other end point). A calculation of the free space received signal strength is made, assuming values for the transmitter power and the transmitter and receiver antenna gains, and using a computed distance separation between the end points. If the two terminals are optically within line-of-sight (LOS) on an uncluttered path with no apparent obstacles, then the actual received signal level should be nearly equal to the computed free space signal level. On the other hand, when the terminals are optically hidden from one another, the received radio signal level will be less than the free space signal level by an amount which depends upon the path length, geometry, vegetation, frequency, etc. Thus, the simplest method to determine intervisibility using microwave methods is to set a radio signal threshold near that observed at optical grazing LOS and that is a function of the distance between the terminals. As long as the actual received level is greater than the threshold, the terminals can be said to be intervisible.

Unfortunately, the actual received signal is not a fixed level, but is variable for a given path length and intervisibility condition (such as when the two terminals are just within optical grazing line-of-sight). The source of the variability is due to the variety of propagation paths, conditions for the obstructions between the terminals, etc. These influences play a role in making a correct decision as to whether the two end points are intervisible to one another.

1.2 Objectives

The first objective of the project was to demonstrate what effects signal variability has on the intervisibility decision process.

The second objective was to identify the possible sources of the signal variability and to estimate the magnitude of each source's contribution to the total variability.

The third objective was to obtain propagation loss data, over various types of terrain and obstructed paths, which could be used to predict received signal variability due to propagation over similar paths. Specifically, the measurements were to be made in the millimeter wave (SHF) band using frequencies near 9.6 GHz and 28.8 GHz, over path lengths of 200 to 10,000 meters, with a variety of obstructions, i.e. paths with abrupt ridges or smooth-rounded ridges and paths having rock outcroppings, trees, tall grasses, or little vegetation. (The measurement system is described in Appendix A).

Based on the effects of signal variability on the intervisibility decision process, and on the results of the propagation measurements, a recommendation was made on the feasibility of a microwave intervisibility measurement system.

2. EFFECTS AND SOURCES OF SIGNAL VARIABILITY ON INTERVISIBILITY DETECTION

2.1 Assumptions and Terminology

The intervisibility system is assumed to be designed using two basic measurements: (1) the distance (d) between the target and observer (transmitter and receiver) and (2) the received microwave signal level.

These measurements may be made by two independent systems and recorded for "off-line" analysis of intervisibility, or they both may be measured by the receiver for "real-time" analysis.

For any instant of recorded time the received signal level W is compared with a threshold level $W_o(d)$, this threshold being a previously determined function of the distance d. (At the very least it should contain the factor d^{-2} to account for simple free space loss.) If $W \geq W_o$, then an alarm is set, the presumption being that at that instant observer and target are intervisible.

Application of the simplest theory (Fresnel knife-edge diffraction) would suggest that W_o should be just 6.02 dB below free space, but we cannot say that this simplest theory is directly applicable to real-life conditions. Rounded and/or irregular obstacles, multiple obstacles, atmospheric layering, scattered reflections from the ground, and scattered reflections from off-path obstructions will all have an effect on the received signal level, usually depressing it from theoretical values, but sometimes enhancing it. The exact effect will depend on a great many variables (some unrecorded or unrecordable); thus the total effect will be that of an apparently random variable W, which only can be treated statistically. The value of W_o, for example, might very well be taken to be the median value of all W measured on grazing paths, i.e. on paths such that the direct optical line between terminals just grazes an obstacle. If such a threshold is chosen, then 50 percent of grazing paths would give an alarm and 50 percent would not.

For generally situated paths it is desired to have an alarm when the terminals are intervisible and not to have an alarm when the terminals are not intervisible. Because of the random variability of path losses, and because of equipment variability and errors in measuring the distance d, this desired situation will not always occur.

Therefore, there will be errors in the record of alarms. These will be of two kinds: the false alarm where the terminals are not intervisible but an alarm is registered and the missed alarm where the terminals are intervisible but no alarm is registered. The question is not whether such errors will occur, but whether they will occur rarely enough to be acceptable.

Clearly, the probability of errors will depend on how much a path is line-of-sight or shadowed. If the radio signal threshold is pegged at the median optical grazing value and if the optical line between terminals lies just barely above grazing, nearly 50 percent missed alarms would be expected. If the path is just barely below grazing, then nearly 50 percent false alarms would be expected. This sort of error must be tolerated. But if the path is in the deep shadow, presumably there will be very few errors (false alarms). The real question here concerns the intermediate conditions and whether the probability of errors decreases fast enough as one passes from grazing either to an optical line-of-sight path or an optically obstructed one.

A parameter is needed to describe quantitatively the amount by which a given path departs from the just-grazing condition. For this parameter the quantity H is suggested as pictured in Figure 2-1. It is the amount by which an obstruction falls short of, or projects beyond, an equivalent direct path (AB) between terminals. It is positive if the path is obstructed, zero at grazing, and negative if the obstruction lies below the line-of-sight path. (On an arbitrary line-of-sight path, it is sometimes difficult to determine just what constitutes "the" obstacle, but we do not investigate this problem here.)

The quantity Y, also pictured in Figure 2-1, is the amount by which a target terminal is displaced from a reference level, here defined to be the "just-grazing path" from the observing terminal to the obstruction. We define Y to have the same sign as H and we can remenber Y's sign by considering that the target (B) would have to rise up (when Y is positive) above the reference line (AB') to be seen by the observer (A) and would have to get down (when Y is negative) to become hidden from the observer. Therefore, we will call Y, the target cover. Since $Y_B = Hd/d_A$ and $Y_A = Hd/d_B$, we see that Y is always larger than H, sometimes extremely so. If the obstacle is at mid-path (so that $d_A = d/2$), then $Y_A = Y_B = 2H$.

The parameter Y might be used to measure the difference between an actual path and a grazing path, but that measure has two disadvantages. The most severe of these is that it is not a symmetric measure and depends on which terminal is considered the observer and which the target. This asymmetry is not present in either the question of intervisibility or in the measured

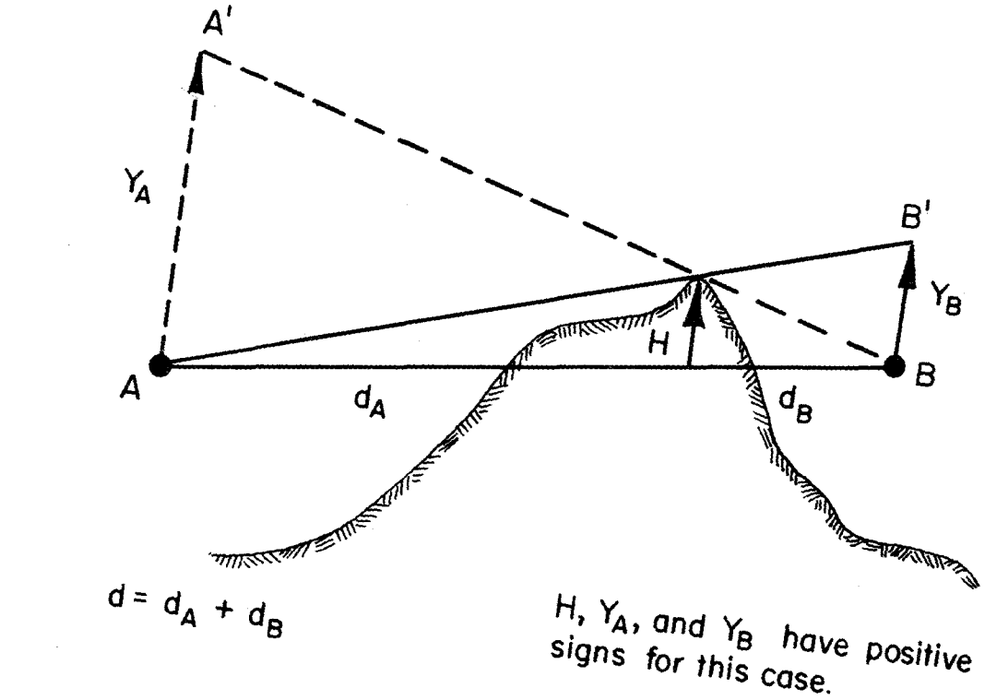

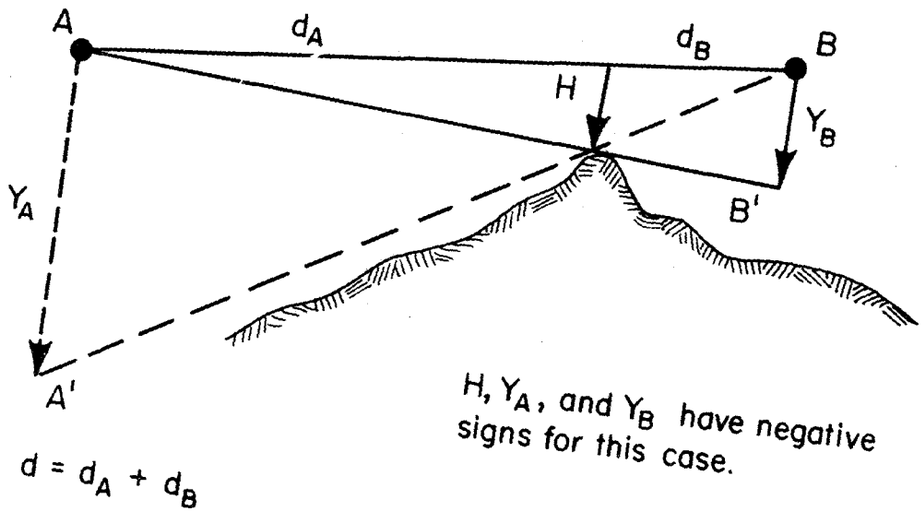

Figure 2-1. Path geometry.

signal levels. Therefore, unless the obstacle is exactly mid-path, a single path is represented by two different values of Y, (Y_A and Y_B in Figure 2-1) despite the fact that all the other pertinent measures of the path have single values. The second disadvantage is that Y does not have very much to do with the electromagnetic properties of the path. That is, a complete description of the path would involve a great many parameters; and from these we should try to choose the single one upon which the received signal level depends most critically. The parameter Y falls short of this desideratum. Admittedly, the parameter H also is not a perfect choice of parameters, but it has a simple geometric meaning and is symmetric with respect to the terminals. In the measurement results that follow in section 4, we will present the results in terms of H and Y.

2.2 Effects of Signal Variability

The output of a measurement program will provide, at the least, mean or median values of radio signal thresholds for the grazing condition and a measure of their variability for a range of values of the distance d and the obstruction height H.

The median values are expected to bear a close resemblance to the theoretical values for a perfect knife-edge. They may deviate somewhat but generally will show the same slope as a function of H. The variability involved is expected to approximate a log-normal distribution; i.e., when measured in decibels, the signal levels will be normally distributed with some standard deviation σ, also expressed in decibels. This distribution is the one that has been experienced at lower frequencies, and we shall assume it will be valid here as well.

Figure 2-2 shows the consequences of these suppositions. The probability of registering an alarm is plotted versus the value of H. Thus, for positive H, this is the probability of a false alarm. For negative H, the complement of this probability (one minus the probability) is the probability of a missed alarm. Parameters used in constructing Figure 2-2 consisted of a distance of 3.5 km, a wave length of 1 cm, and with the obstacle at mid-path. However, the results are not very sensitive to the actual values of these parameters; changing one of them by as much as a factor of 2 will produce only small changes in the curves as we will note later in this discussion.

It has been suggested that the threshold might be biased so as to favor one situation or another. For example, one might insist that an alarm should be registered in 75 percent of the cases where the direct optical ray is just grazing, a situation easily obtained by lowering the threshold value to a suitable level. The consequences of such a bias are pictured in Figure 2-3. The missed alarms have been greatly reduced but the false alarms have, in compensation, increased.

On the other hand, the standard deviation σ is critical as the two curves of Figure 2-2 demonstrate. Figure 2-4 shows the curves redrawn, presenting here the probability of error versus the assumed standard deviation. The parameters in these figures assume a wave length of 1 cm and distance d of 1, 3.5, 7, and 10 km.

The probability of an alarm or of no alarm curves deserve some clarifying remarks:

1. In Figure 2-2 the asymptotes for large negative H are undoubtedly wrong. They have been drawn assuming (1) the measured attenuation medians at the grazing condition will be exactly the Fresnel knife-edge value of 6.02 dB and (2) the standard deviation remains constant. Furthermore, they assume that no matter how clear the path, there always will be ground reflections large enough to frequently cancel out the direct ray, thus producing a missed alarm. But (1) measured medians undoubtedly will be different from Fresnel knife-edge values and (2) experience indicates that σ will decrease to zero as H becomes large and negative.

2. The curves in Figures 2-2 and 2-3 are valid only for an instantaneous determination of intervisibility. In practice the terminals will be in motion and in any small interval of time there may be many determinations of intervisibility. If they are independent, then a combined estimate would be much more accurate. An analysis of the increase in accuracy requires a knowledge of how the received signals vary within small areas. Perhaps a "correlation distance" or some similar parameter is needed.

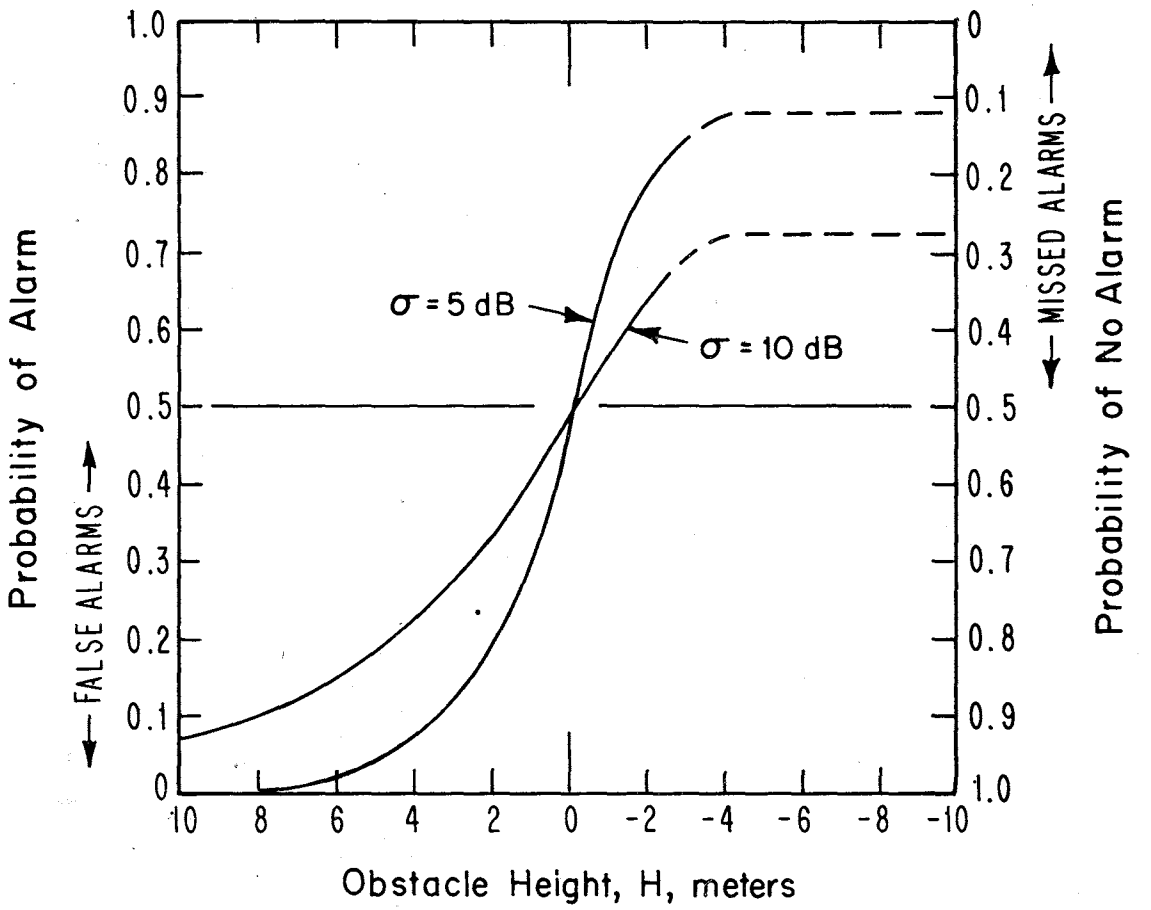

Figure 2-2. Probability of alarm assuming two different values of the standard deviation of signal level variability. Parameters: d = 3.5 km, frequency = 30 GHz.

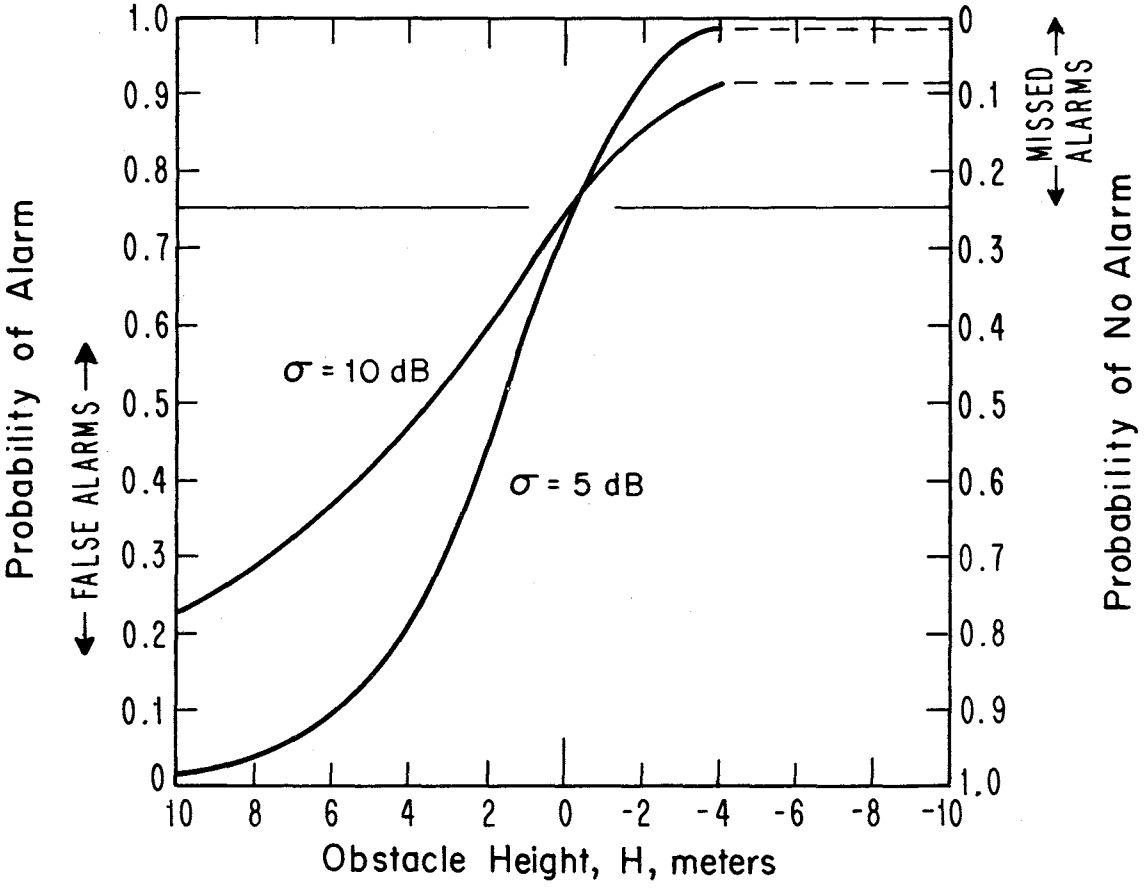

Figure 2-3. Probability of alarm when the threshold is offset. Parameters: d = 3.5 km, frequency = 30 GHz.

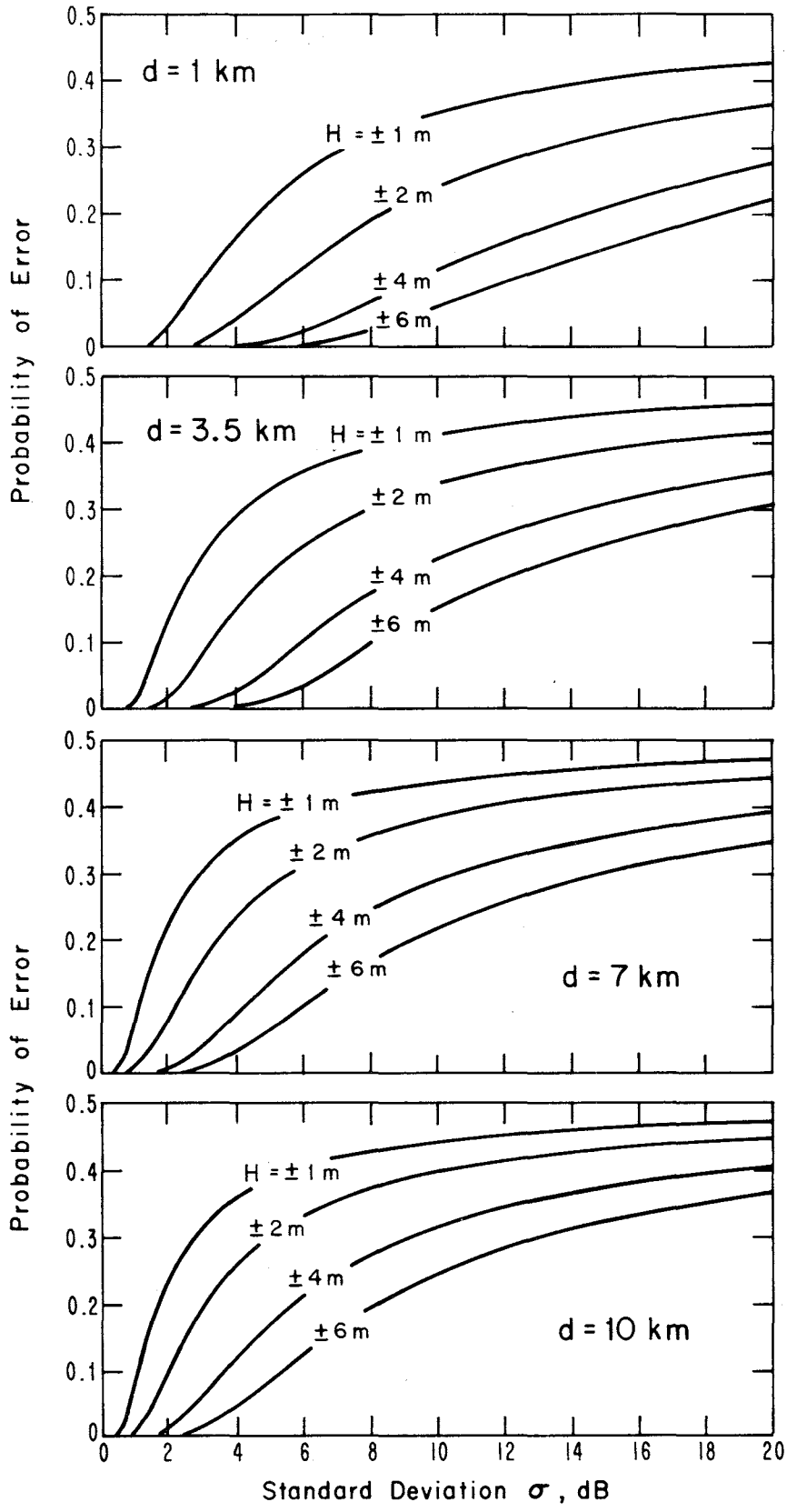

Figure 2-4. Probability of error versus standard deviation of signal level variability. Frequency = 30 GHz.

2.3 Sources of Signal Variability

Estimates of what value of σ a measurement program will discover are presented next. In practice it will have several statistically independent sources, which are listed here:

1. Time variability. This refers to the variability of the received radio signal one would observe with the passage of time due to changes in atmospheric conditions, seasonal conditions, and local conditions. With the short paths under discussion, one would expect very little variation in time. The standard deviation should be less than 1 dB.
2. Local variability. This refers to the variability observed as one moves the terminals over short distances--say from 1 to 10 meters. It usually is due to multipath signals, i.e. to the combination of many signals arriving over different paths because of reflection and scatter. The most severe situation leads to a Rayleigh distribution whose standard deviation is 5.6 dB.
3. Path-to-path variability. This refers to the variabilty observed when the paths are distinctly different while retaining the same values of d and H. Past experience at lower frequencies would indicate that this probably will be the largest single component of the total variability. The usual estimate given is a standard deviation of 10 dB, although Longley [1976] would raise that (for the high frequencies involved) to 25 dB. These large estimates, however, are for standard land mobile situations where only the distance d is provided; the additional knowledge provided by the value of H should reduce the variability somewhat. On the other hand, Longley et. al. [1971] have shown that if one uses some of the best available prediction methods where the entire terrain profile between terminals is provided, standard deviations of the order of 7 to 9 dB are still found.
4. Region-to-region variability. This refers to the variability involved when exercises are carried out in entirely different locations. The differences in climate, general terrain irregularity, and the overall types of vegetation present all lead to an additional component of variability. Estimates of standard deviation at lower frequencies usually have ranged from 3 to 5 dB.

5. Equipment variability. In real-life practice, variability in recorded signal levels will include a variability due to the different, time-varying equipments. Both transmitters and receivers would be involved. If desired, this variability can be included with that due to pure propagation effects. An estimate of its standard deviation would be on the order of 2 to 3 dB. The question of antenna gains and patterns also should be considered.

6. Range measurement or position errors. Again this is a source of variability that can, if desired, be included in the estimate of total system variability. If the only effect (or the major effect) of distance on the assumed threshold is in the associated free space loss, the standard deviation of signal level variability can be expressed in the formula $8.7\ \sigma_d/d$, where σ_d is the standard deviation of distance errors and is measured in the same units as is d. If σ_d is 10 m and d is 3.5 km, this becomes 0.02 dB, which is too small to be of concern. But if d is to be decreased to as little as 50 m, this standard deviation increases to 1.7 dB.

These different components of variability, or at least those which seem pertinent to the operation in question, should be combined as a root-sum-square. Note that such a combination will largely emphasize the largest of the assumed standard deviations.

Thus, a combined standard deviation of 5 dB seems very optimistic. Values of 10 dB or higher probably are more realistic.

3. MEASUREMENT PATHS

All paths measured were located on the Ft. Hunter Liggett, CA test range and chosen with the guidance of U.S. Army CDEC and support contractor personnel knowledgeable in battlefield strategy and types of cover that players utilize. Many different terrain features were selected to determine the applicability of microwave propagation to electronically monitored intervisibility between players. A total of nine separate paths were measured. The first five paths (1 through 5) provided abrupt obstacles with at least one side that fell away from the obstacle's crest rapidly. Path 5

was nearest to a knife-edge obstacle because an abrupt rock outcropping was used. The obstacle on path 6 was somewhat more gradual, and path 7 had a very large radius of curvature. A more or less flat path through mostly dead oak trees with some shorter brush and stumps was selected for path 8. A double obstacle of gradual curvature was used for path 9. Paths 1, 5, 6, 7, and 9 were free of trees and other outstanding features above the regular terrain except for the obstacle itself. Tree cover was prominent on paths 2, 3, 4, and 8. Table 3-1 gives a general outline of the features of each path. Figures 3-1 through 3-23 are photographs of each path as indicated.

Figure 3-1 shows the location of paths 1, 2, 3, and 4 on a section removed from the Hunter Liggett Special Edition (1-DMATC) enlarged by two times. The same map and enlargement are used for Figure 3-2, showing the location of paths 5, 6, 7, and 8 as well as Figure 3-3 which locates path 9. The arrows indicate the direction from the transmitter to the receiving terminal.

Figure 3-4 is a photograph of the initial standard path used to calibrate the system after assembly at Hunter Liggett. The transmitter on the adjustable tower is in the foreground at a measured distance from the receiver, located at the center of the photograph.

Path 1, crest to transmitter, appears in Figure 3-5. The transmitter and tower are in front of the tree limb at the center, and the instrumentation on the tripod, and electrotape for distance measurements, appears at the upper right at the estimated location of the crest. The crest to receiver of path 1 is shown in Figure 3-6, and Figure 3-7 views the crest from the receiving terminal.

Photographs in Figures 3-8 and 3-9 show path 2 from crest to receiver and from receiver to crest, respectively. In Figure 3-9 the transmitter is located directly in line with the receiver mast just beyond the top of the grassy knoll.

Figure 3-10 is a view behind the receiver looking toward the crest on path 3. Photographs of Figures 3-11 and 3-12 show the transmitter and crest of path 3.

Figures 3-13 and 3-14 show the view of path 4 receiver to crest and transmitter to crest, respectively.

In paths 5 and 5b the obstacle was a rock outcropping. Path 5 is shown in Figure 3-15 with a view from the receiver toward the obstacle. Figure 3-16 is a view from the outcropping to transmitter, the configuration for path 5b. The transmitter is located at the center of the photograph just in front of the trees. Figure 3-17 is a photograph of the outcropping and receiver as employed in path 5b.

Path 6 looking from the receiver toward the transmitter is shown in Figure 3-18. Figure 3-19 views the transmitter looking toward the crest of path 6. A view from the crest looking to the transmitter is shown for path 6 in Figure 3-20.

The very rounded obstacle, gradual slope in either direction from the crest, used for path 7 is seen looking from the receiver in Figure 3-21.

Photographs of path 8 are not included because none were available which adequately described the path.

The photograph of Figure 3-22 is taken from the crest nearest the transmitter looking toward the transmitter terminal on path 9. Figure 3-23 shows the receiver looking toward the second crest of path 9.

4. PROPAGATION MEASUREMENTS RESULTS

4.1 Path Categories

As shown by the photographs given in the previous section, all of the measurement paths had terrain features which were irregular; i.e., the path terrain profiles from each transmitter location to its horizon and from each receiver location to its horizon were not smooth, monotonic lines and the horizons were not long, straight transverse ridges. Although all of the paths had at least one obstruction, several paths appeared to have just a single dominant obstruction which would affect the received signal level and its variability. For these paths, the obstruction was an uncluttered ridge with no trees or rock outcroppings on the ridge line or along the path (see the photographs of path 6, Figures 3-18 through 3-20). Other paths had cluttered ridges for a dominate obstruction with many "almost obstructions" along the path (see the photographs of path 3, Figures 3-10 through 3-12). In describing the measurement results, two categories will be considered. The first will be the irregular paths with uncluttered obstructions and the second

Table 3-1. General Outline of the Features of Each Path

Path No.	Location Grid Nos. from Hunter-Liggett Special Map 1-DMATC	Length (m)			Type Obstacle	Vegetation
		Total	Crest to Transmitter	Crest to Receiver		
1	Milpitas Grid 53-54X92-93	199.4	40.8	158.6	Abrupt	Grass, Sparse trees
2	Milpitas 54-55X92-93	492.0	40.84	451.2	Abrupt	Grass and trees
3	Milpitas 52-53X92-93	472.3	49.07	423.2	Abrupt	Grass and trees
4	Milpitas 52-53X92-93	440.4	323	117.4	Abrupt	Grass and trees
5	Stony Valley 55-56X80-82	1036	14	1022	Very abrupt	Grass
5B		≃1025.3	1022	≃4.3	Rock out-cropping	
6	Stony Valley 53-55X82-84	3620	60	3560	Gradual	Short grass
7	Stony Valley 53-57X80-82	≃900	≃Midpath	≃Midpath	Rounded	Tall grass
8	Nacimiento Valley 52-53X81-82	1498	No Crest		Flat	Trees
9	Gabilan 60.61X74-75	831	88	64	Gradual	Short grass

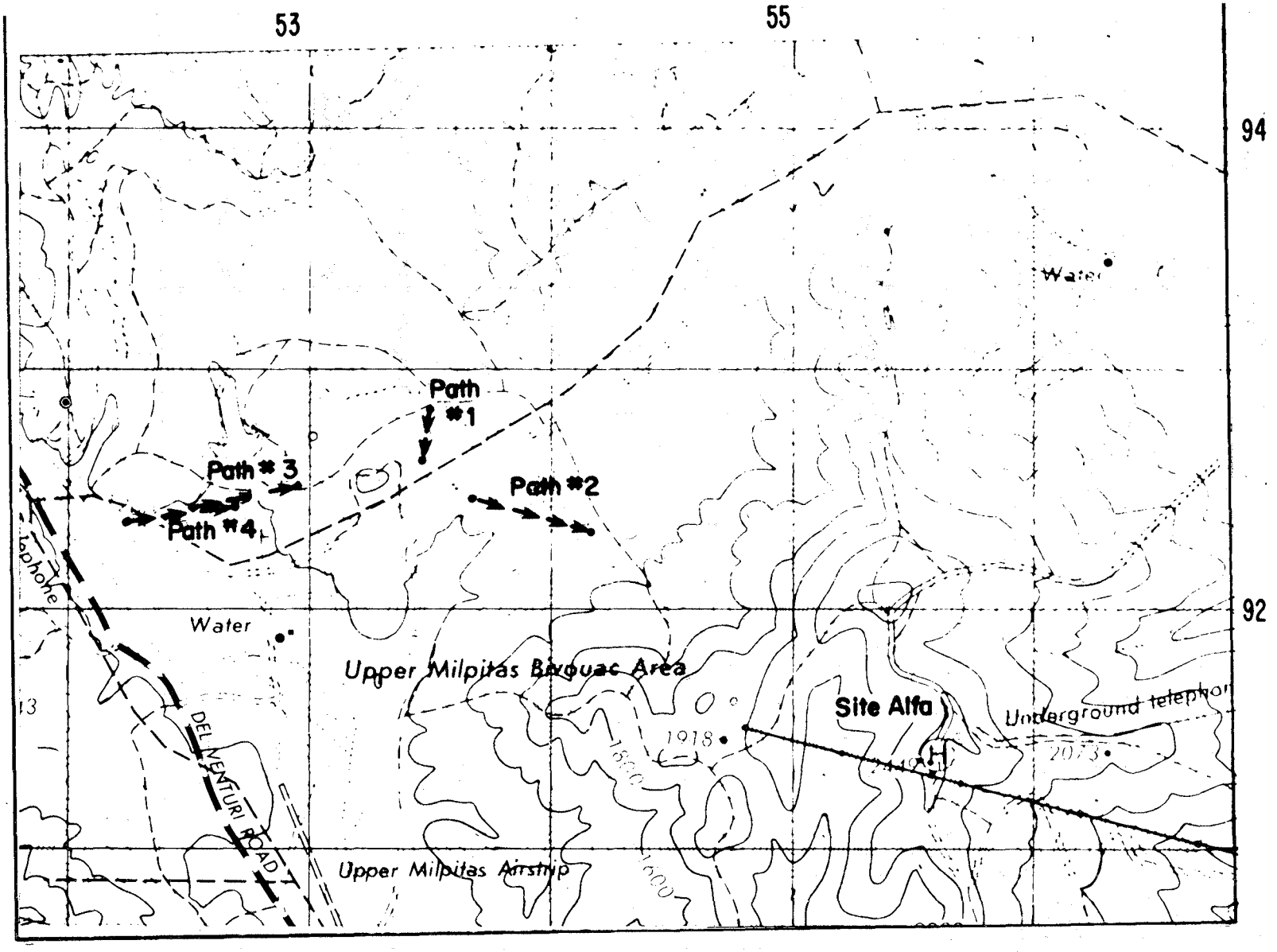

Figure 3-1. Location of paths 1, 2, 3, and 4 for March 79 propagation measurements.

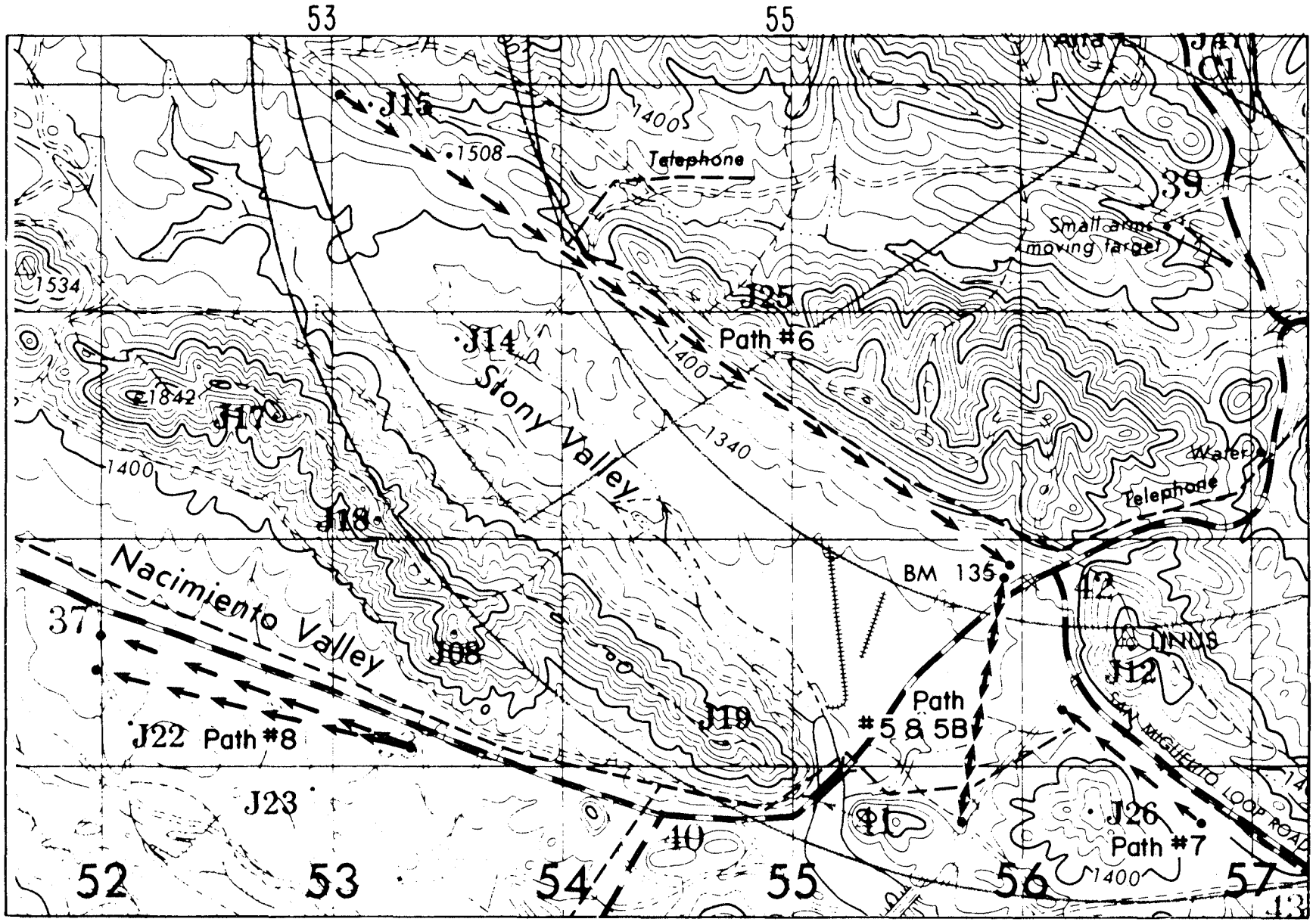

Figure 3-2. Location of paths 5, 6, 7, and 8 for March 79 propagation measurements.

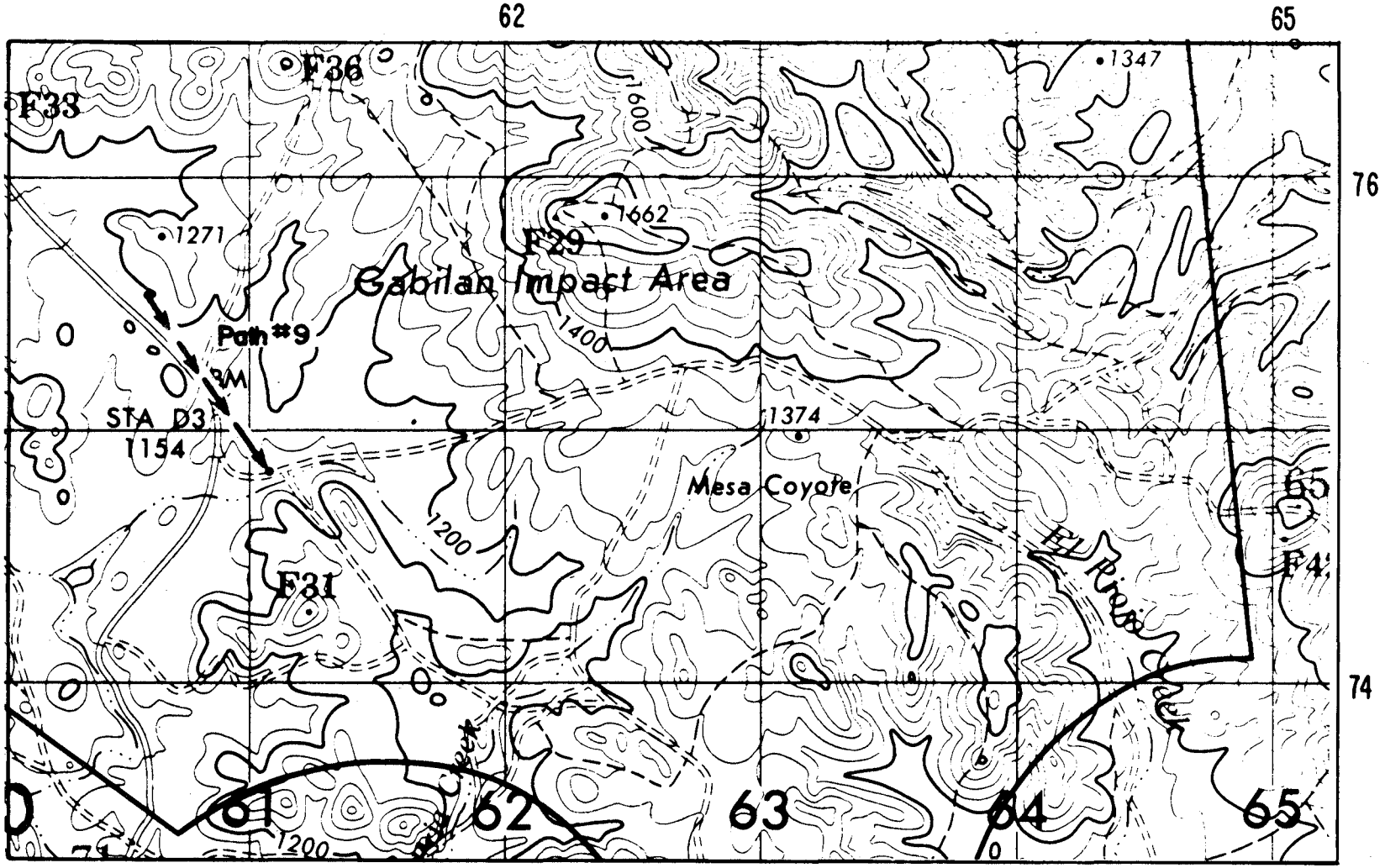

Figure 3-3. Location of path 9 for March 79 propagation measurements.

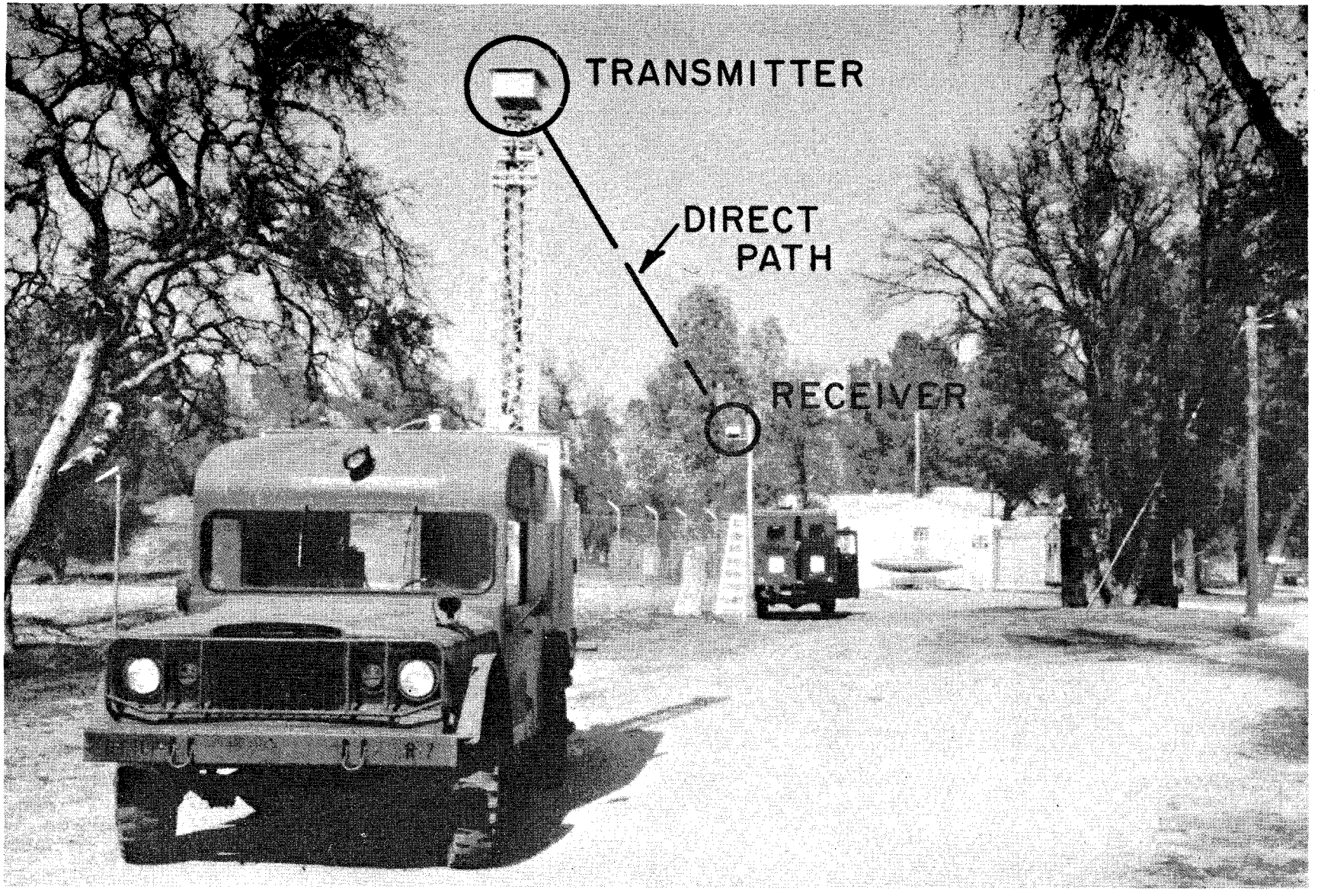

Figure 3-4. A standard path calibration setup.

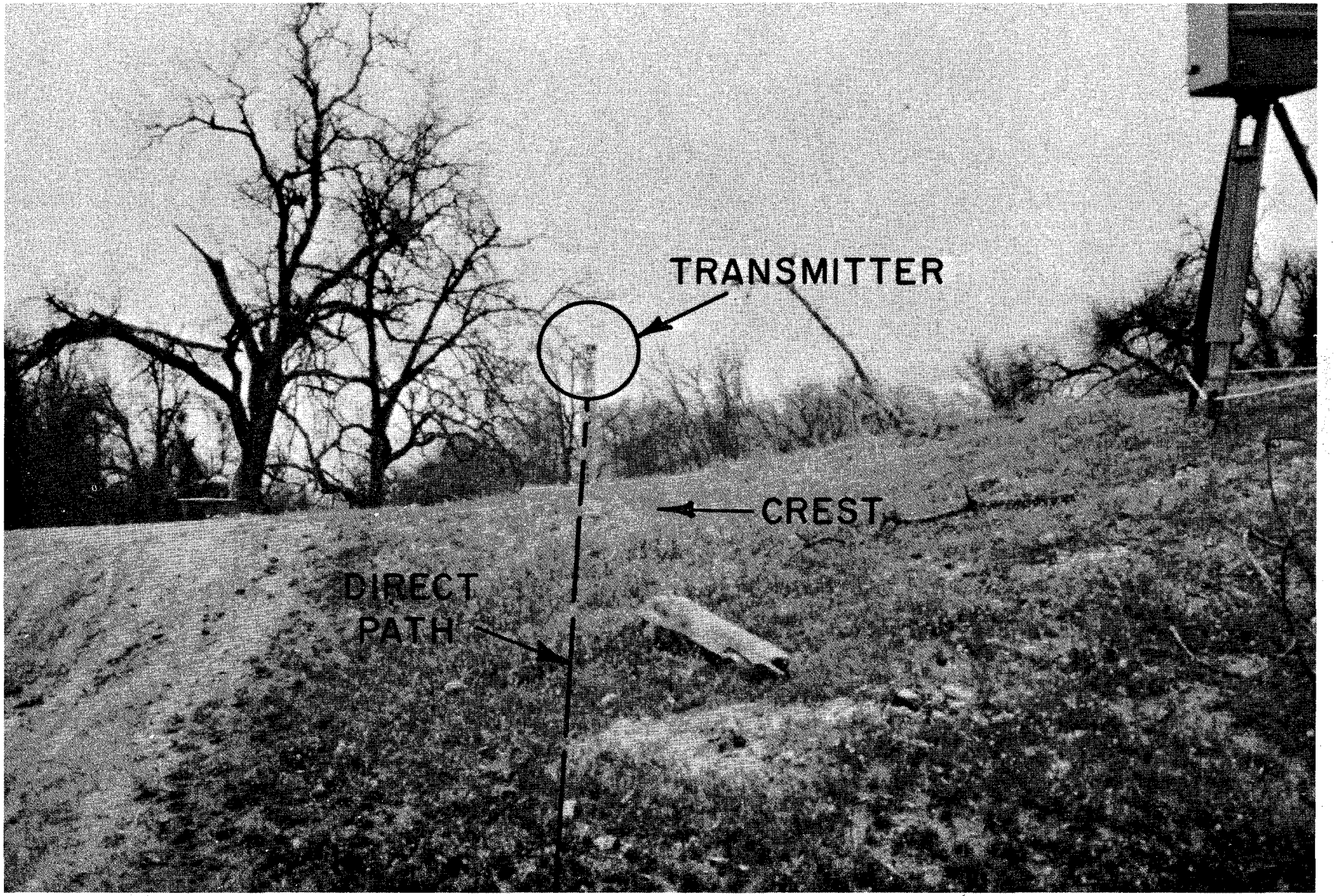

Figure 3-5. Path 1 crest to transmitter.

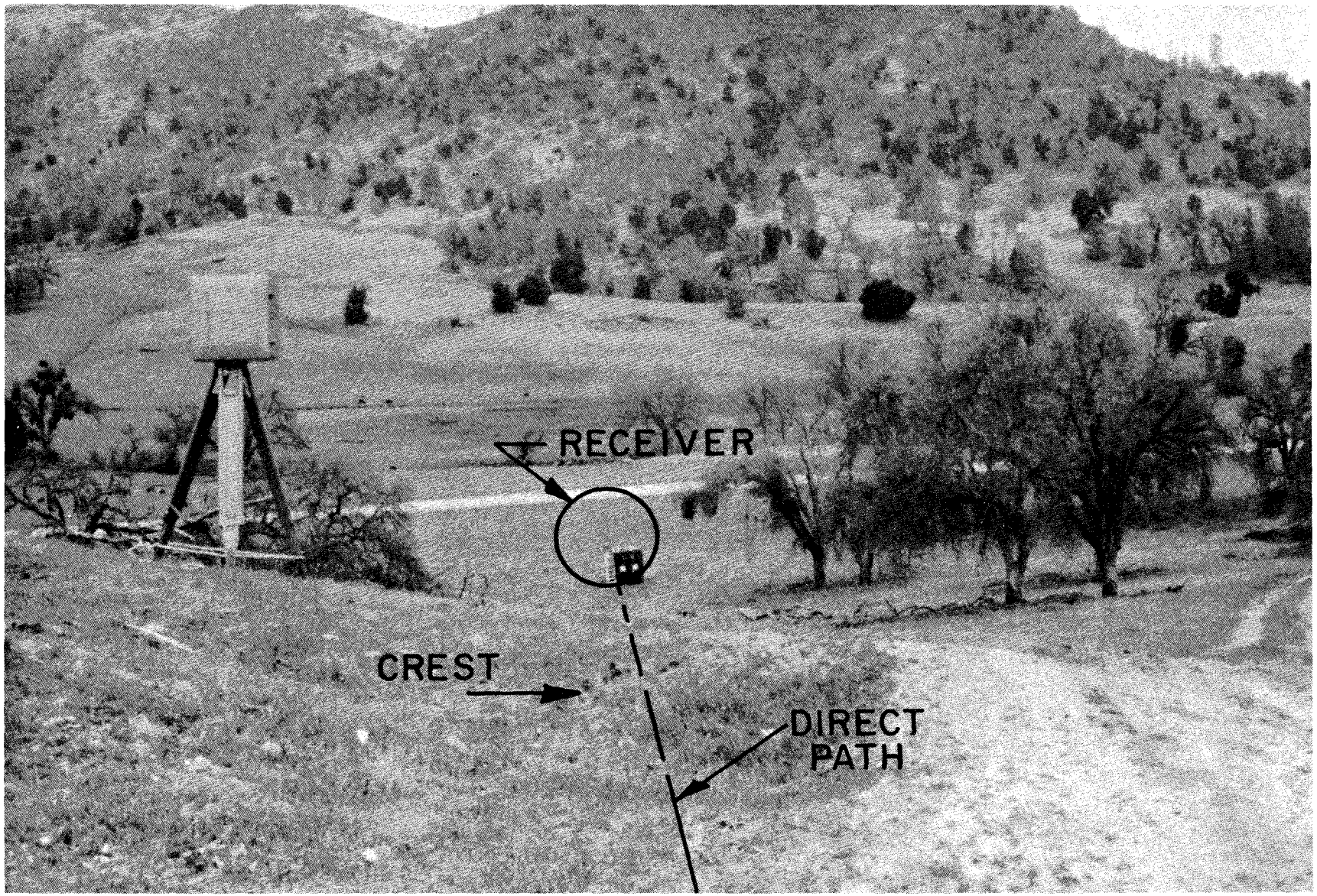

Figure 3-6. Path 1 crest to receiver.

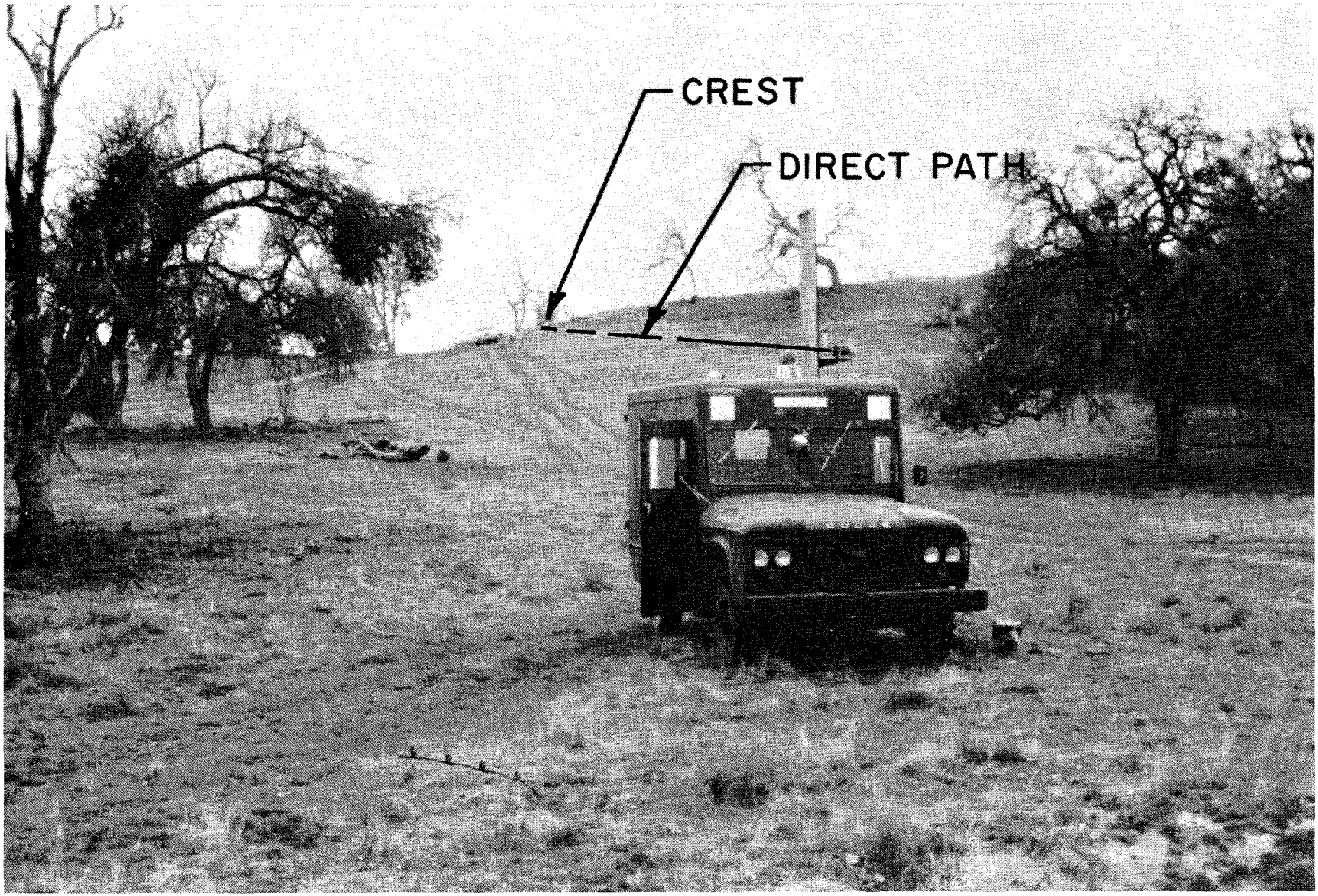

Figure 3-7. Path 1 receiver to crest.

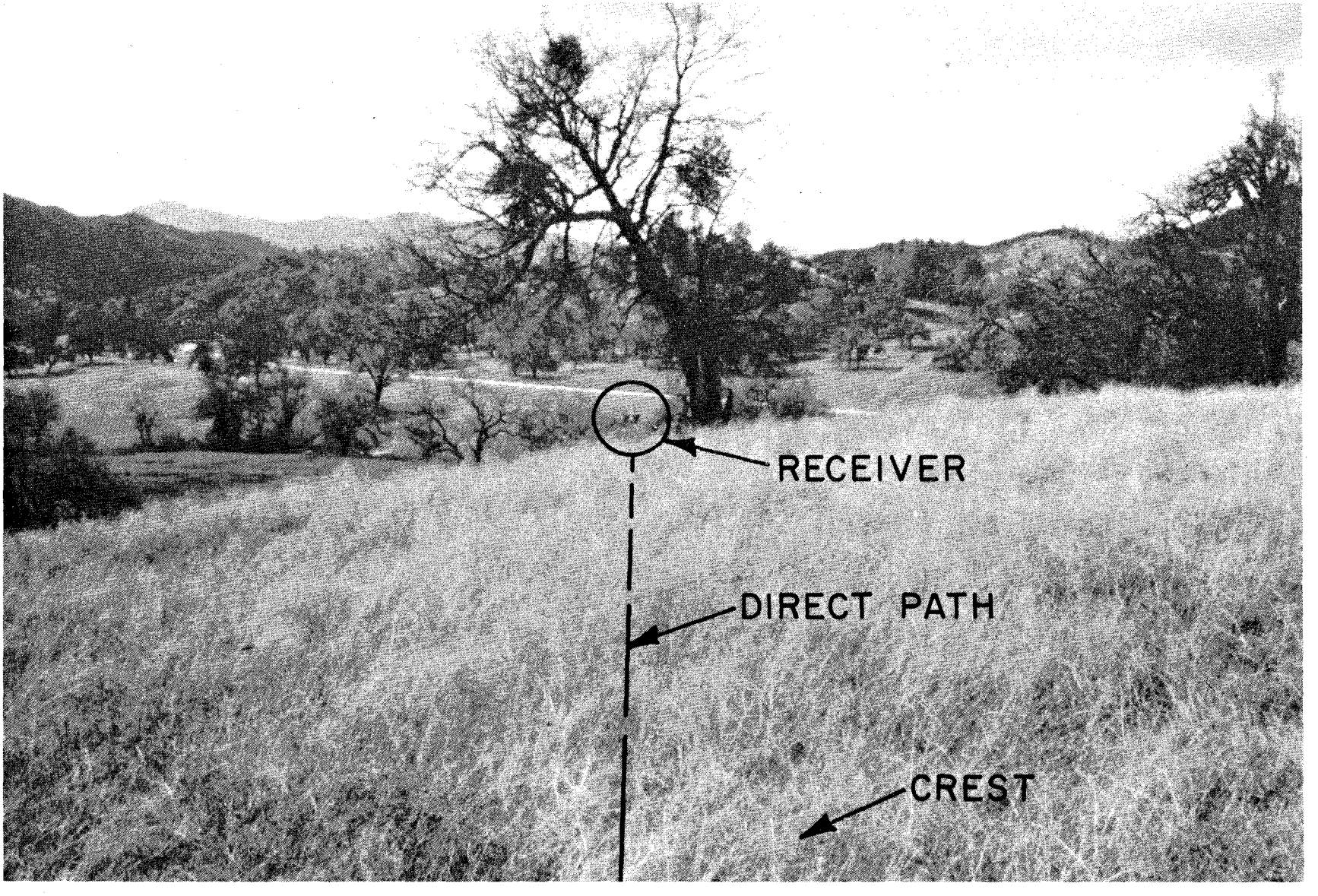

Figure 3-8. Path 2 crest to receiver.

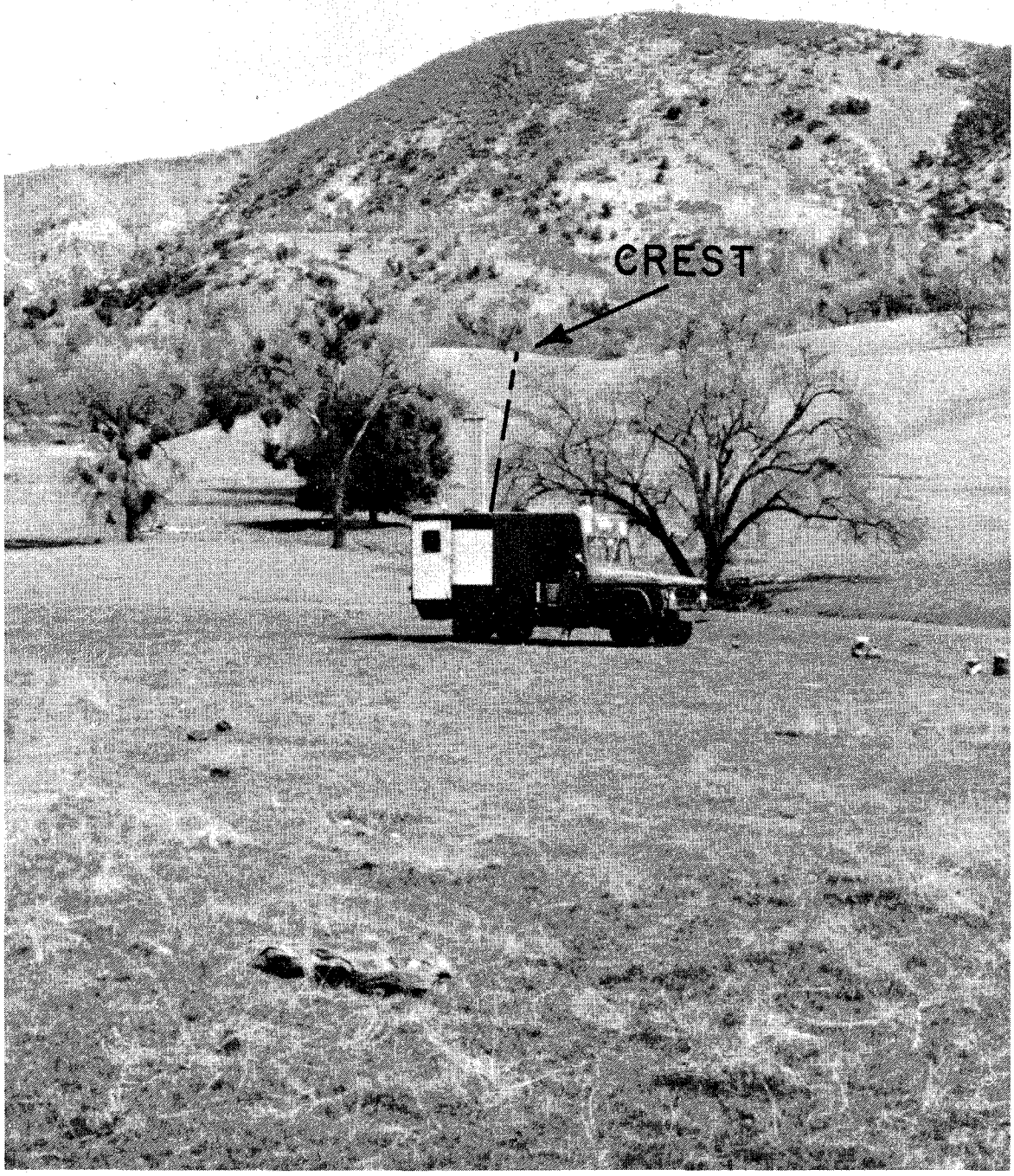

Figure 3-9. Path 2 receiver to crest.

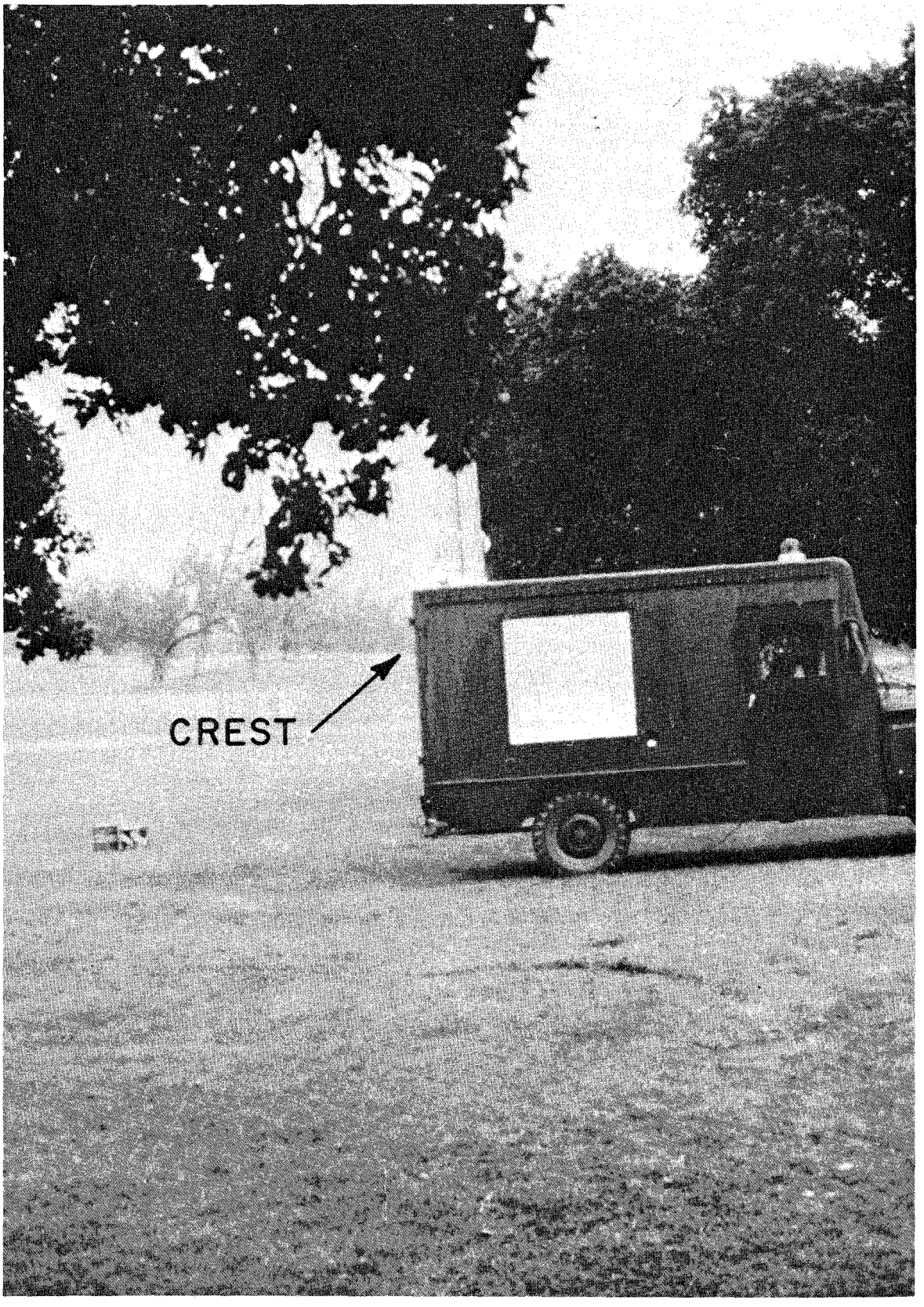

Figure 3-10. Path 3 receiver to crest.

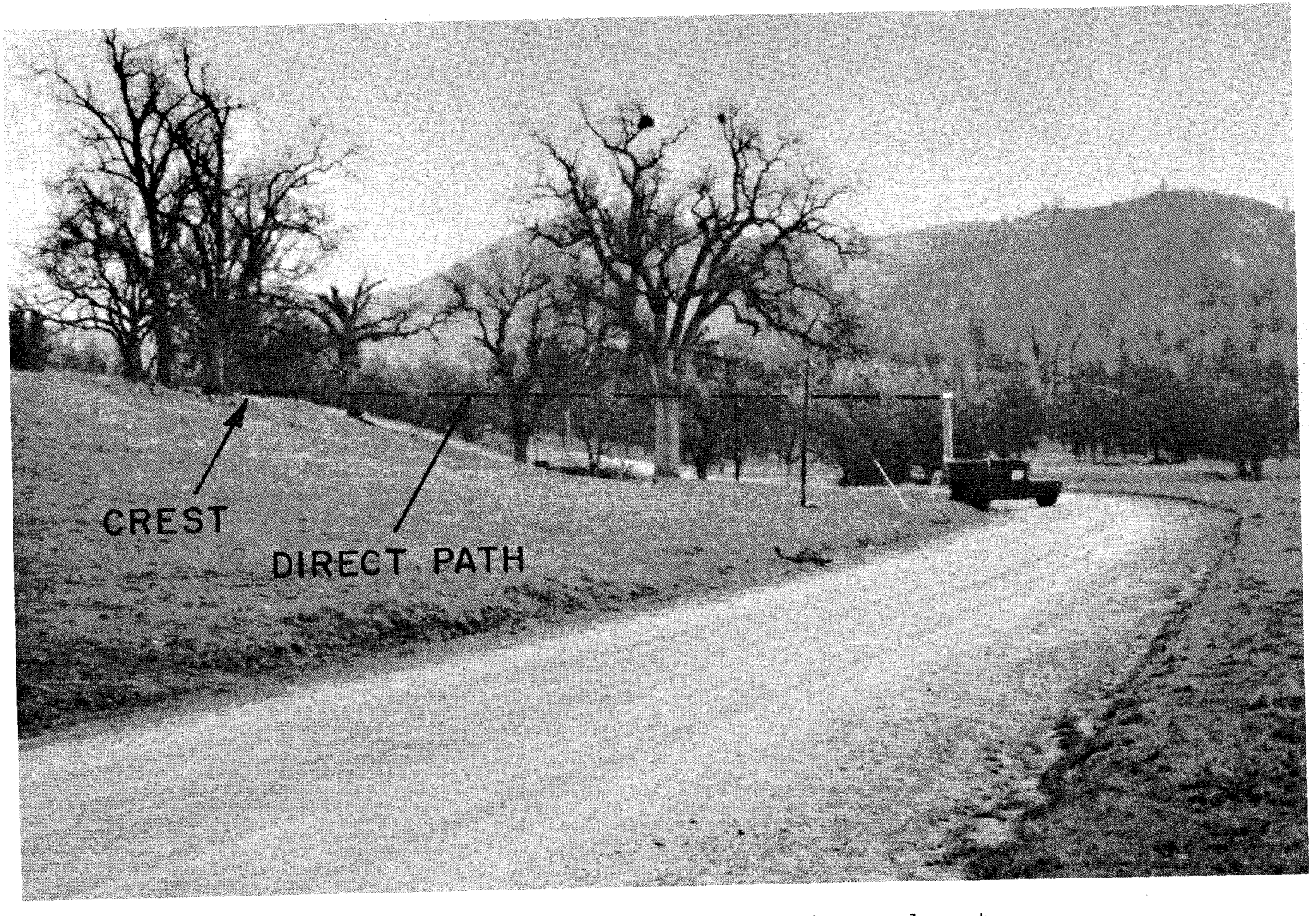

Figure 3-11. Path 3 side view of transmitter and crest.

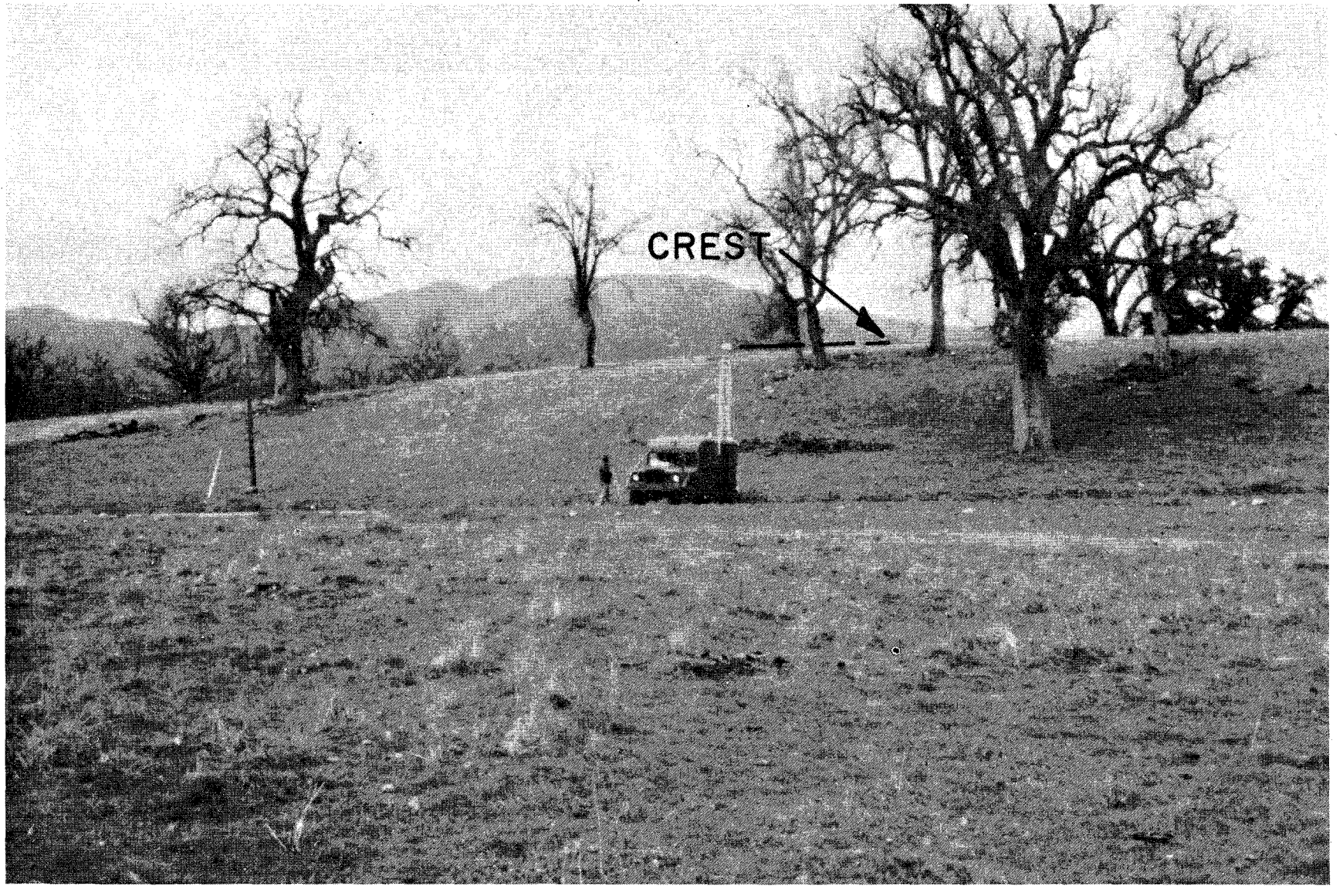

Figure 3-12. Path 3 transmitter crest.

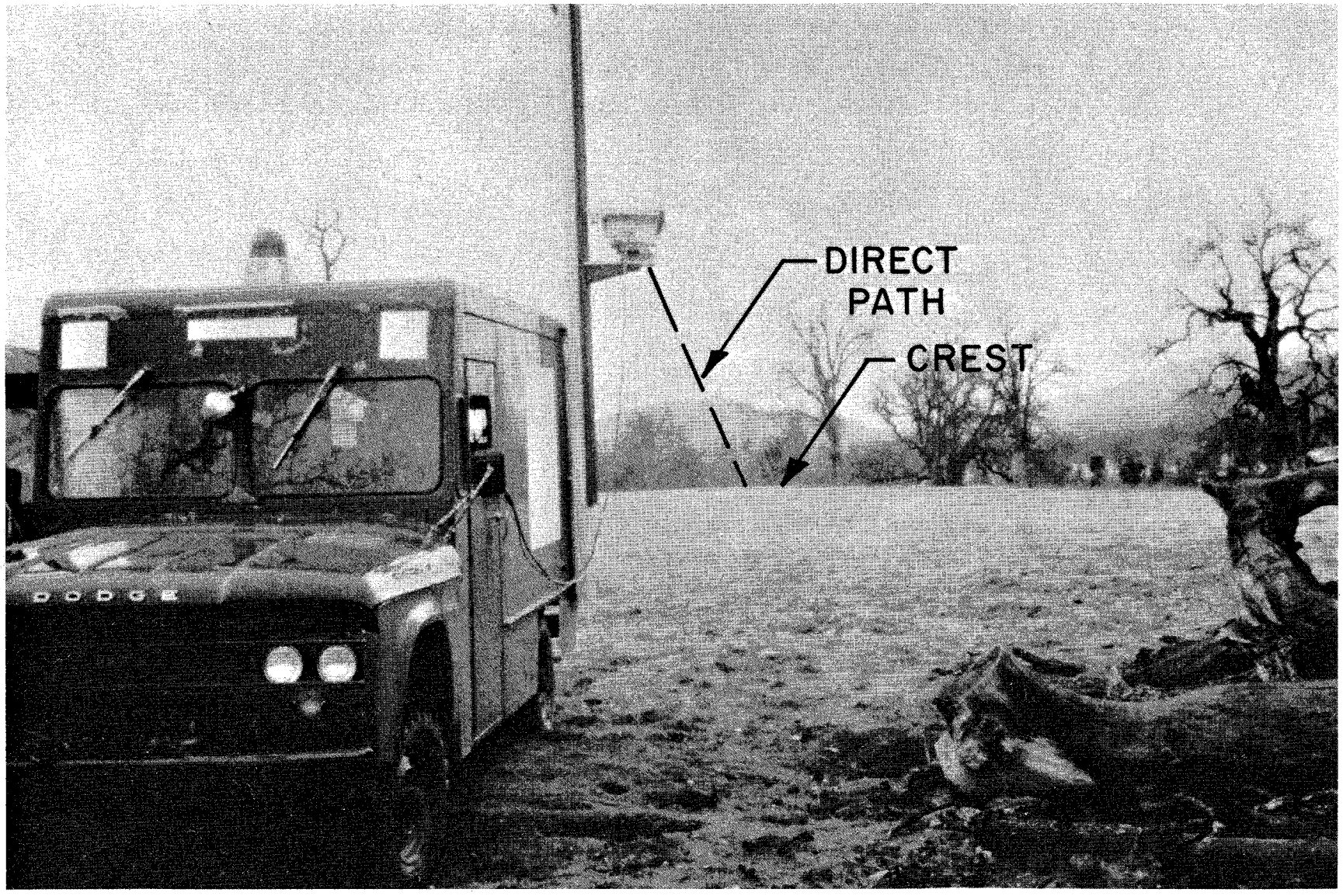

Figure 3-13. Path 4 receiver to crest.

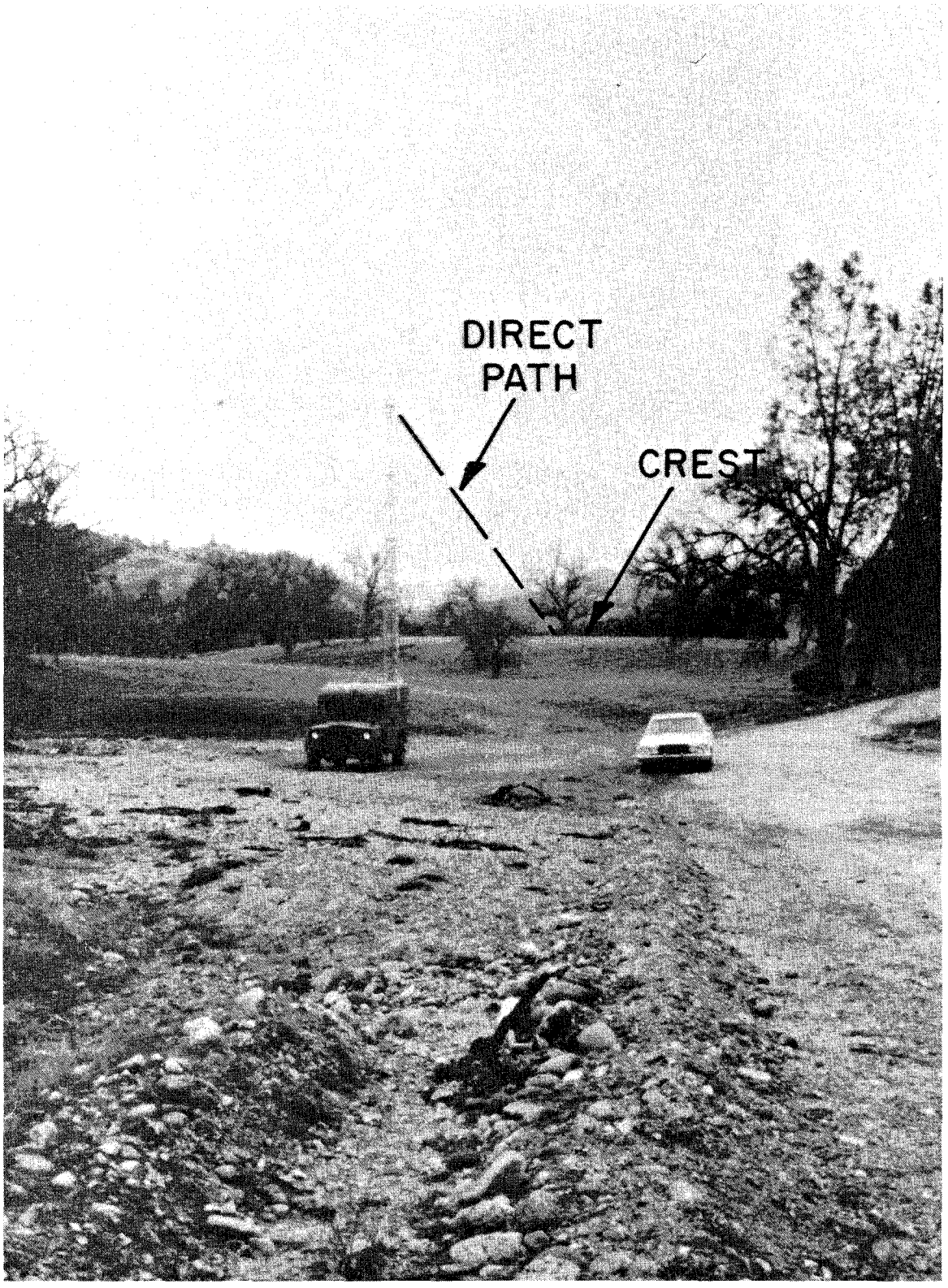

Figure 3-14. Path 4 transmitter to crest.

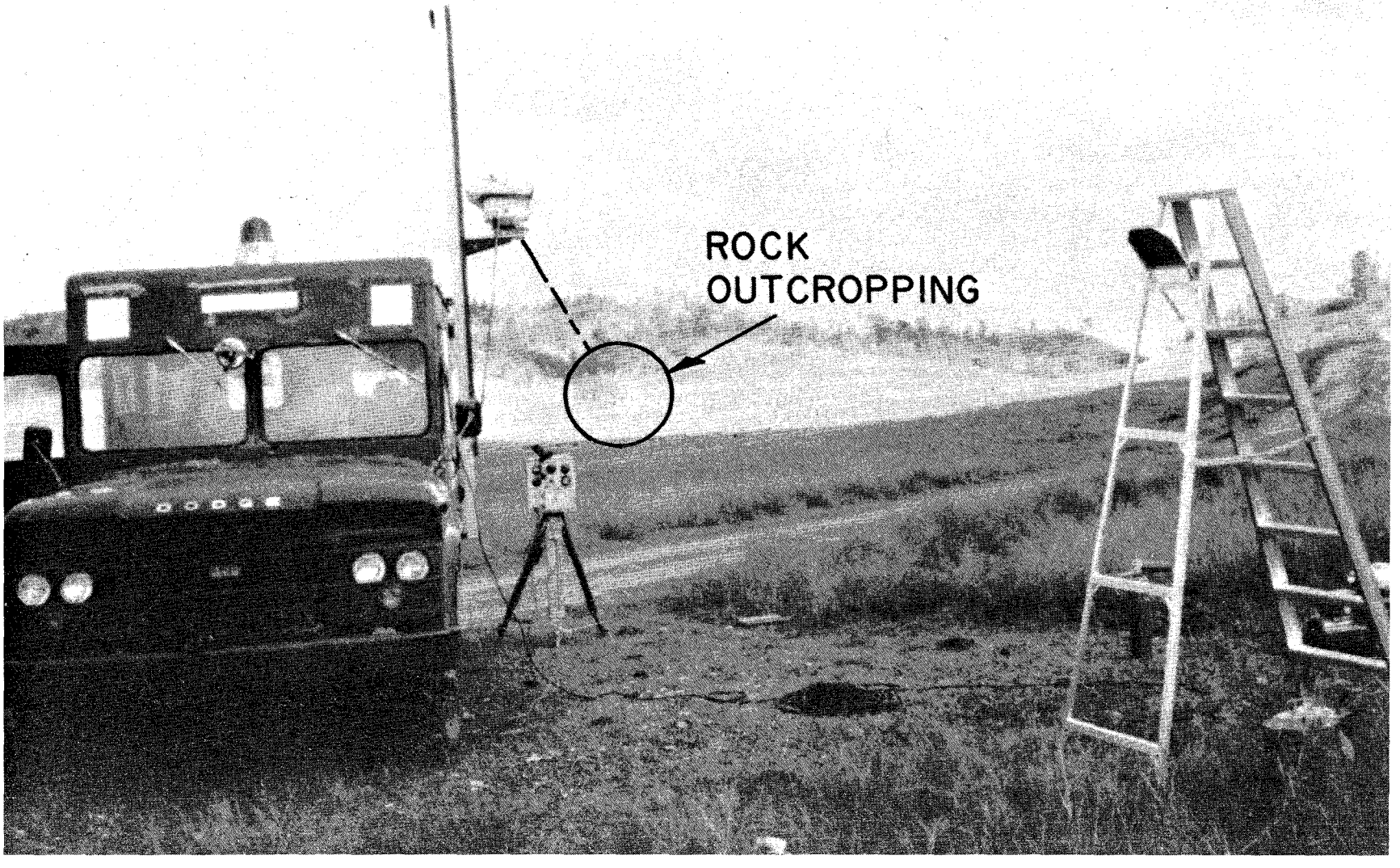

Figure 3-15. Path 5 receiver to rock outcropping.

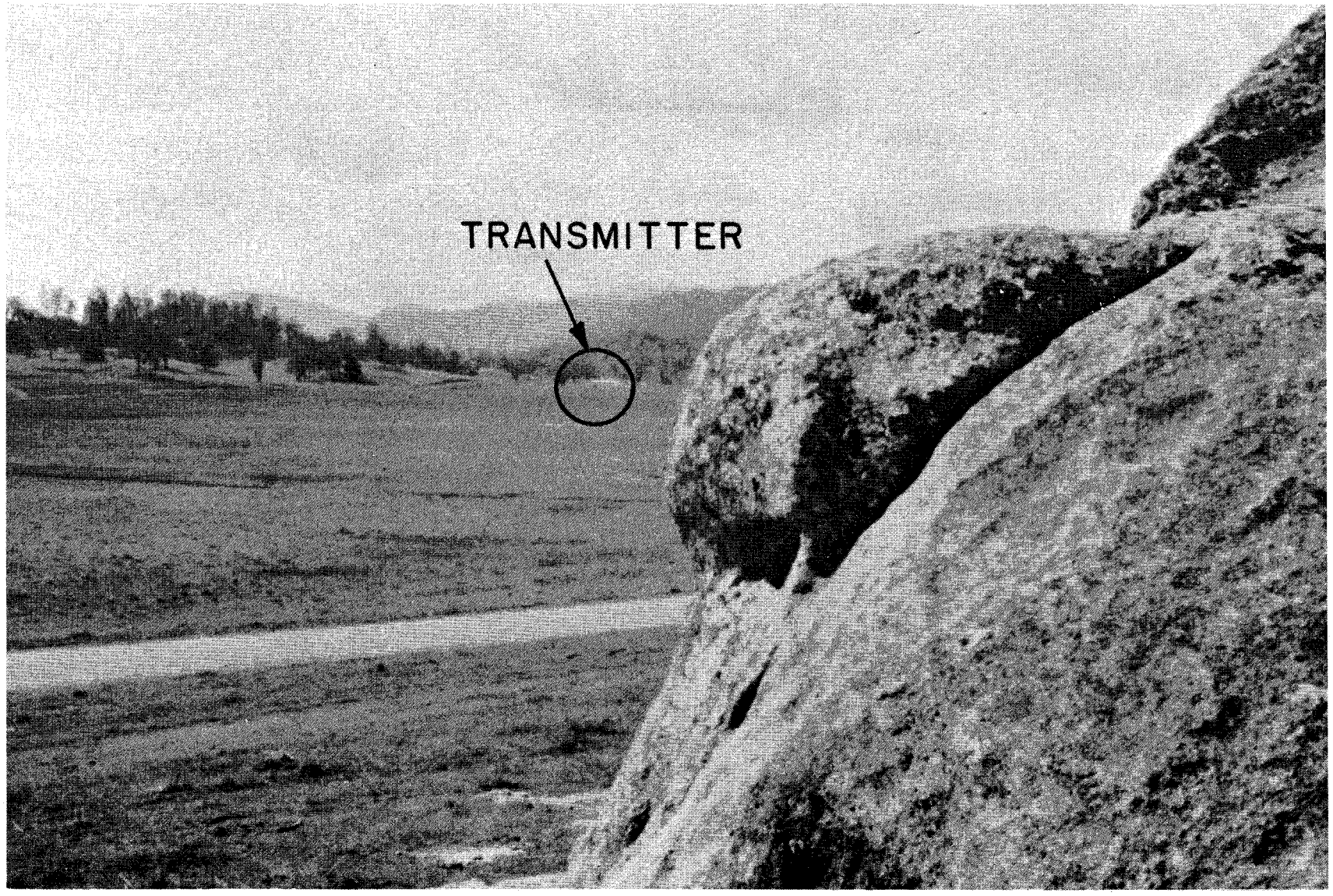

Figure 3-16. Path 5B receiver to transmitter.

Figure 3-17. Path 5B receiver behind rock outcropping.

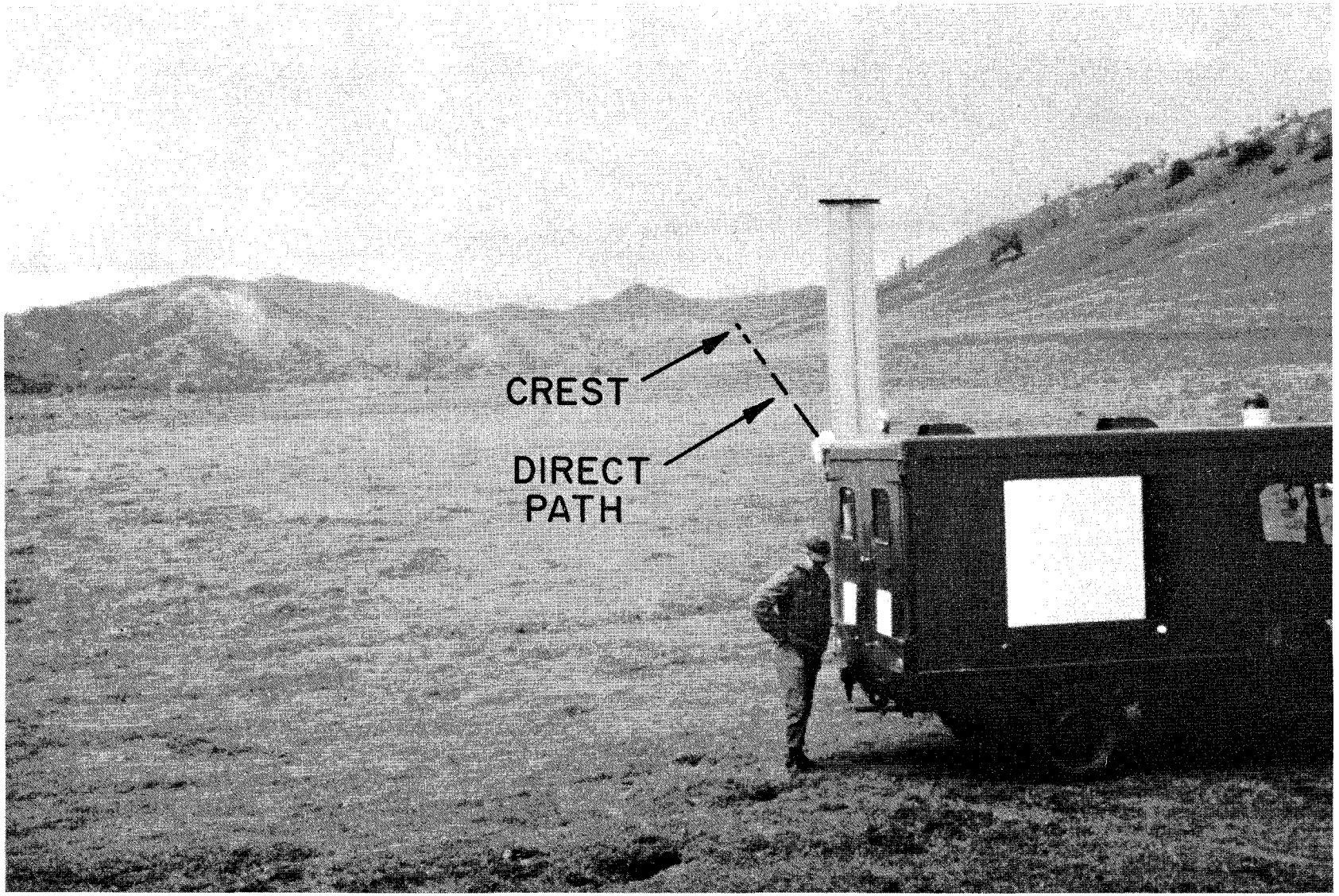

Figure 3-18. Path 6 receiver to transmitter.

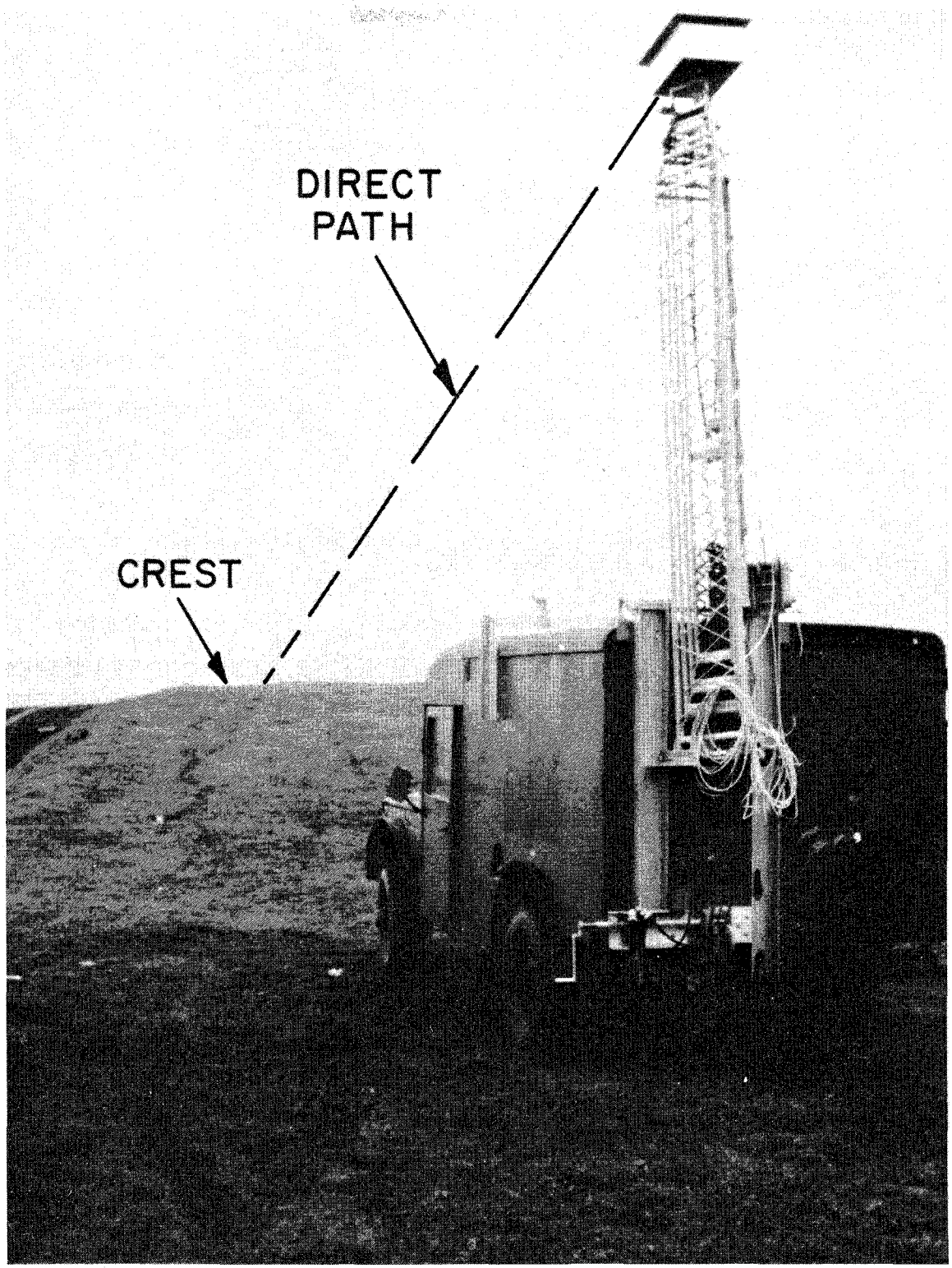

Figure 3-19. Path 6 transmitter to crest.

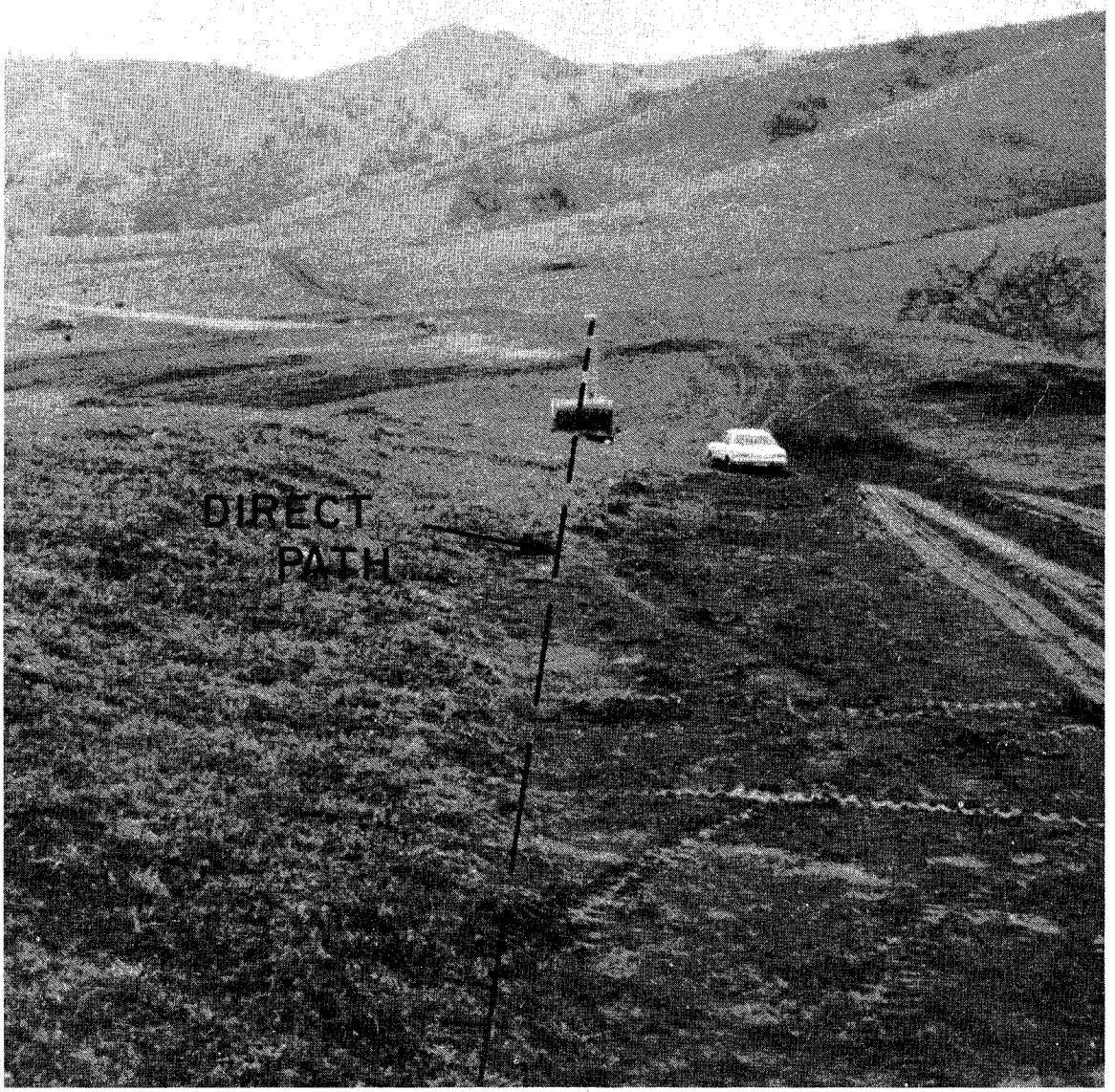
DIRECT
PATH

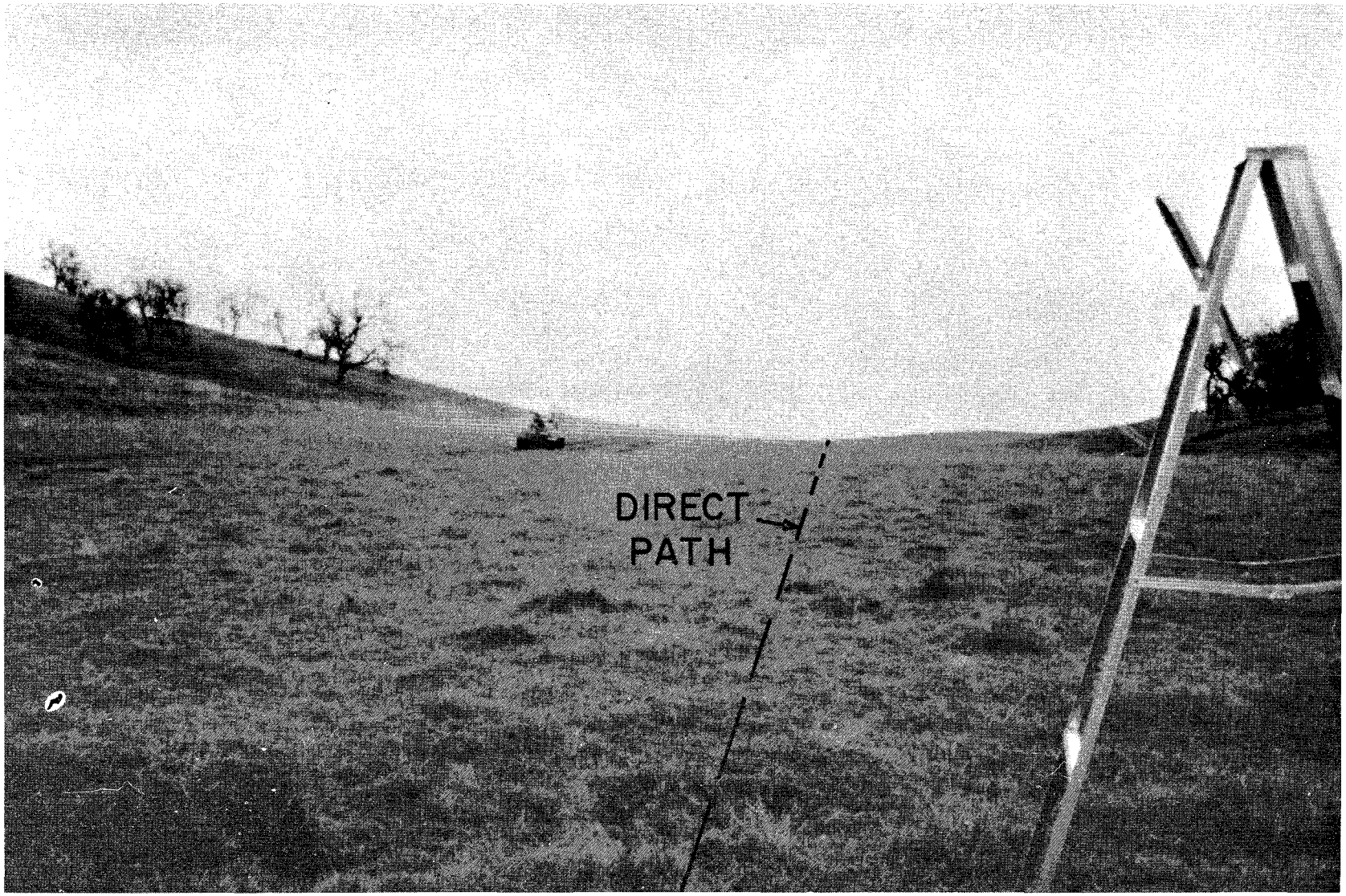

Figure 3-21. Path 7 receiver to transmitter.

Figure 3-22. Path 9 second crest to transmitter.

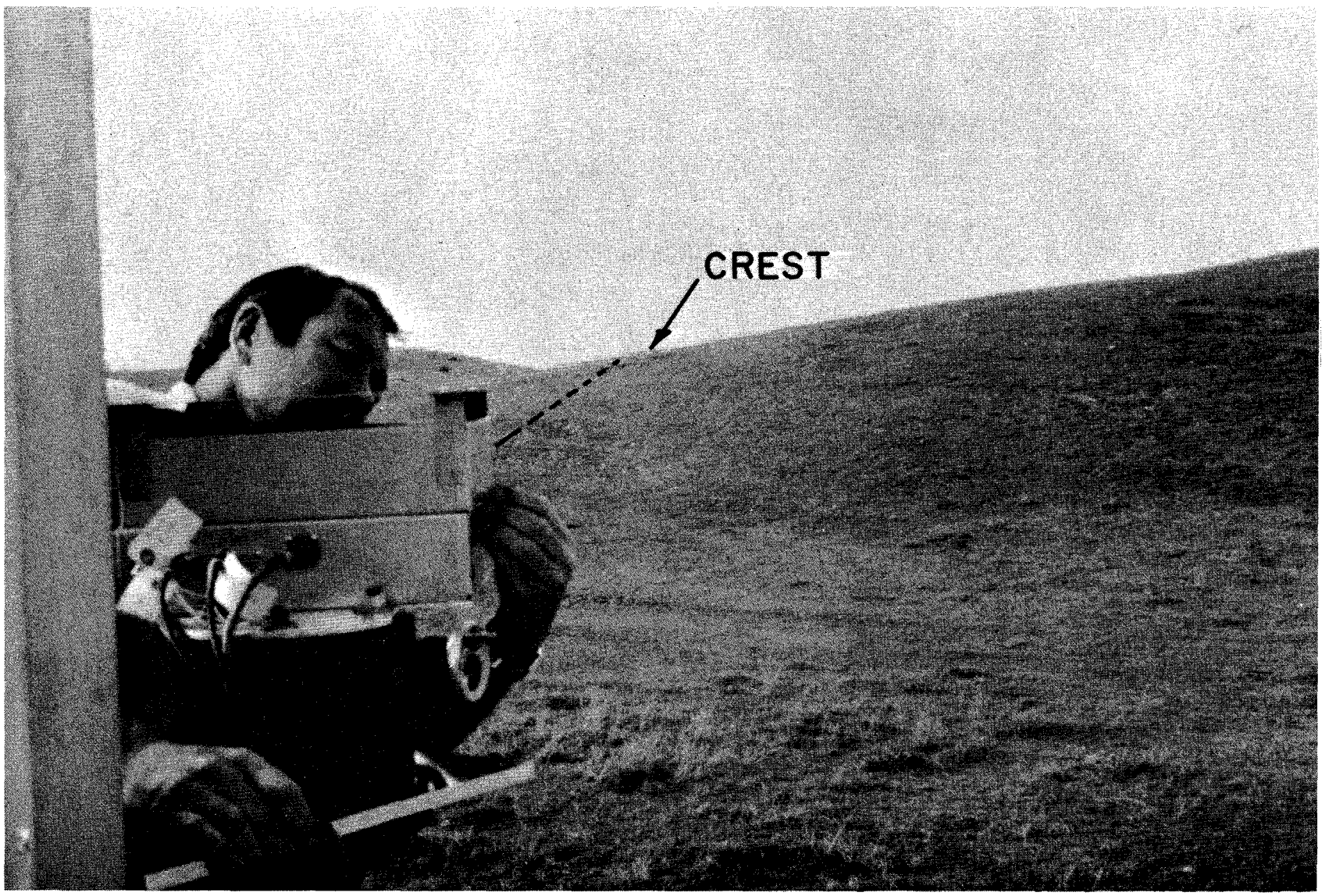

Figure 3-23. Path 9 receiver to second crest.

will be those that had cluttered obstructions. We will divide the paths into these categories only to show how the clutter affects the signal variability.

4.2 Results for Uncluttered, Irregular Paths

Figure 4-1 shows sketches of paths which have well-defined surfaces. Along each path, the common horizon between the transmitter and the receiver antennas is an infinitely long, horizontal ridge which is transverse to the path. A cross-section of the upper ridge shows that it is a knife-edge surface, while a cross-section of the lower ridge shows that it is a smooth and round surface. The antennas are positioned such that a direct ray from one antenna to the other just grazes the ridge. Vertical movement of one of the antennas above this line is defined as displacement of the target (and the radio path) above the grazing condition. For this condition, the two antennas are optically line-of-sight (LOS), but as we shall soon see the radio signal is affected by the obstruction until the antenna is raised well above the reference line defined by the just-grazing ray. Vertical movement of one of the antennas below the reference line is defined as the "below grazing" condition. In moving one of the antennas from above grazing ray to below it, we optically go from a "now you see it" condition to a "now you don't" condition. The radio signal, on the other hand, degrades gracefully as the antenna is lowered from above grazing to below grazing. The effects of an obstruction on radio propagation can be demonstrated by transmitting a signal from one of the antennas and measuring the received signal at the other antenna using the relation:

$$P_R = P_T + G_T + G_R - L_{\text{FREE SPACE}} - L_{\text{DIFFRACTION}}$$

where

P_R = measured received signal level, dBm

P_T = transmitted power, dBm

G_T = transmitted antenna gain, dBi

G_R = receiver antenna gain, dBi

$L_{\text{FREE SPACE}}$ = free space loss

$$= 20 \log (\text{frequency}_{\text{MHz}}) + 20 \log (\text{distance}_{\text{meters}}) - 27.55$$

$L_{\text{DIFFRACTION}}$ = diffraction loss due to the obstruction.

Using the same notation as we developed in Section 2, Figure 4-2 shows the theoretical effects on diffraction loss of ridges with several well-defined radii of curvature (adapted from Dougherty and Maloney, 1964 or Rice et al, 1967). For an ideal knife-edge ridge, the radius of curvature, P, is 0; for a rounded ridge, the radius of curvature approaches 1. Note that at grazing (obstacle height equals 0), the diffraction loss varies from 6.02 dB for the ideal knife-edge ridge to greater than 15 dB for a ridge with a radius of curvature equal to 1. As the radio path is raised above the grazing path (the obstacle height becomes more and more negative), the diffraction loss experiences a damped oscillation about the 0 dB axis.

Consider now specific paths and propagation measurements. Path 6 was a long path with apparently a single obstruction between the transmitter and receiver. Figure 4-3 shows the path 6 obstruction's effect on the measurement signals at 9.6 GHz and 28.8 GHz. As in all of the figures, the diffraction loss is the difference between the measured received radio signal level and the computed free space signal level. The diffraction loss has been plotted as functions of obstacle height, H, and target cover, Y. Recall from Section 2, target cover is defined as negative when the observer is optically able to see the target and positive when the observer is unable to see the target. Because the target is relatively close to the obstruction, Y and H are nearly equal; in fact, $H = 0.98Y$.

There are two curves plotted on each figure; the transmit antenna's platform was set initially below grazing, and then during data recording the platform was raised above grazing and finally returned below grazing. Although the platform moved continuously during the measurement period, the data recording was not continuous as evident by the gaps in the 28.8 GHz curves. The gaps are due to the data collection process, since for every 30 seconds of measurement time approximately 25 seconds were spent collecting data and 5 seconds were used to compute signal statistics and print the results to the terminal.

For this particular type of path, a threshold could be set for either frequency such that if the received radio signal threshold were exceeded, the transmitter and receiver could be said to be optically line-of-sight or intervisible to one another.

Path 7 was a short path compared to path 6, but was similar in the sense that it was relatively free of clutter (e.g. trees and rock outcroppings). The crest of path 7 had a sparse stand of about 0.5 meter tall grass, although when viewed from a distance, the stand of grass appeared to be dense. Figure 4-4 shows the effects of the grassy crest on the path 7's diffraction loss at 9.6 and 28.8 GHz. As with path 6, a threshold could be used to determine when the two end points of the path were intervisible to one another. Figure 4-5 shows the signal variability as the receiver was moved horizontally transverse (perpendicular) to the path while maintaining line-of-sight conditions.

Path 9 was a double horizon path fairly clear of clutter. As the transmitter was lowered below the grazing ray, two crests simultaneously blocked the signal as illustrated in Figure 4-6. Figure 4-7 shows the effects of the double horizon on the diffraction loss.

In general, for paths that have intervening ridges relatively clear of clutter, it appears that a threshold, based on the separation distance between two mobile units, can be set to determine when the two units are intervisible.

4.3 Results for Cluttered, Irregular Paths

Along the first half of path 3 from the receiver to the obstruction, the path was clear of clutter; however, the last half was lined with live and dead oak trees, on both sides of the path, well within the 3 dB beamwidths of the antennas. None of the trees blocked the direct ray from the transmitter to the receiver. The effects of the trees are shown in Figure 4-8. Both frequencies appear to exhibit the effects of multipath fading, especially when the transmitter antennas were lowered below the grazing ray. Due to the signal scattering, probably caused by the trees along either side of the path, a fixed signal threshold would result in periods of both missed and false detections of intervisibility between the transmitter and receiver.

Path 4 was approximately the same length as path 3; however, the path 3 crest-to-transmitter distance was about one-tenth of the total path distance, while the path 4 crest-to-transmitter distance was about three-fourths of the total distance. Both paths had trees which were within the 3 dB beamwidths of the antennas. As Figure 4-9 shows, any threshold setting for either frequency would be subject to periods of false or missed intervisibility detections.

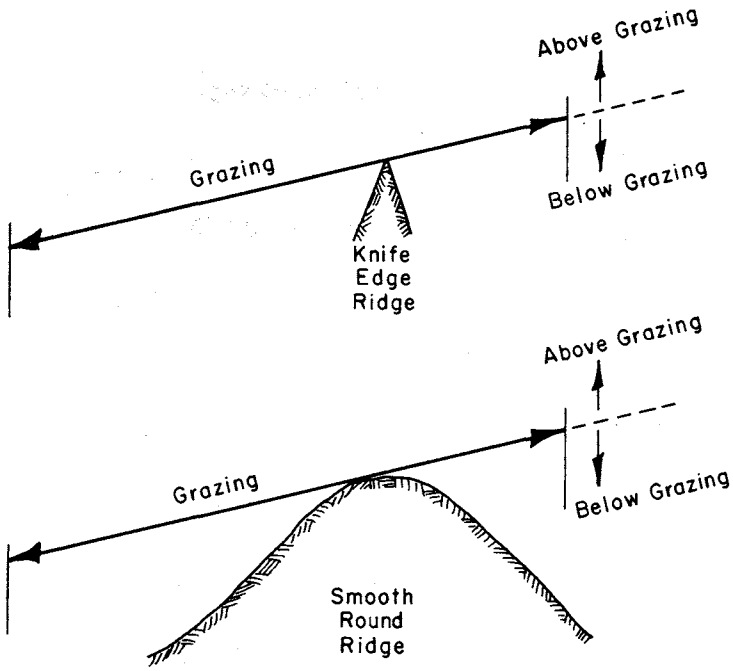

Figure 4-1. Examples of clear, well-defined paths.

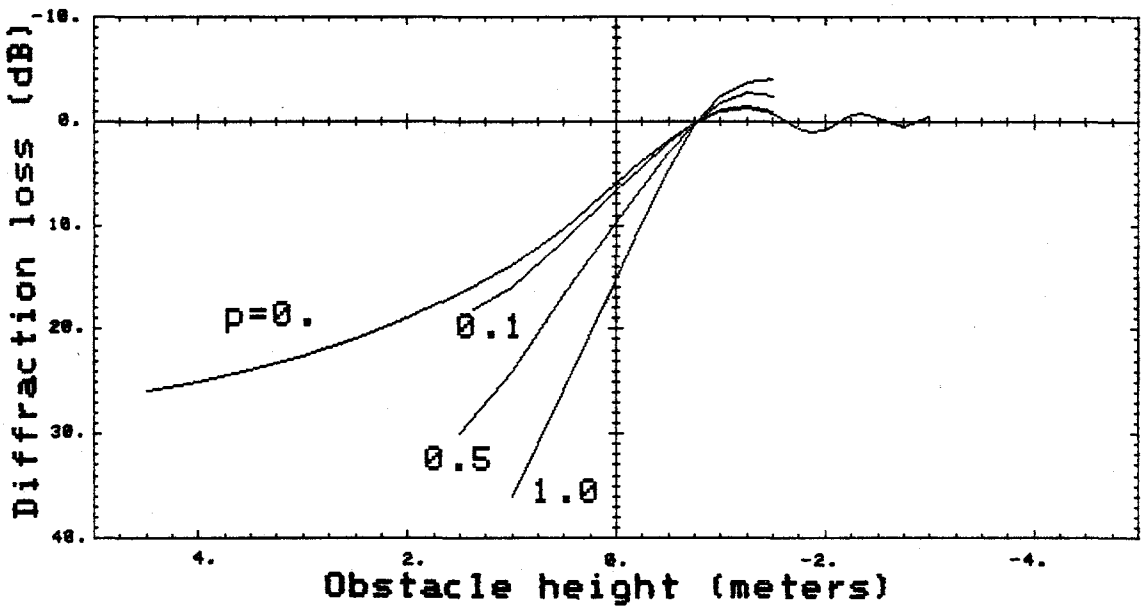

Figure 4-2. Theoretical diffraction loss for ridges with several well-defined, normalized radii of curvature. Parameters: d_A = 1000 meters, d_B = 250 meters, frequency = 30 GHz.

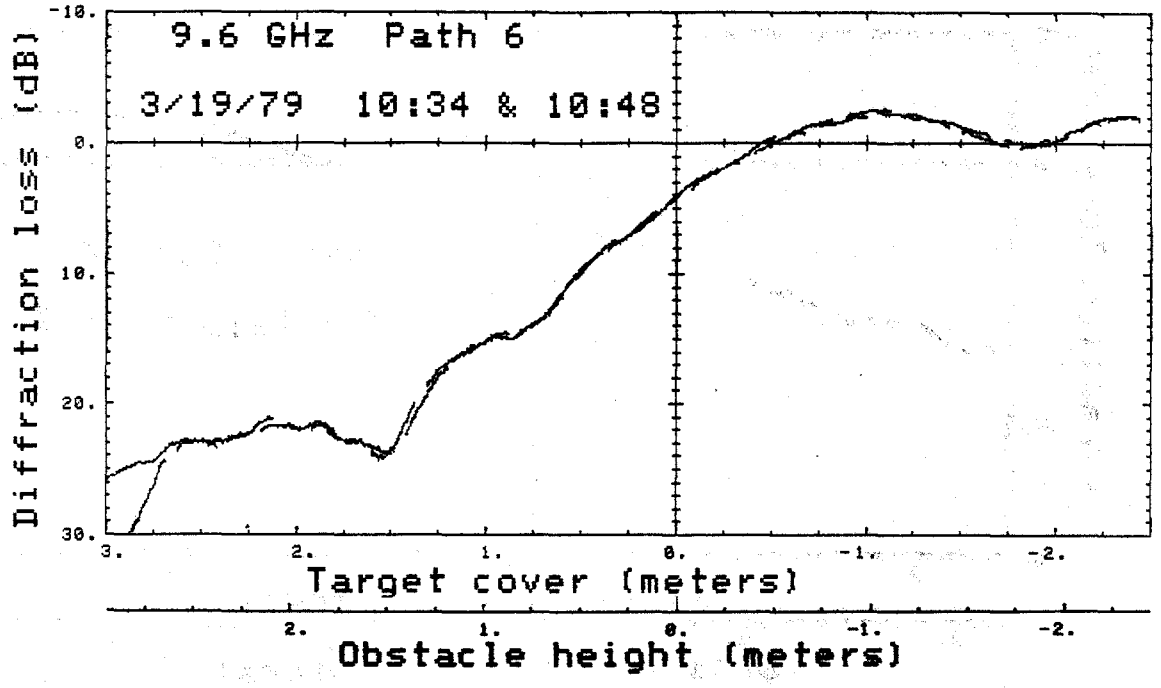

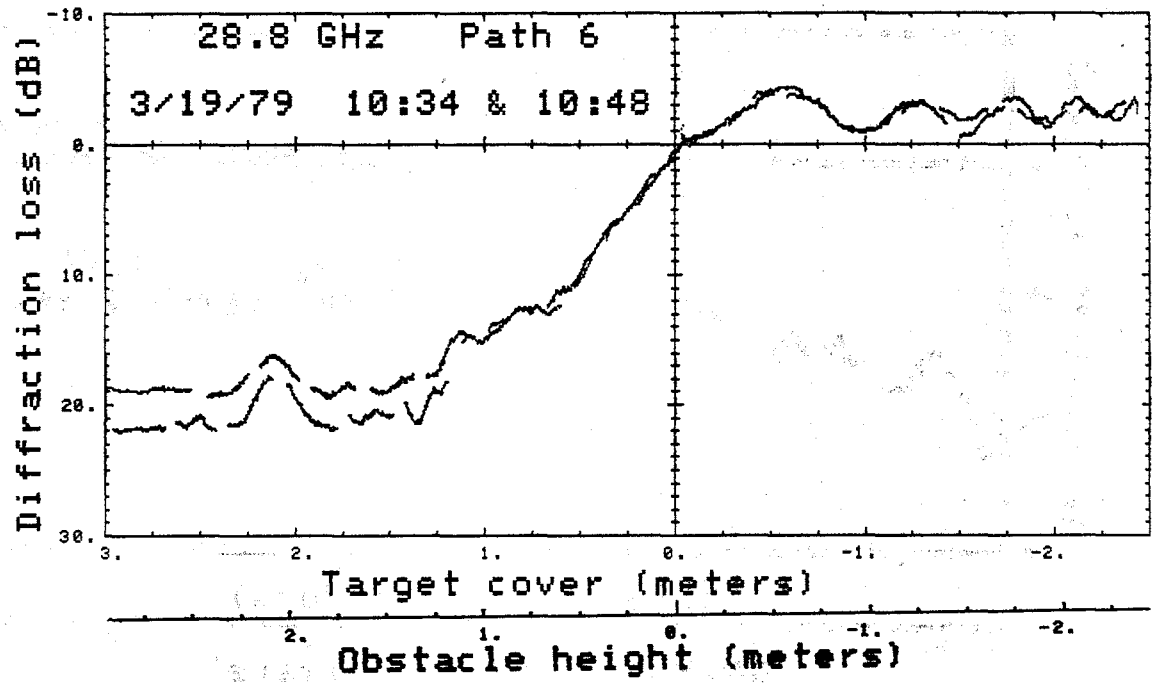

Figure 4-3. Diffraction results for path 6.

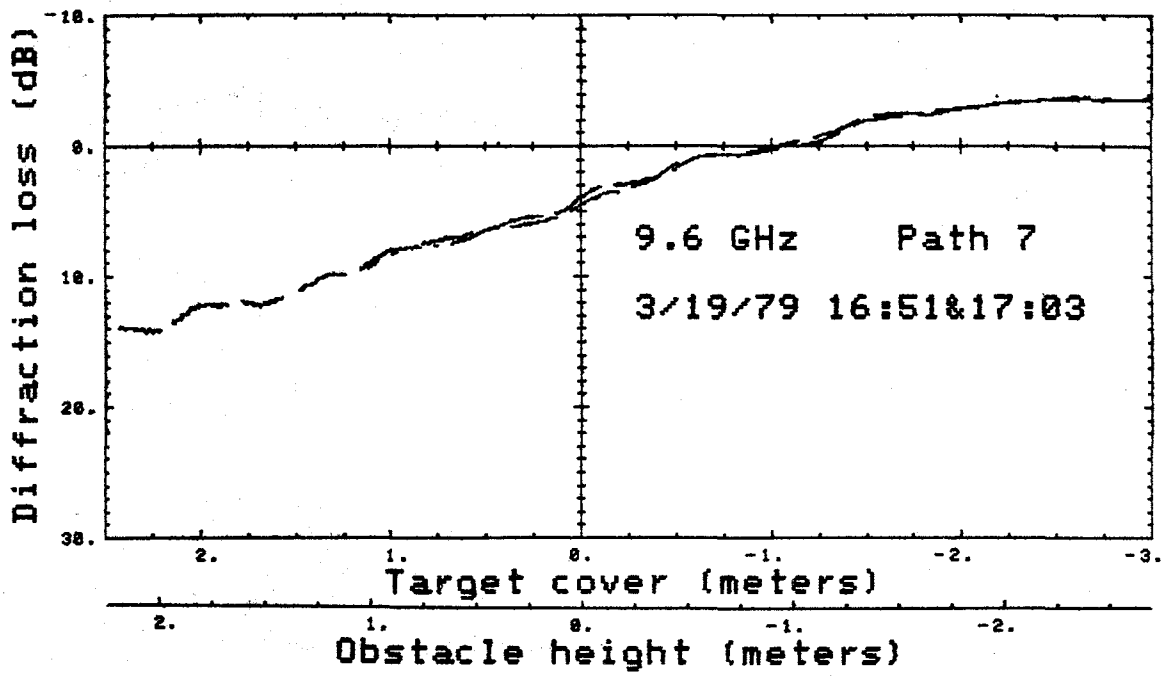

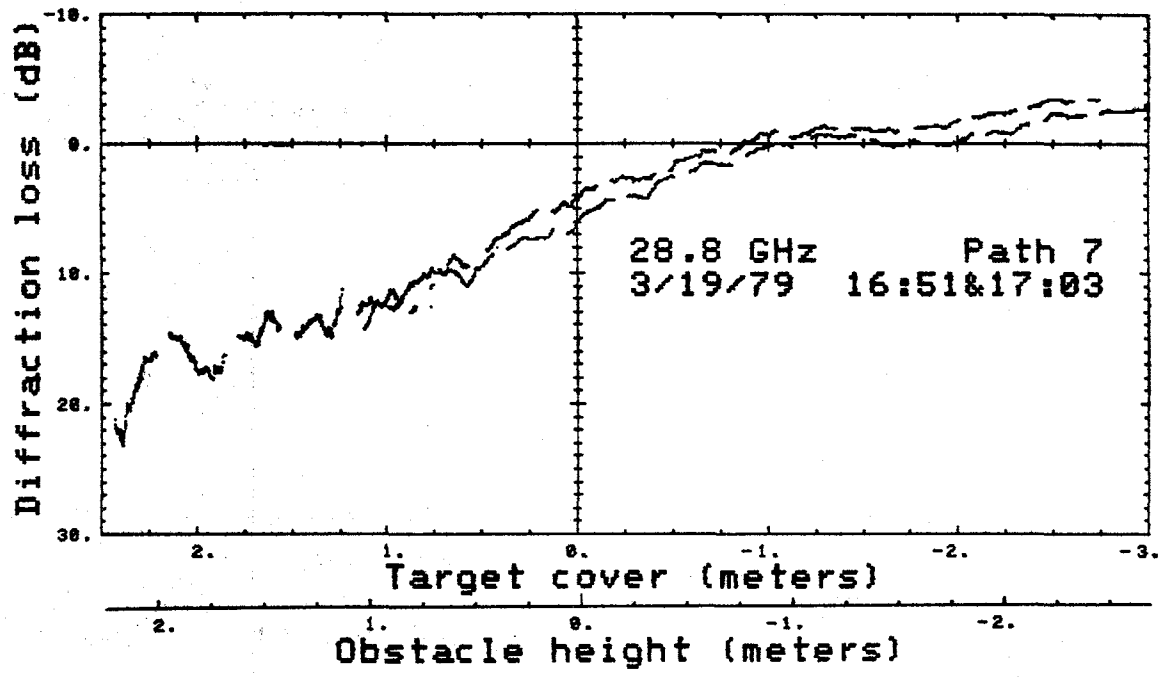

Figure 4-4. Diffraction results for path 7.

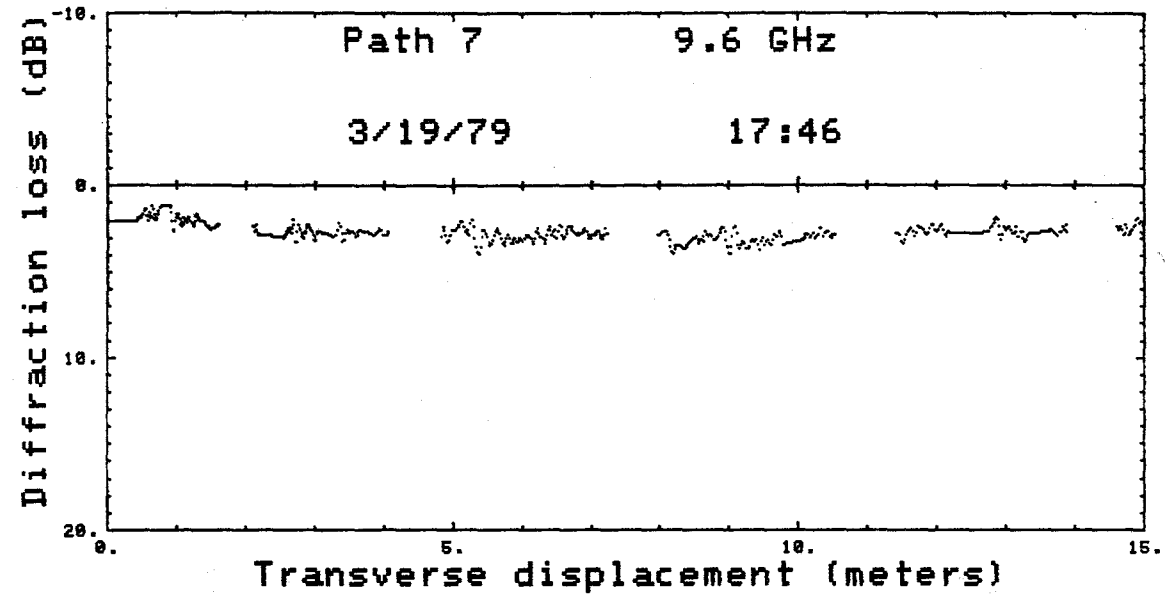

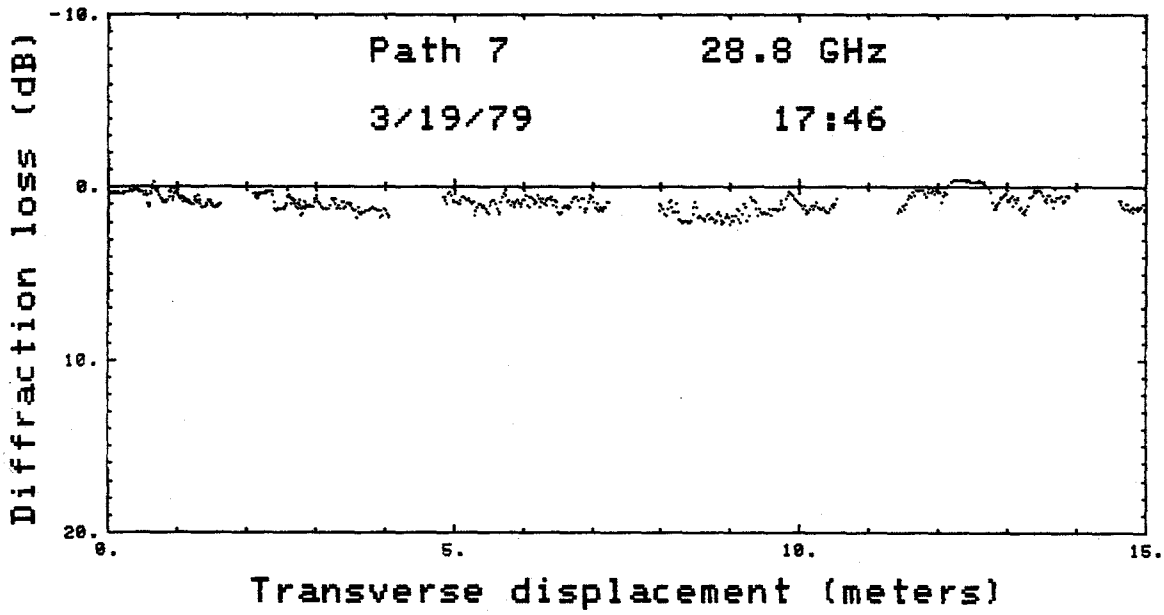

Figure 4-5. Diffraction loss for path 7, with transverse displacement of the receiver.

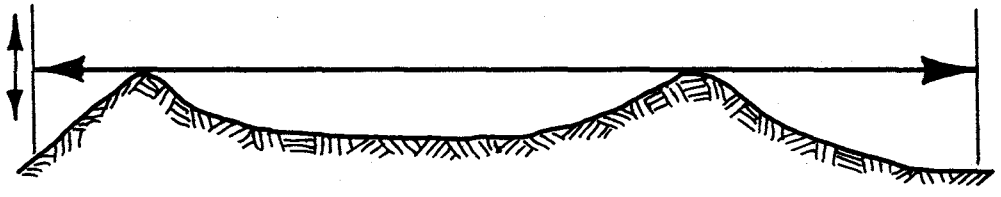

Figure 4-6. Sketch of path 9's profile.

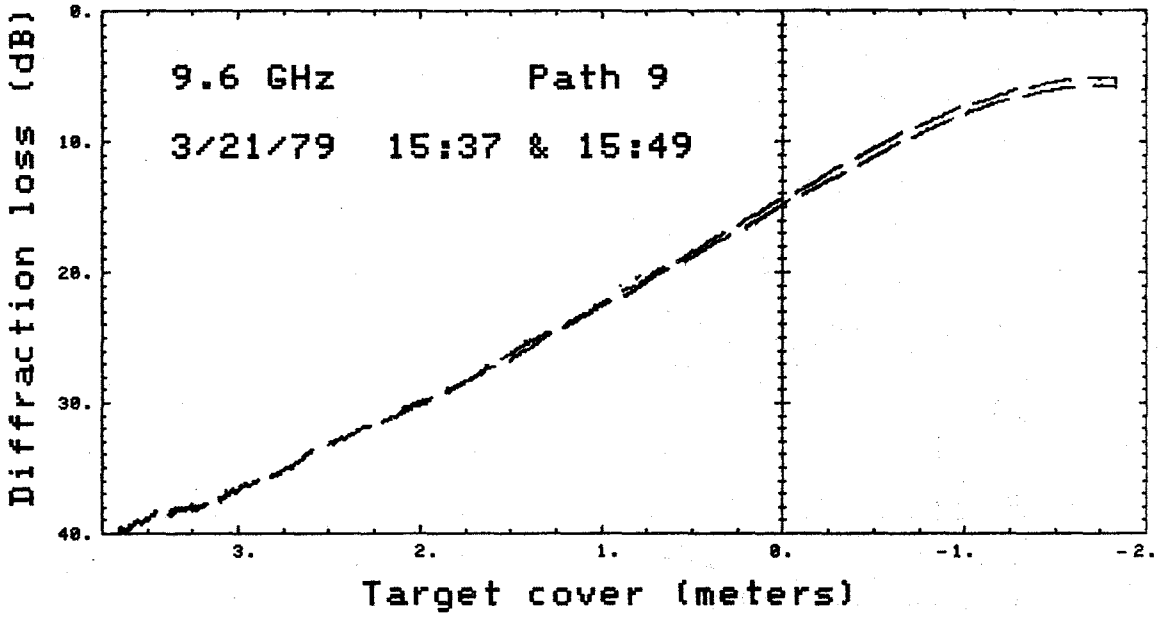

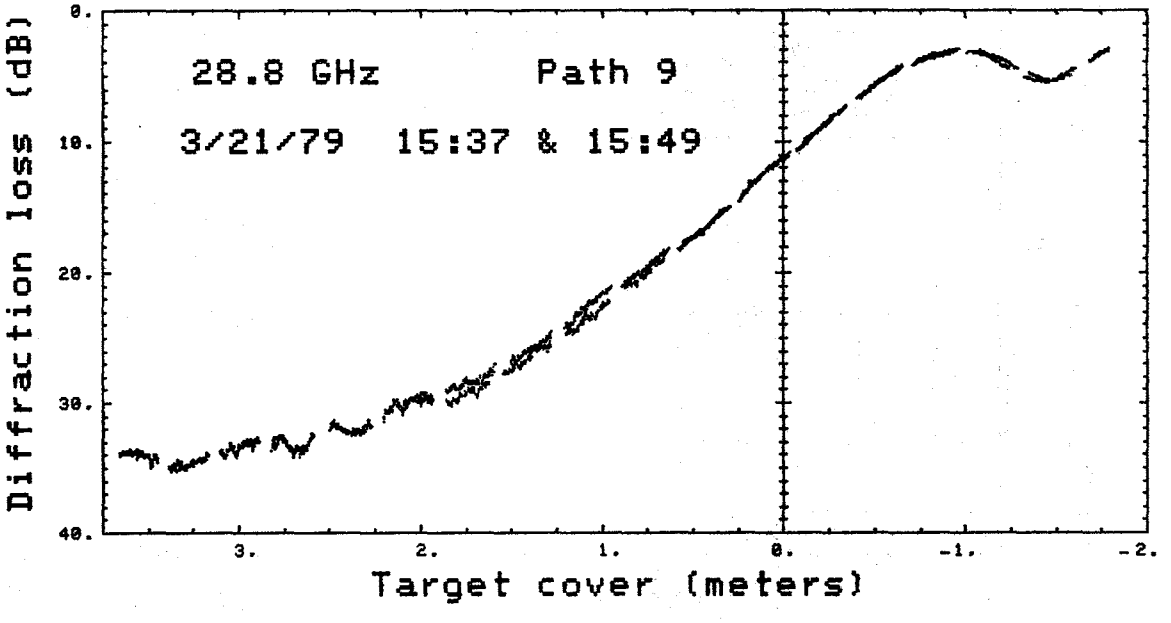

Figure 4-7. Diffraction results for path 9.

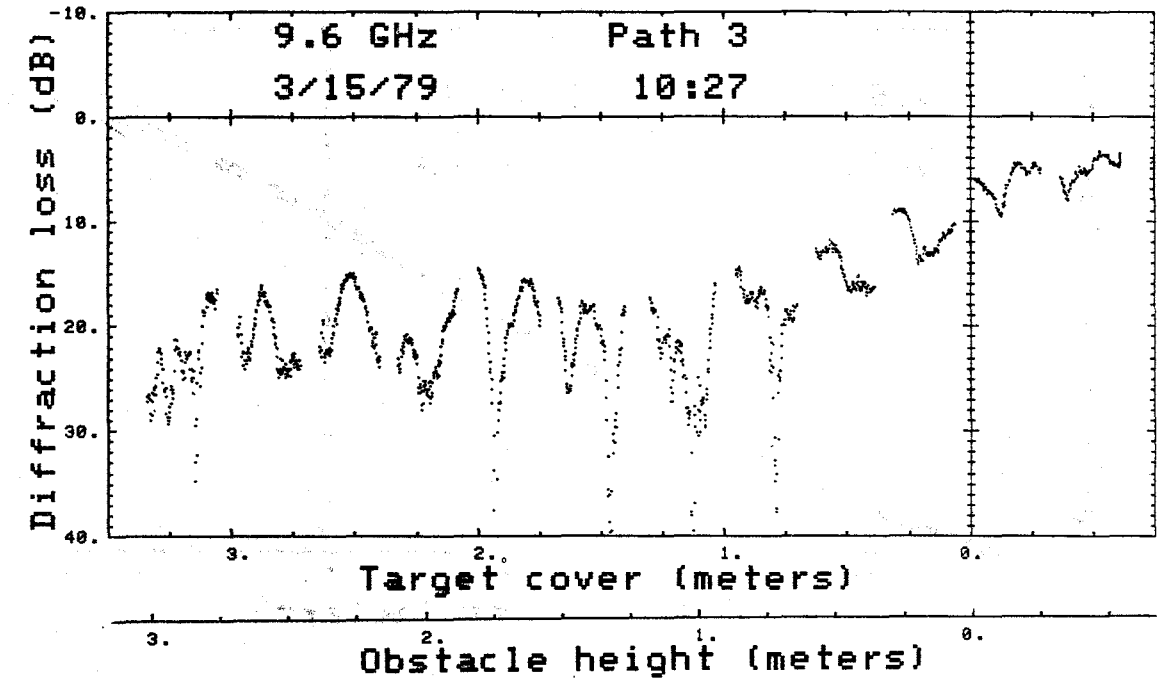

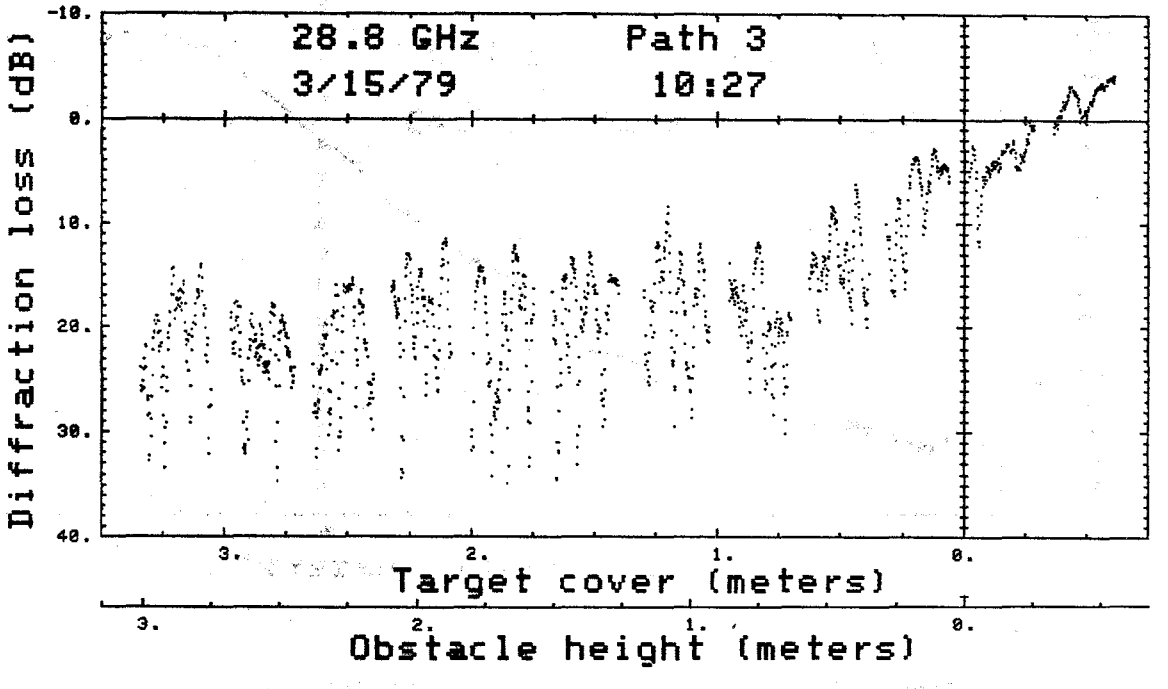

Figure 4-8. Diffraction results for path 3.

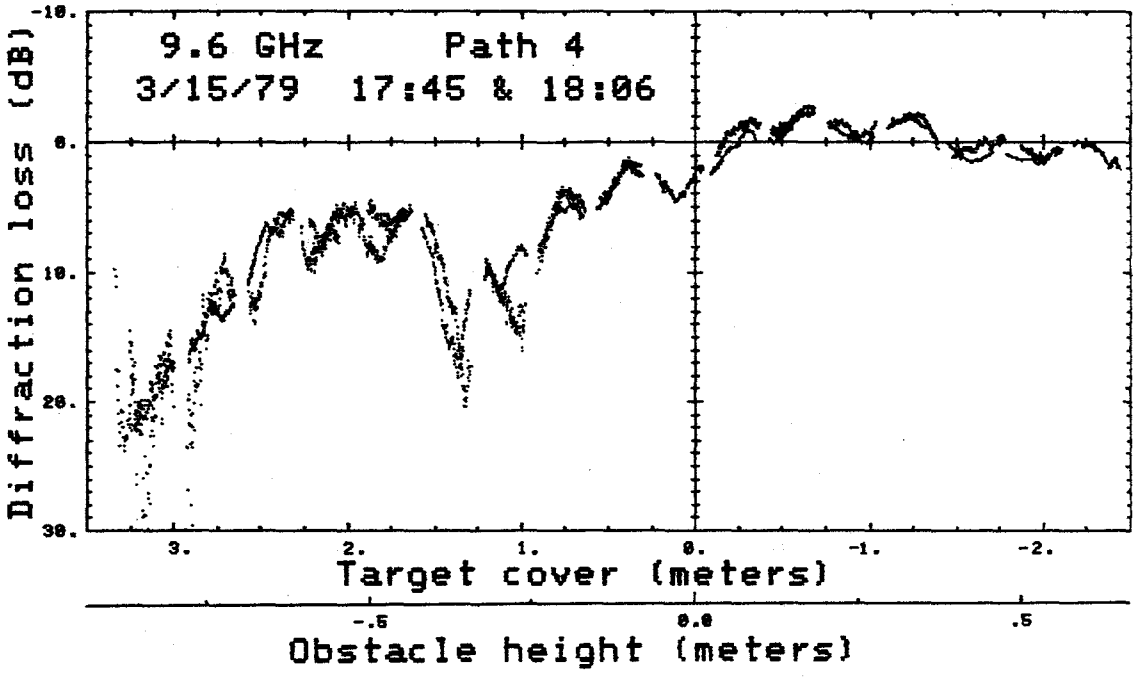

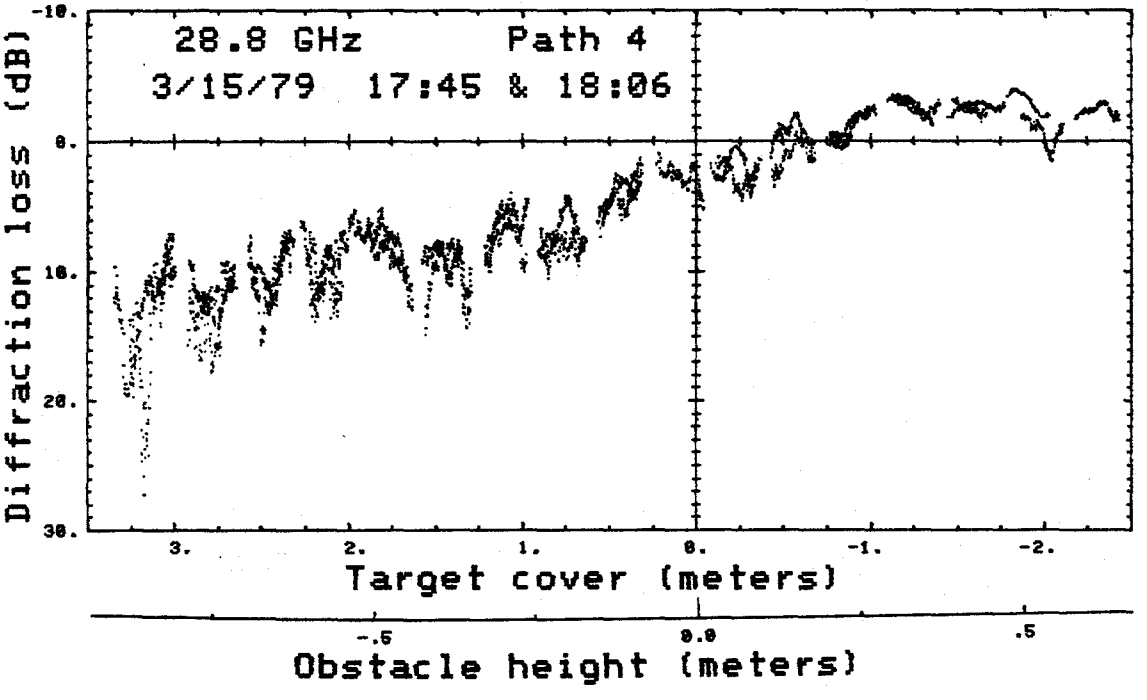

Figure 4-9. Diffraction results for path 4.

The obstacle along path 5 was a large rock outcropping. The transmitter was positioned a few meters behind the outcropping and then raised and lowered relative to the grazing ray. Figure 4-10 shows the results when the transmitter was 14 m behind the outcropping (about 1.3 percent of the total path distance) and Figure 4-11 shows the results with the transmitter 44 m behind the outcropping (about 4 percent of the total path distance). In either case the results at each frequency are quite similar; signal reflections off the rock outcropping enhance or reduce the received signal level depending upon the path geometry when the two end points are clearly intervisible. For this type of obstacle, any signal threshold for either frequency would result in false and/or missed intervisibility detections.

For the measurements made on the path identified as 5B, the transmitter and receiver positions were exchanged so that the receiver was close to the rock outcropping. The receiver was moved horizontally and transverse to the path; for the following figures; a positive exposure indicates that the transmitter and receiver were intervisible. Figure 4-12 shows the diffraction loss results when the receiver was approximately 15 m behind the rock outcropping and about 2 m below the top of the outcropping. For Figure 4-13, the receiver was moved to about 4 m from the outcropping. Again, signals reflected from the outcropping significantly affect the received signal such that a signal threshold would be impossible to set without a high incidence of missed alarms when the two end points are clearly intervisible.

Because the data collection process was different for paths 1 and 2, their results are presented separately in Appendix B.

In general, for the types of paths that had identifiable obstacles such as trees or rock outcroppings along the sides of the path, the received signal at either frequency was affected by the multiple scatterers from the trees or rock surfaces. Due to the received signal's variability, even when the end points are clearly intervisible, a signal threshold for estimating intervisibility could not be set reliably without periods during which a large number of false alarms or a large number of missed alarms are registered.

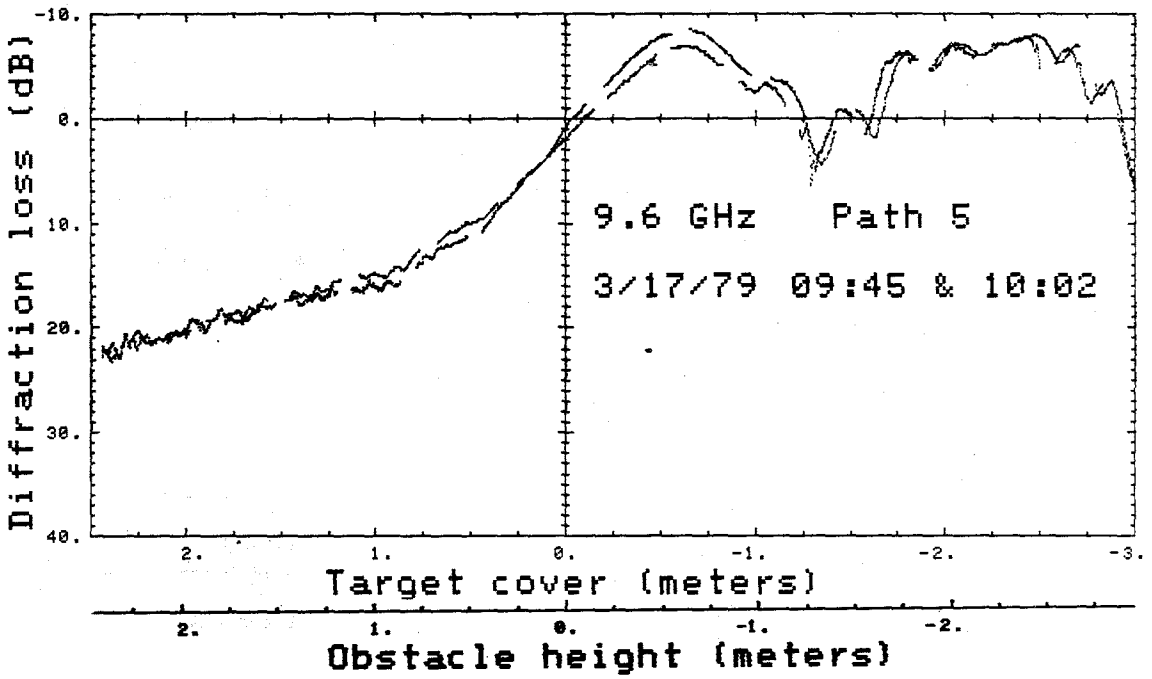

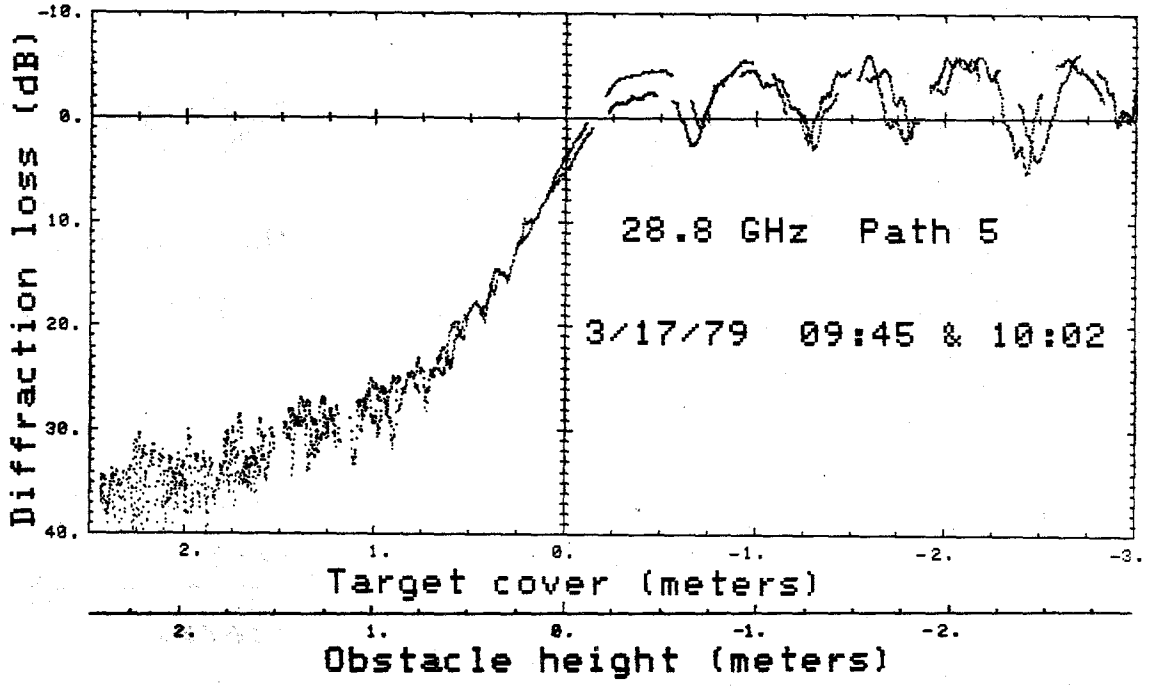

Figure 4-10. Diffraction results for path 5, first location.

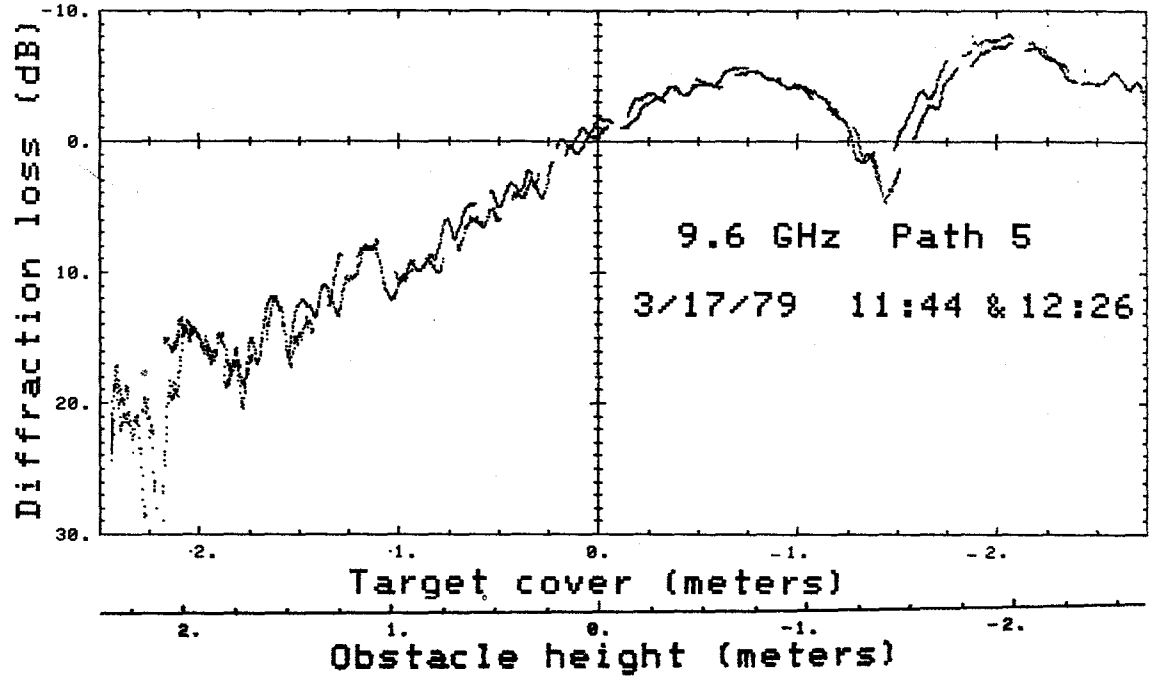

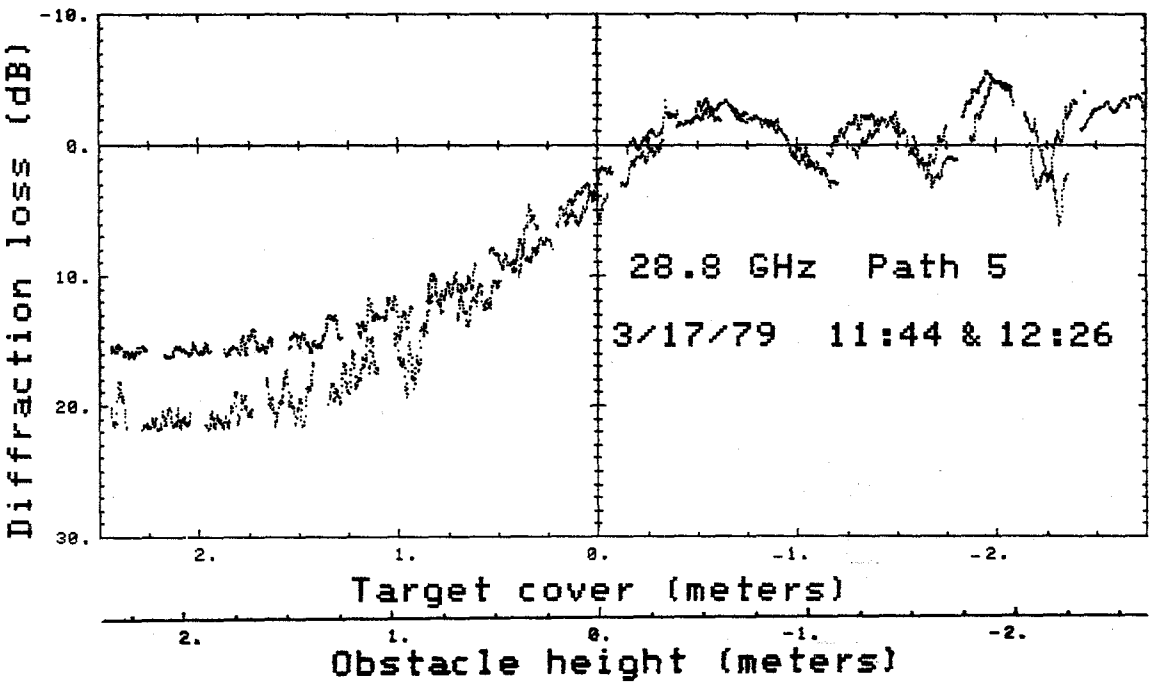

Figure 4-11. Diffraction results for path 5, second location.

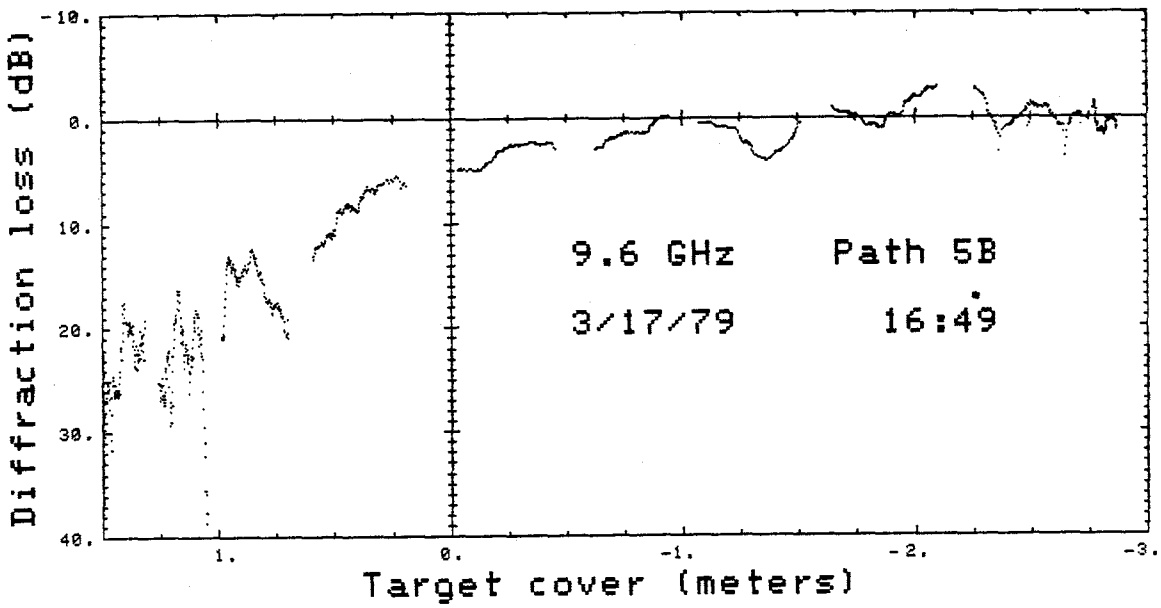

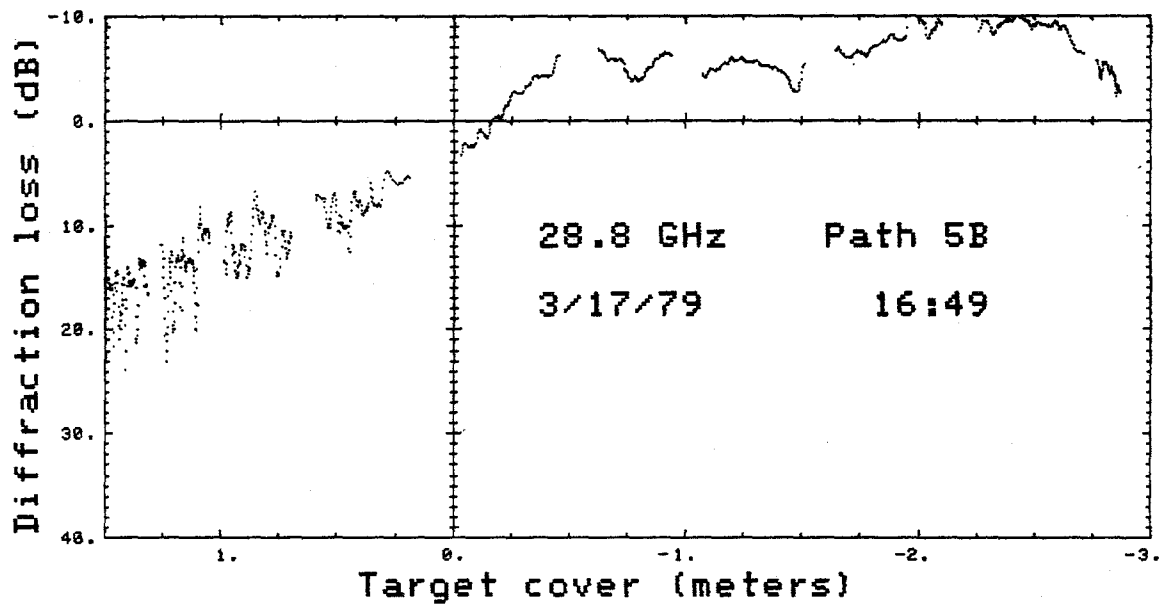

Figure 4-12. Results for path 5B, transverse movement of receiver about 15 meters behind rock outcropping.

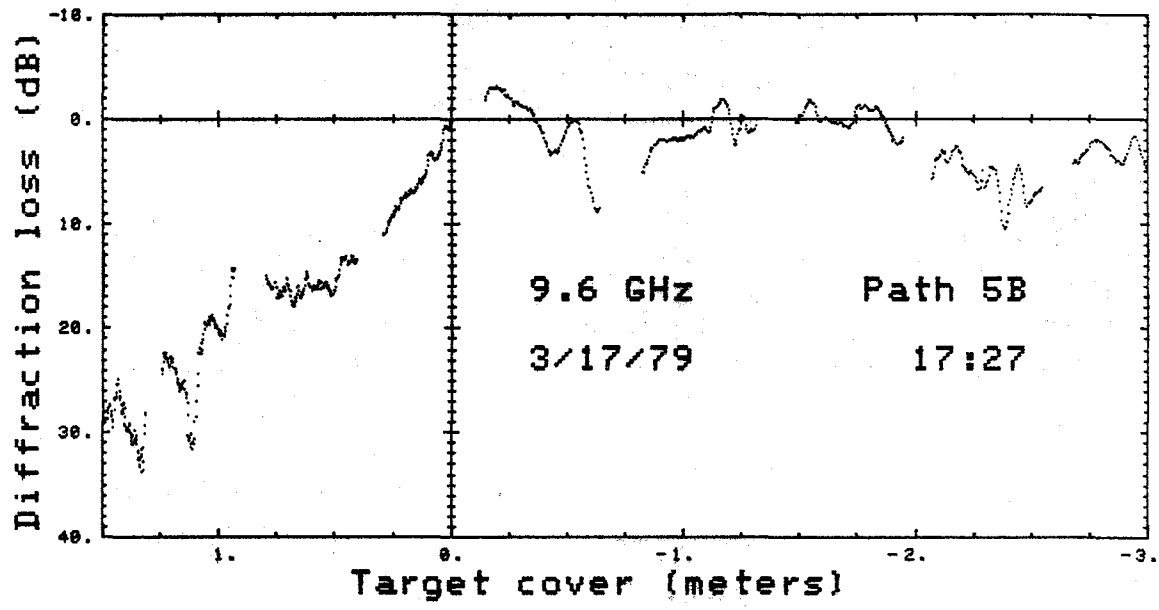

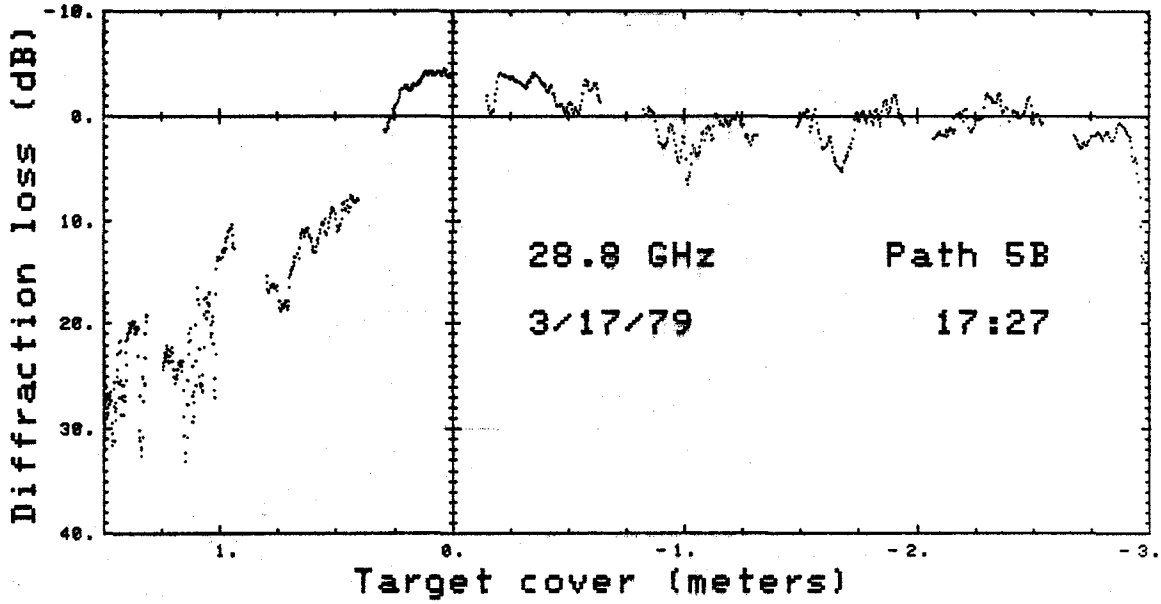

Figure 4-13. Results for path 5B, transverse movement of receiver about 4 meters behind rock outcropping.

4.4 A Normalized Set of Results for All Single Horizon Paths

In the report by Dougherty and Maloney (1964) the Fresnel-Kirchoff parameter V is defined. Parameter V can be used to normalize all paths of differing lengths at different frequencies. The sketch in Figure 4-14 shows the path geometry and definition for V. Figure 4-15 shows the results of diffraction loss versus V for the well-defined obstacles of Figure 4-1. We note 4 points about the curves of diffraction loss versus V:

1) the loss is 6.02 dB at V=0 for the ideal knife-edge ridge
2) the loss is 0 dB at V = -0.8 for all of the idealized ridges
3) the loss has a damped oscillation about the 0 dB axis for V < 0
4) the loss for the ideal knife-edge has a peak (actually a diffraction gain) at V = -1.25 with smaller peaks at V = -2.3, etc.

Figures 4-16 through 4-21 show the results of diffraction loss versus V for paths 3 through 7, all normalized to the same scales.

The most interesting feature to note is that when the curves of Figure 4-15 are superimposed on the measured data of Figures 4-16 through 4-20, paths 3, 4, 5, and 6 exhibit characteristics of knive-edge to near-knife-edge obstacles, i.e. the measured data has the slope characteristic below grazing and the oscillation characteristic above grazing for obstacles having a normalized radius of curvature p from 0 to 0.1.

Path 7's crest does not appear to have any of the characteristics displayed by the well-defined obstacles of Figure 4-15. This may be due to path 7's crest topography, which was much like a flattened Gaussian surface. Because of the crest's gradual roll-off towards both the transmitter and the receiver, the exact position of the peak of the crest along the path was very difficult to determine. If the transmitter-to-crest and receiver-to-crest distances are in error, the calculation of V will be in error also and could explain why the plots given in Figures 4-21 (path 7) do not correspond to any of those curves in Figure 4-15.

Up to this point in the discussion, it has been assumed that the optical grazing ray is the same as the electrical (9.6 GHz and 28.8 GHz) grazing ray. The grazing point (obstacle height = 0 for Figure 4-3 etc., and V = 0 for Figures 4-16 through 4-21) was determined by an optical observation at the

time of the measurements. However, for some conditions it was difficult to determine when optical grazing occurred. Uncertainty were due to the long path lengths, coupled with poor optics, and the vegetation growing at the grazing crest. Suppose the location of the V = 0 axis for each of the Figures 4-16 through 4-21 was not known yet. One method to determine the location would be to determine under what conditions the theoretical knife-edge curve produces the best fit to the measured data. This is done by first overlaying the theoretical curve (Figure 4-15) on the measured data (say Figure 4-20). Then, an interval is chosen (say V = 0.5 to -2.0) over which the difference between the theoretical diffraction loss and the measured diffraction loss at each data point is determined. The mean and the standard deviaton of all the computed differences within the interval then are computed. Next, the overlayed theoretical curve is displaced by an incremental amount along the V axis and the process is repeated. Table 4-1 shows an example of this procedure to determine the best fit between the theoretical knife-edge curve and the measured 28.8 GHz data of path 6.

Note that the standard deviation of the differences between the measured diffraction gains and the theoretical diffraction gains reaches a minimum when the theoretical knife-edge curve's V = 0 axis leads the measured data's V = 0 axis by 0.25 units (overlay the theoretical V = 0 axis 0.25 units to the left of the Figure 4-20's V = 0 axis). Then, when the theoretical curve is raised by 2.4 dB, the best fit occurs. This similarity can be demonstrated visually by overlaying Figure 4-15 on Figure 4-20 by the computed offsets. The computation of the mean and standard deviation of the differences made use of an approximation (Vogler, 1979) to the knife-edge curve, given by:

for V > 0

$$\text{diffraction loss} = 20 \log_{10}\left[\frac{1}{\sqrt{2}}\ P(V)\right] \quad \text{dB} \quad ;$$

for V < 0

$$\text{diffraction loss} =$$

$$-20 \log_{10}\left[\frac{1}{\sqrt{2}}\left[2\ [1 - \sqrt{2}\ P(V)\ \cos D] + P^2(V)\right]^{1/2}\right] \quad \text{dB} \quad ;$$

where

$$P(V) = \left[f^2(V) + g^2(V)\right]^{1/2} \quad ,$$

$$D = \frac{\pi}{2} V^2 + \frac{\pi}{4} - \tan^{-1}\left[\frac{g(V)}{f(V)}\right] \quad ,$$

$$f(V) = (1 - 0.926(V))/(2 - 1.792(V) + 3.104(V)^2) \quad ,$$

$$g(V) = 1/(2 - 4.142(V) + 3.492(V)^2 - 6.670(V)^3) \quad .$$

Finally, Tables 4-2 and 4-3 show what conditions give the best fit between the theoretical knife-edge and the measured data. Note that the "cluttered" paths (paths 3 and 4) showed the highest standard deviation between the measured and theoretical data points. The least cluttered path (path 6) had the lowest standard deviation. Note that for none of the paths does the diffraction loss for the optical grazing point (as determined by the data takers) correspond exactly to the ideal knife-edge loss at grazing. Finally, note that the last column indicates the mean difference between the measured diffraction loss and the theoretical diffraction loss usually was negative (less loss was measured than would be predicted). Dougherty (1979) explains that the lower loss than predicted is quite possible since, for transverse obstructions that are convex rather than linear, the grazing loss will tend to be less than that for the linear (Dougherty 1969, 1970). Dougherty (1979) also notes that the measured diffraction loss is within the bounds that he had estimated (i.e., at grazing for V=0 the diffraction loss is within 6 ± 3.5 dB for all terrain).

4.5 A Theoretical Prediction for the Double Horizon Path

Path 9 was a double horizon path which took a considerable amount of time to line up for the measurements. The difficulty in creating the path tends to indicate that this type of path would not occur very often. However, in military exercises where the intervisibility measurement system would be used, many of the players will be using nearby terrain obstacles for cover; thus double horizon paths may not be as uncommon as first expected.

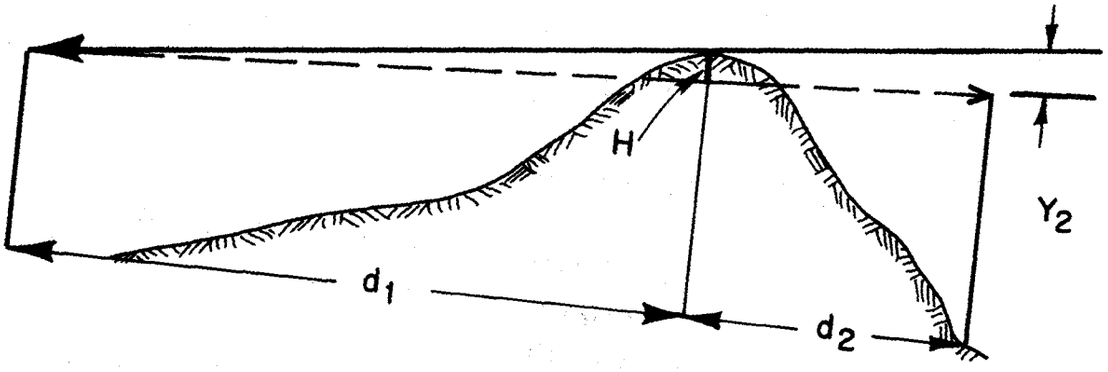

$$V \equiv \sqrt{\frac{2d_1}{\lambda d_2 (d_1 + d_2)}}\, Y_2$$

$$\equiv \sqrt{\frac{2\,(d_1+d_2)}{\lambda\, d_1\, d_2}}\, H$$

Y_2 = Target Cover
H = Obstacle Height

Figure 4-14. Path geometry and definition for V.

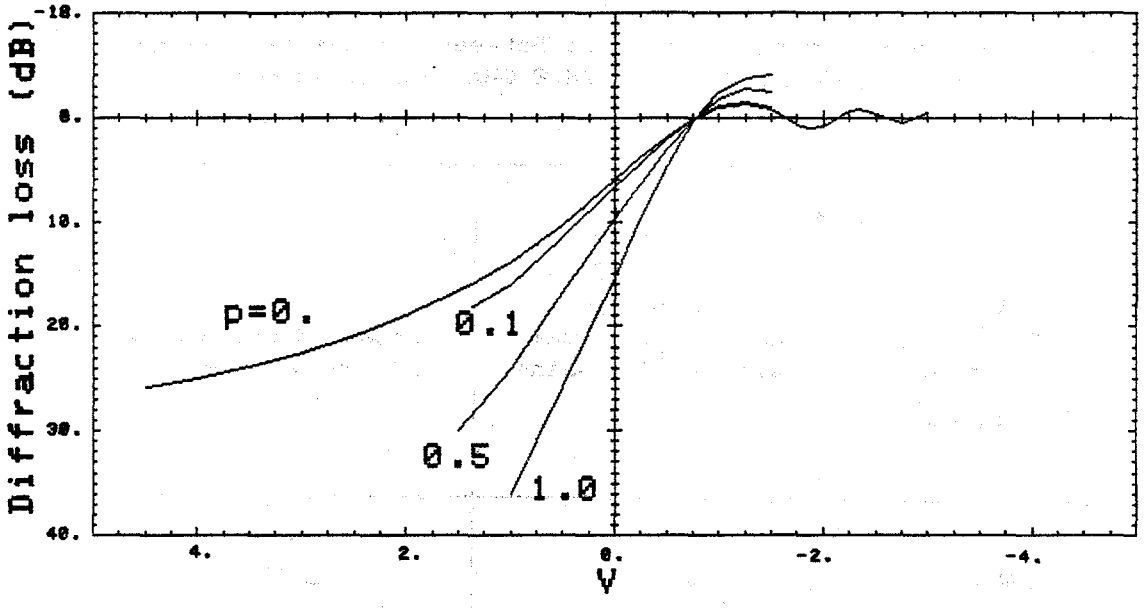

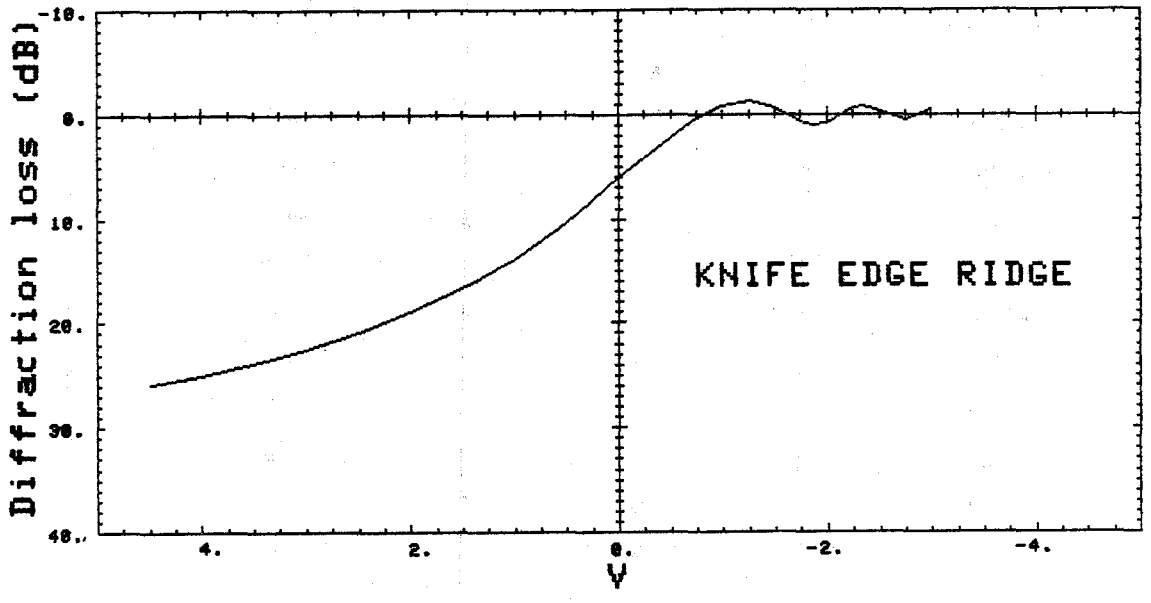

Figure 4-15. Results for an obstacle having a normalized radius of curvature from 0 to 1.0; the lower figure is for an ideal knife-edge ridge alone.

Table 4-1. Determination of Best Fit Between the Theoretical Knife-Edge Curve and the Measured 28.8 GHz Data of Path 6

V Offset ($V_{theoretical} - V_{measured}$)	Mean Difference (Measured Diffraction Gain-Theoretical Diffraction Gain) dB	Standard Deviation of the Difference dB
-.500	5.56	3.57
-.450	5.28	3.40
-.400	5.03	3.21
-.350	4.78	3.01
-.300	4.55	2.80
-.250	4.33	2.57
-.200	4.12	2.34
-.150	3.92	2.10
-.100	3.73	1.86
-.050	3.55	1.62
.000	3.36	1.39
.050	3.18	1.16
.100	2.99	.95
.150	2.80	.77
.200	2.62	.63
.250	2.43	.58
.300	2.25	.63
.350	2.09	.75
.400	1.93	.92
.450	1.80	1.09

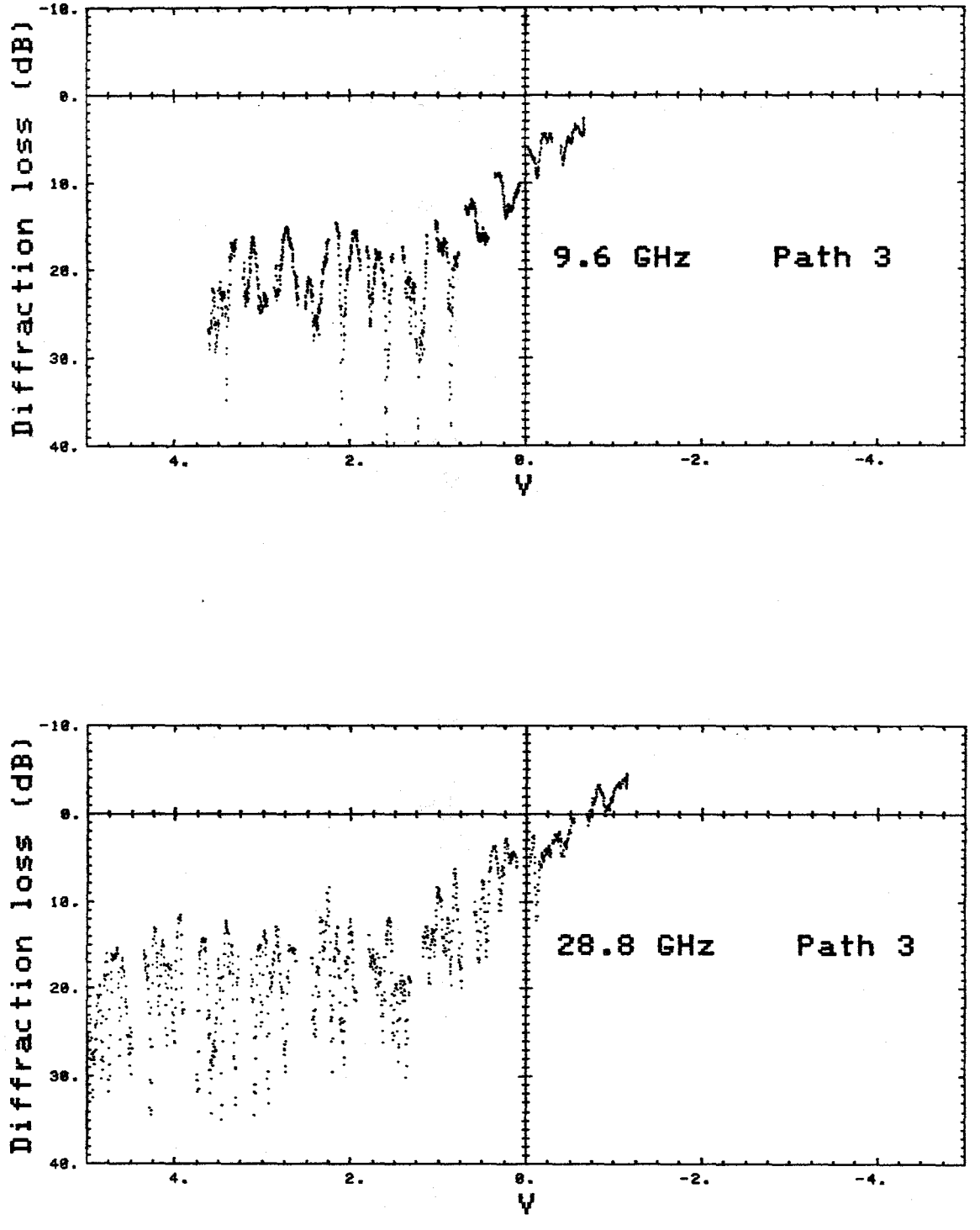

Figure 4-16. Normalized results for path 3.

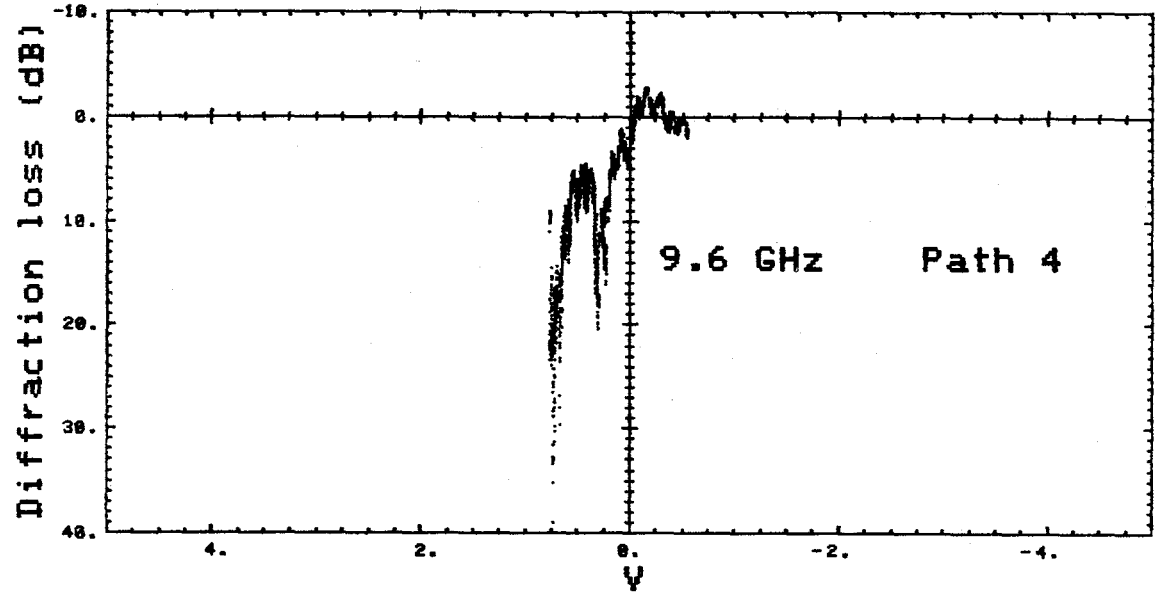

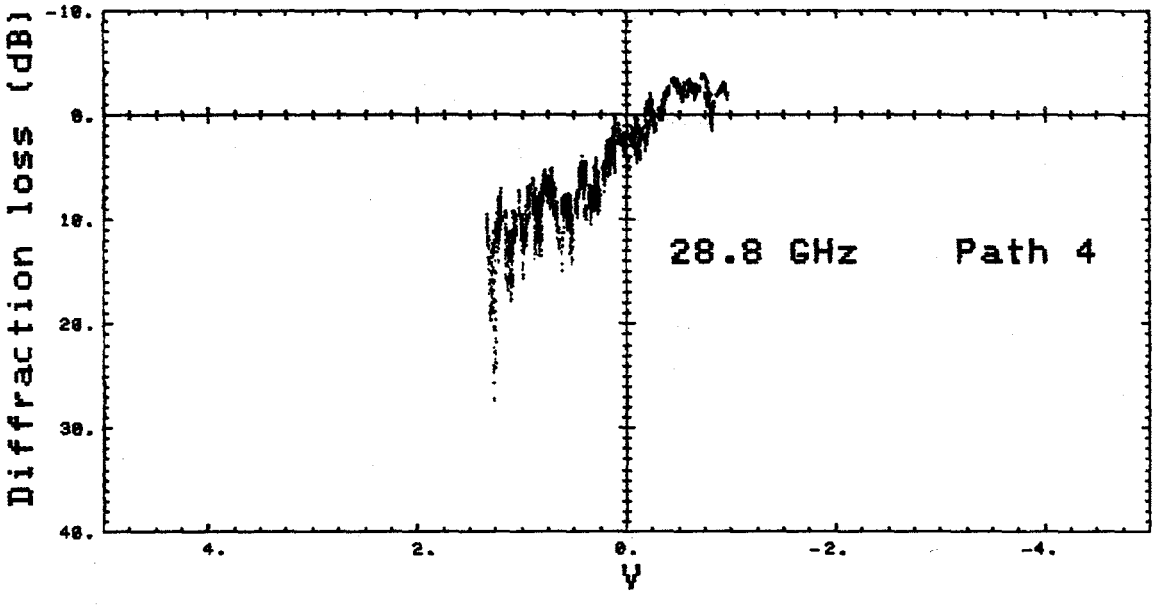

Figure 4-17. Normalized results for path 4.

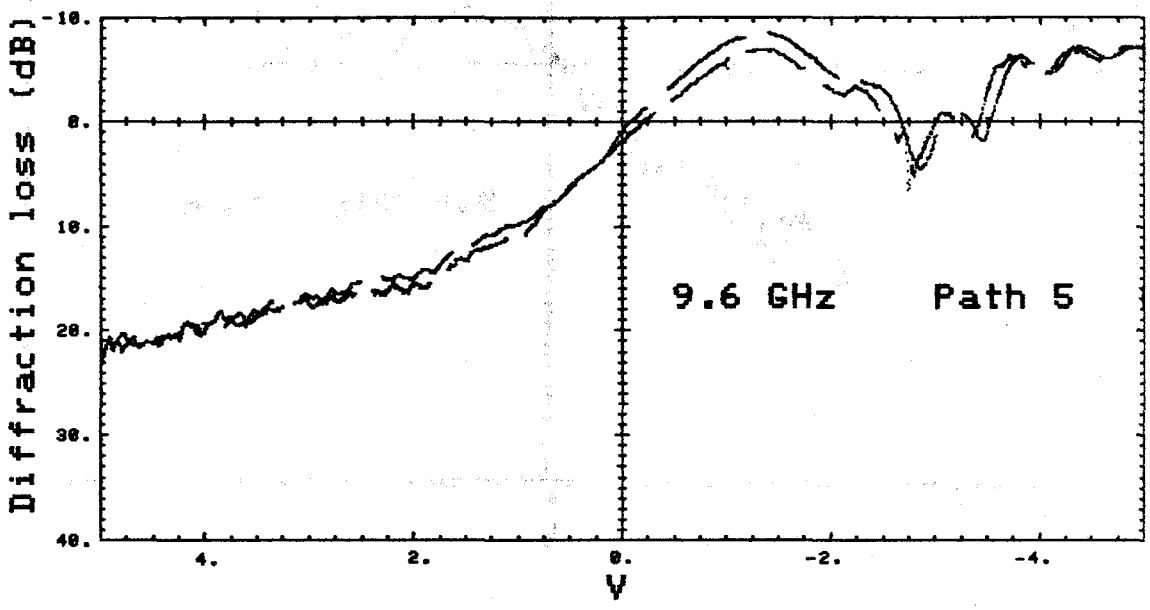

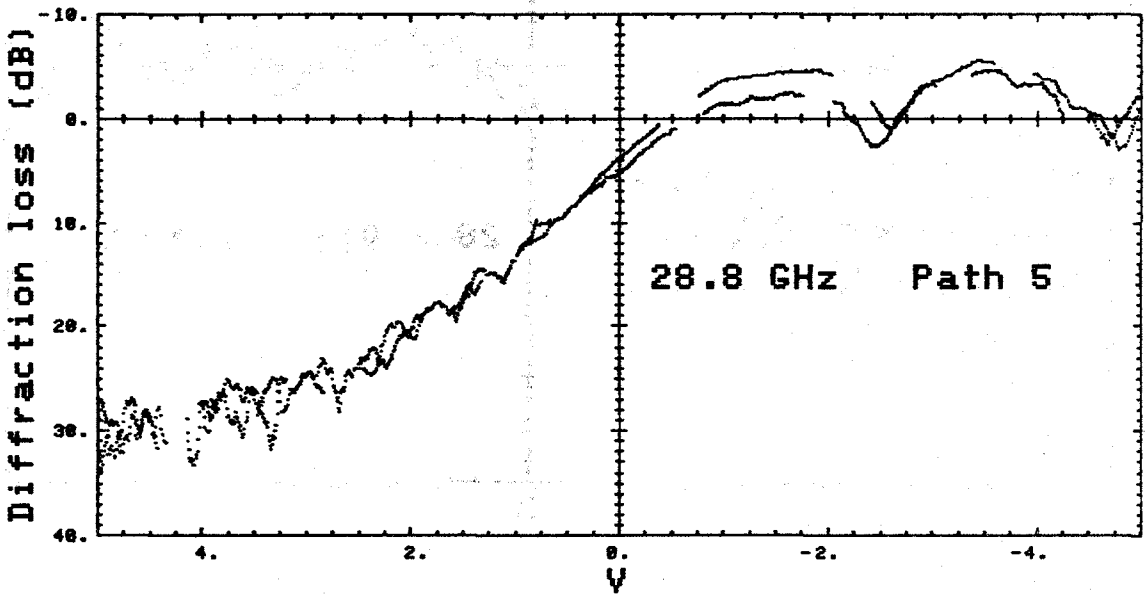

Figure 4-18. Normalized results for path 5, first location.

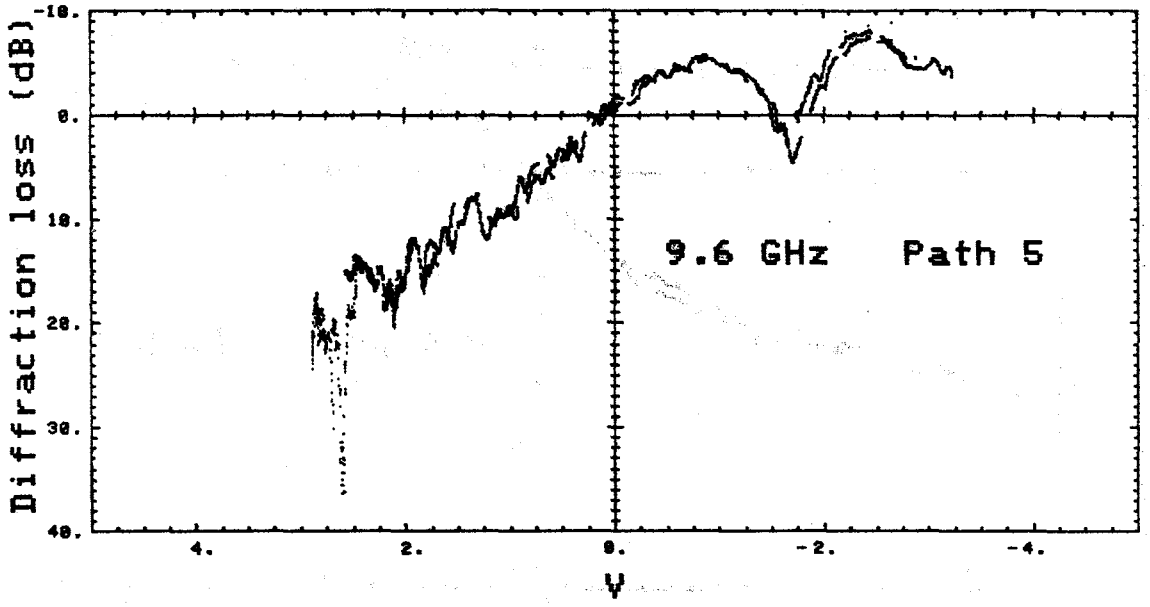

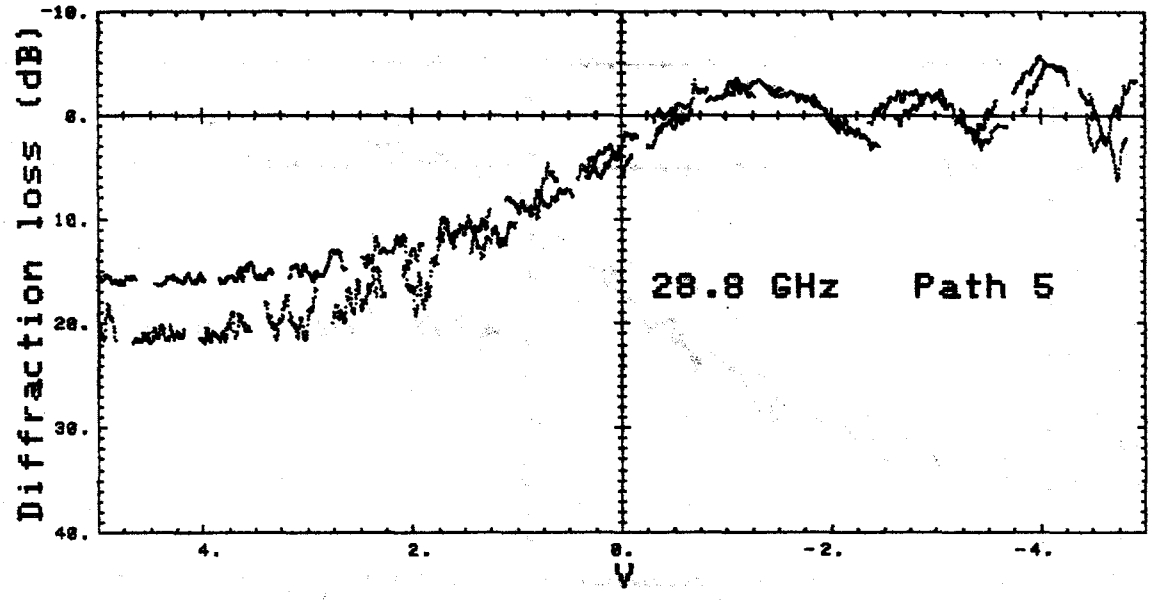

Figure 4-19. Normalized results for path 5, second location.

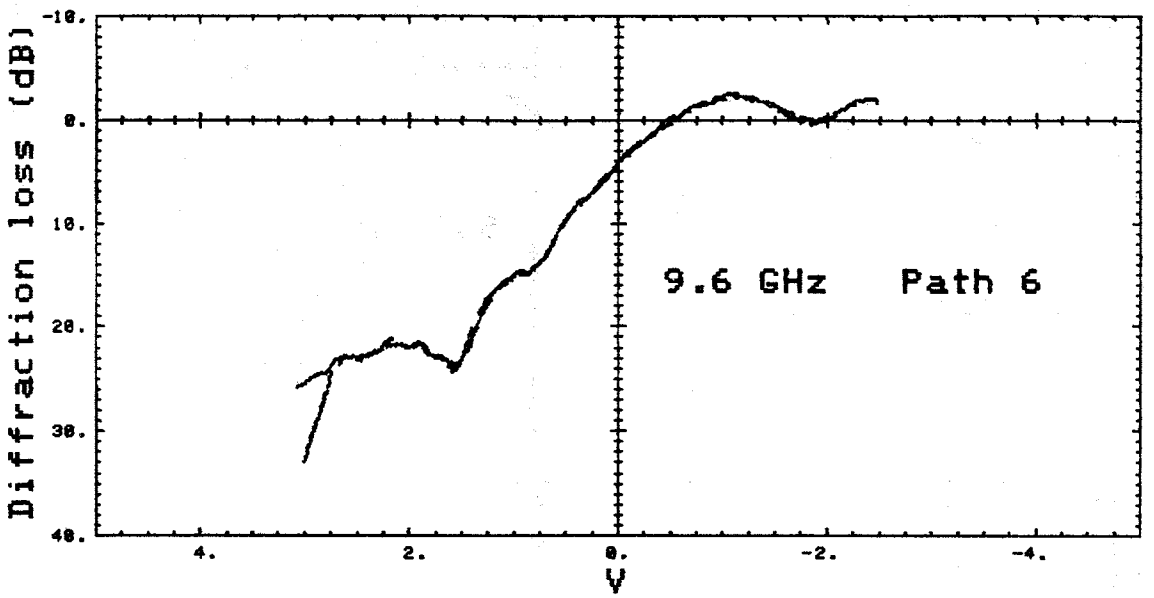

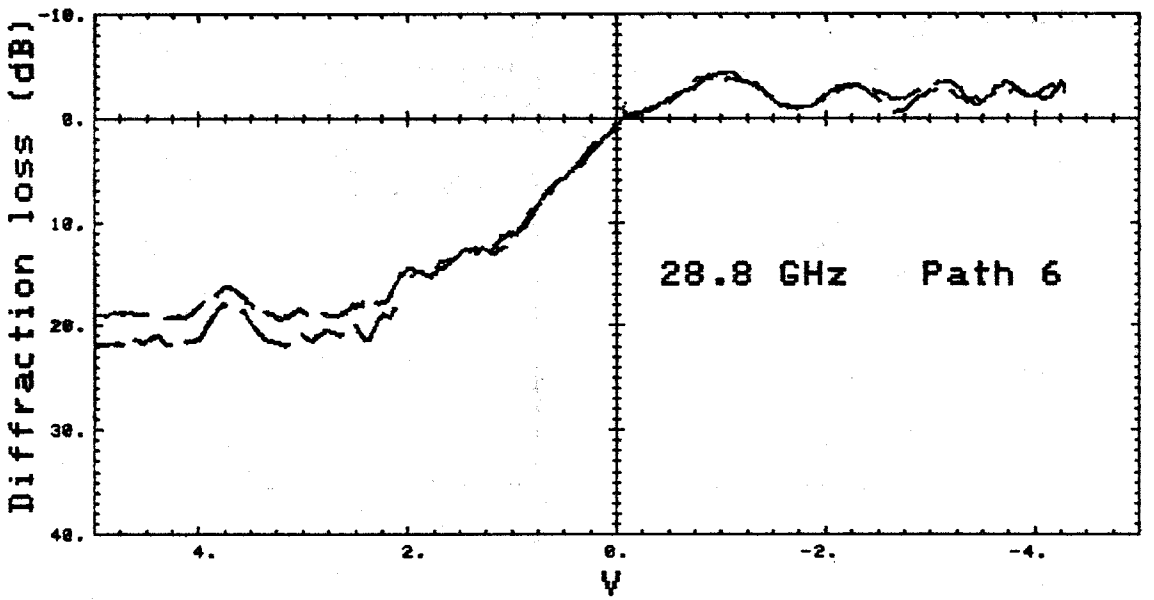

Figure 4-20. Normalized results for path 6.

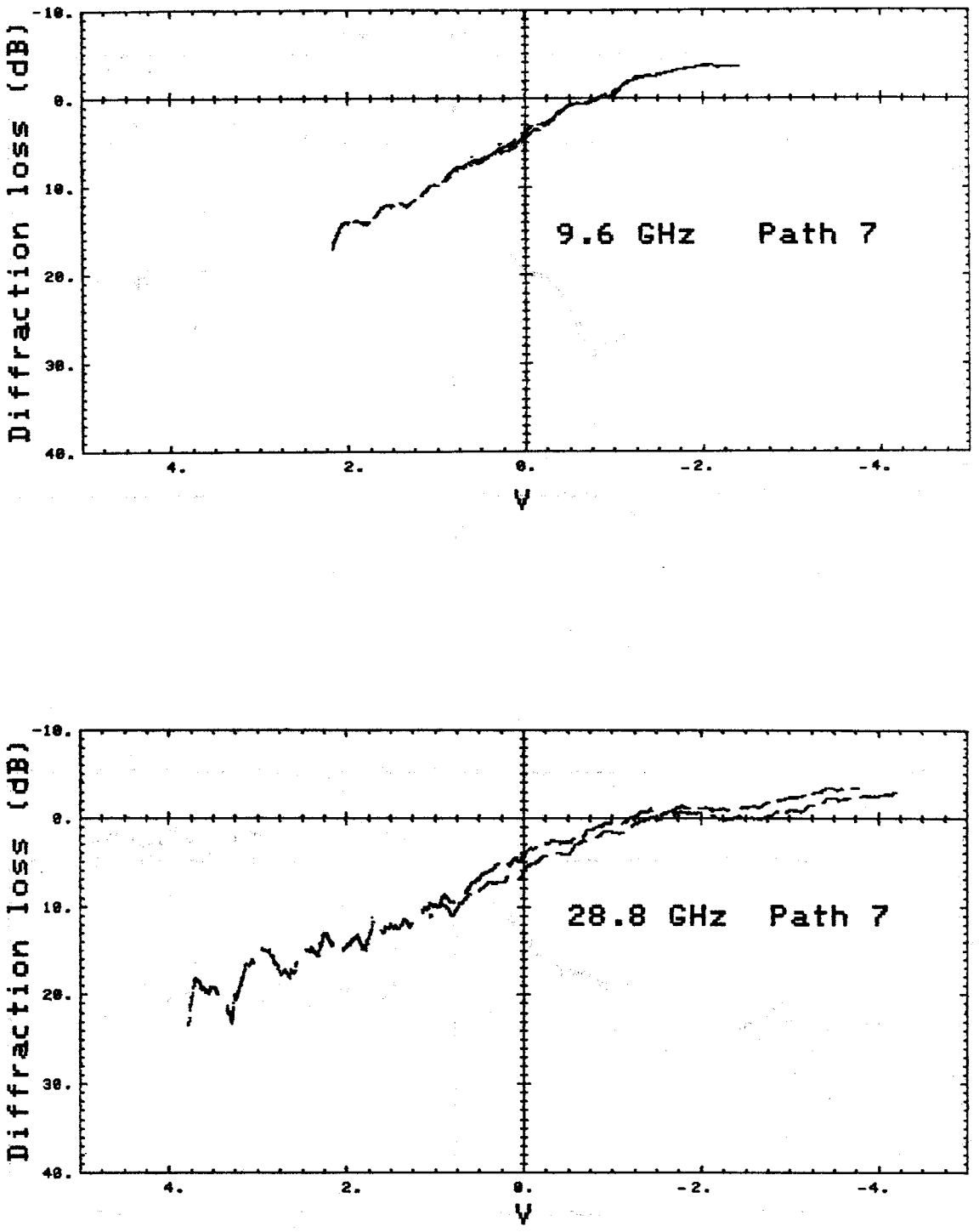

Figure 4-21. Normalized results for path 7.

Ott (1979) has applied a double horizon approximation (Wilkerson, 1966) to the measured path parameters; the comparison of the measured data with the predicted double horizon diffraction loss is shown in Figure 4-20. The agreement between the measured and predicted diffraction gain is surprisingly good. For double horizon paths, the normal setting of the intervisiblity decision threshold will result in a large number of missed intervisibility alarms when the two players are intervisible.

4.6 Results for Paths with Trees, Vehicles, or People

Path 3 had trees alongside the path between the transmitter and receiver, but none of the trees blocked the line-of-sight view between the end points. Path 8 measurements were made through a grove of dead oak trees (so named because they drop their leaves during the fall and winter). At the time of the measurements no new foliage appeared on the branches. The length of path 8 was approximately 1500 meters and, as the receiver was moved transversely to the path, the path between the transmitter and the receiver was continuously changing from a clear one to one blocked by the trees. The difference in signal level between clear and blocked conditions was greater than 20 dB for both 9.6 GHz and 28.8 GHz. Figure 4-24 shows a strip chart recording of the two signals as the receiver was moved about 100 meters. The sharp downward spikes on the strip chart that occur simultaneously on both receivers indicate when the data collection system was not taking data, but was computing the statistics for the previous block of data. As with path 3, conditions existed when the transmitter and receiver were intervisible, but the clutter (trees) along the path provided a received signal level below the level expected for the clear path case. Signal attenuation measurements also were made with people and vehicles on the obstacle's crest. When the vehicles or people were off to the side of the direct signal path, the signal variability was less than 1 dB. However, when the vehicles or people blocked the direct path, the signal was attenuated about 20 dB by vehicles and about 15 dB by people.

5. PERFORMANCE OF A SIMULATED MICROWAVE INTERVISIBILITY MEASUREMENT SYSTEM

The data from the measured paths can be used to determine the performance of a simulated microwave intervisibility system (MIS). As described in Section 2, with no knowledge of the terrain, the intervisibility decision

Table 4-2. Best Fit Between Measured 9.6 GHz Data and Theoretical Knife-Edge Approximation

Path	Figure	Correlation Interval		Minimum Standard Deviation	Offset from Plotted V=0 Axis	Mean Difference Between Measured Data and the Approximation
		V_{max}	V_{min}	(dB)		(dB)
3		+2.0	-1.0	3.68	-0.02	+3.9
4		+1.0	-0.5	4.22	-0.19	-0.1
5		+2.0	-2.5	1.00	+0.15	-5.2
5A		+1.0	-2.0	1.55	-0.34	-3.0
6		+0.5	-2.0	0.31	-0.075	-1.0

Table 4-3. Best Fit Between Measured 28.8 GHz Data and Theoretical Knife-Edge Approximation

Path	Figure	Correlation Interval		Minimum Standard Deviation	Offset from Plotted V=0 Axis	Mean Difference Between Measured Data and the Approximation
		V_{max}	V_{min}	(dB)		(dB)
3		+2.0	-1.0	3.30	-0.12	+1.0
4		+1.0	-0.5	1.76	-0.01	-3.0
5		+2.0	-2.5	1.36	+0.10	-1.6
5A		+1.0	-2.0	1.01	-0.12	-1.9
6		+0.5	-2.0	0.52	-0.24	-2.5

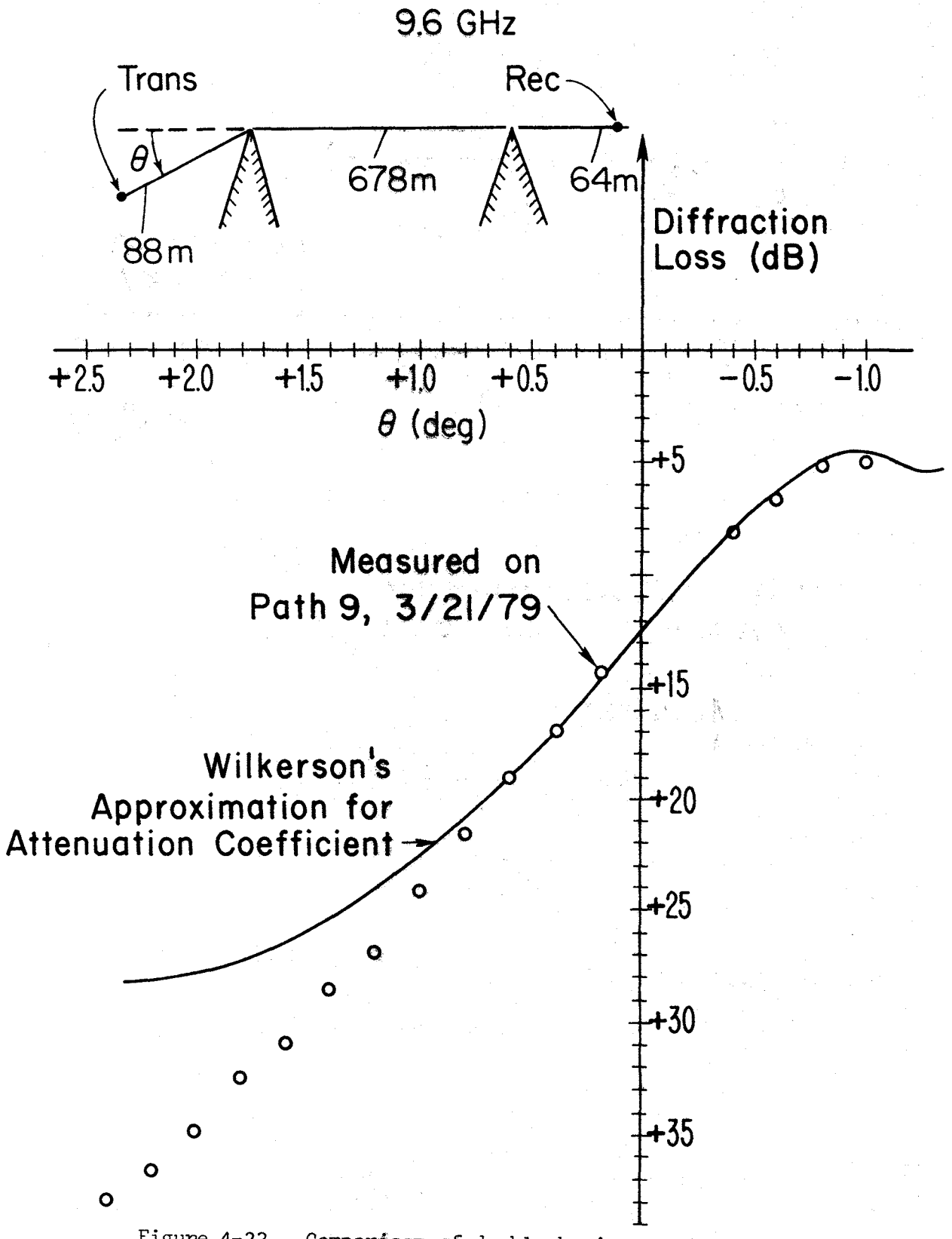

Figure 4-22. Comparison of double horizon path data with Wilkerson's approximation at 9.6 GHz.

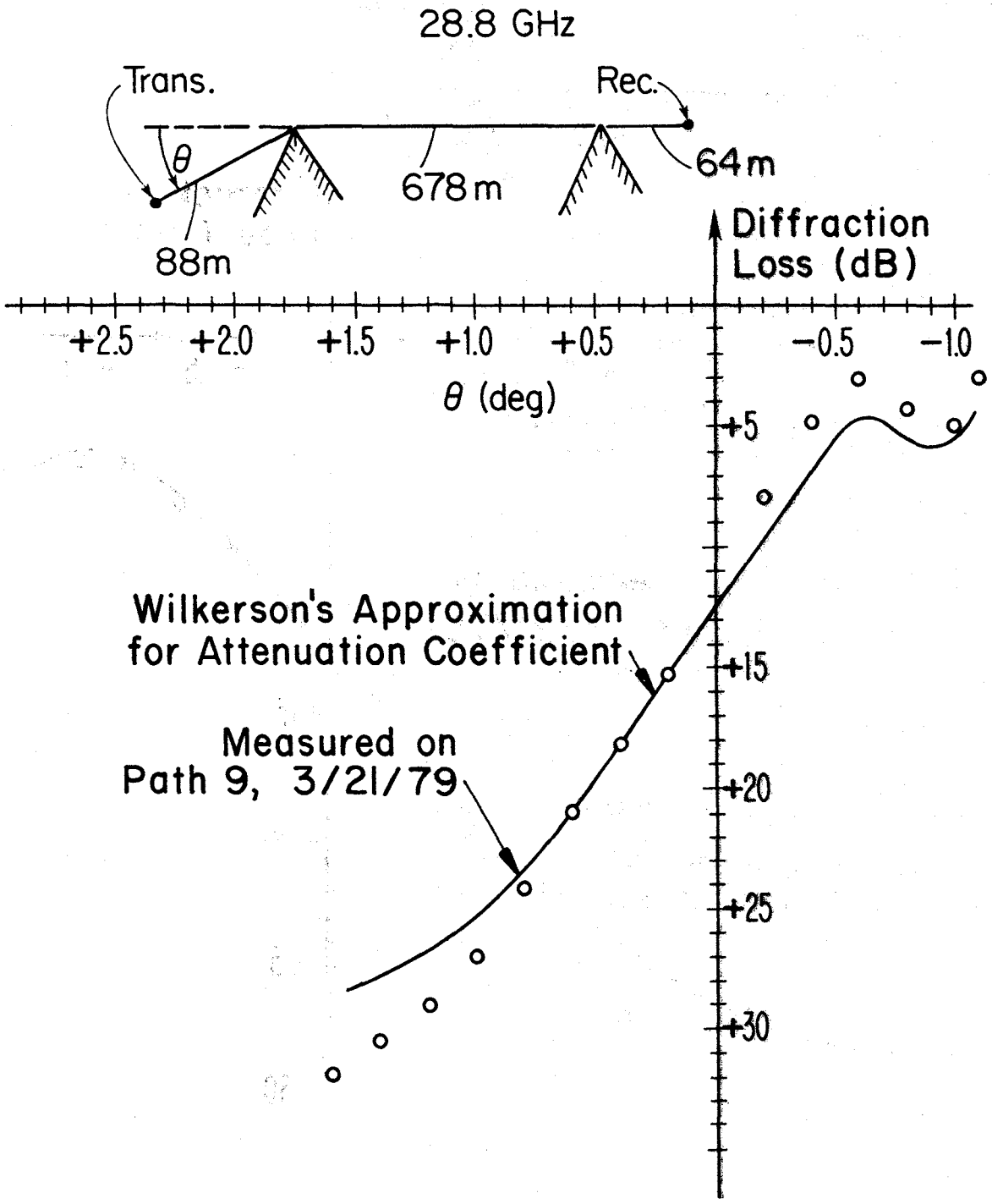

Figure 4-23. Comparison of double horizon path data with Wilkerson's approximation at 28.8 GHz.

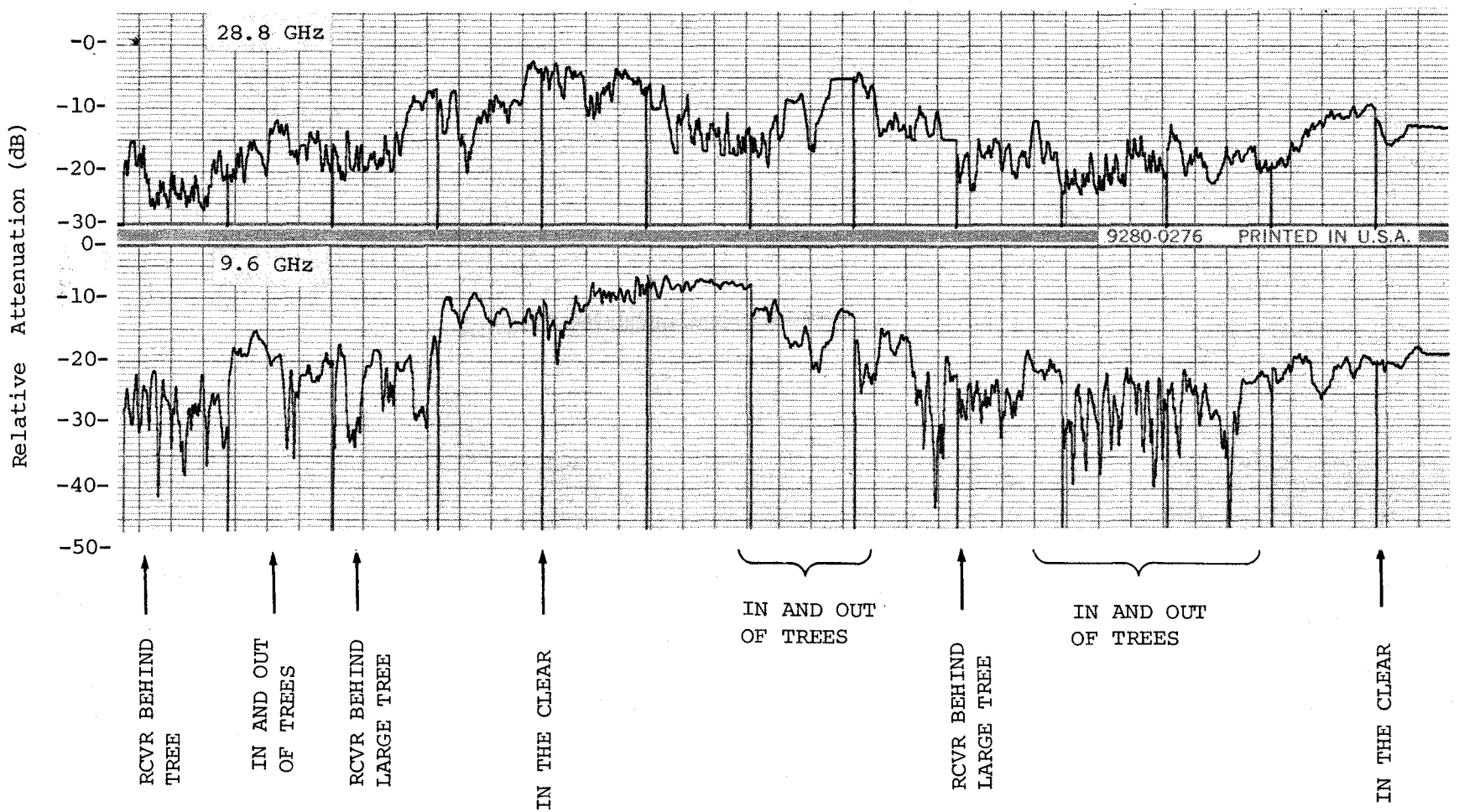

Figure 4-24. Signal variability as receiver is moved about 100 meters horizontally and transversely to the path.

threshold might be set at 6.02 dB below the free space signal level for any path between the transmitter and receiver. The measured data indicates that the threshold should be less than 6.02 dB; therefore, the decision threshold will be based on the measured data. Table 5-1 lists the computed mean diffraction loss at grazing and its standard deviation. The values listed under Radio Grazing in Table 5-1 are computed from the data given in Tables 4-2 and 4-3. A similar computation is made to obtain the optical grazing values. The means listed on the lower half of Table 5-1 were computed from single measured values of diffraction loss at grazing for the paths. The table shows that different methods can be used to arrive at the needed decision thresholds.

The computed "optimum" thresholds to be used by the simulated microwave intervisibility system in the Ft. Hunter Liggett terrain will be the mean diffraction loss values of 4.4 dB at 9.6 GHz and 4.0 dB at 28.8 GHz. The data, such as given in Figure 4-3 for path 6, are operated on by the simulated MIS to determine its performance. As discussed in Section 4-2, the measured diffraction loss is determined from:

$$(L_{DIFFRACTION})_{MEASURED} = P_T + G_T + G_R - L_{FREE\ SPACE} - P_R.$$

False alarms will occur whenever the two antennas are above optical grazing and

$$L_{DIFFRACTION} > 4.4 \text{ dB at } 9.6 \text{ GHz}$$

or

$$L_{DIFFRACTION} > 4.0 \text{ dB at } 28.8 \text{ GHz}.$$

Missed alarms will be counted whenever the two antennas are below optical grazing and

$$L_{DIFFRACTION} < 4.4 \text{ dB at } 9.6 \text{GHz}$$

or

$$L_{DIFFRACTION} < 4.0 \text{ dB at } 28.8 \text{ GHz}.$$

Appendix C contains tables for each path listing the total number of data points in each 0.25 meter height bin along with the number and percentage of false alarms or missed alarms for each bin. Appendix C also contains tables illustrating what happens if a threshold other than an optimum one is used.

Table 5-1. Mean Diffraction Loss and its Standard Deviation for the Measured Paths

	9.6 GHz	28.8 GHz
Optical Grazing (mean and s.d. computed on differences between measured data and knife-edge approximation over selected intervals for paths 3, 4, 5, 5A, and 6)		
mean diffraction loss at grazing	4.4 dB	4.0 dB
standard deviation	3.9 dB	2.7 dB
Radio Grazing (least squares fit between measured data and knife-edge approximation over selected intervals for paths 3, 4, 5, 5A, and 6)		
mean diffraction loss at grazing	4.9 dB	4.4 dB
standard deviation	3.6 dB	2.3 dB
Optical Grazing (computed mean and s.d. based on single value at grazing from paths 1, 2, 3, 4, 5, 5A, 6, 7, and 9)		
without path 9		
mean diffraction loss at grazing	2.6 dB	3.5 dB
standard deviation	3.6 dB	4.3 dB
with path 9		
mean diffraction loss at grazing	3.9 dB	4.3 dB
standard deviation	6.2 dB	5.6 dB

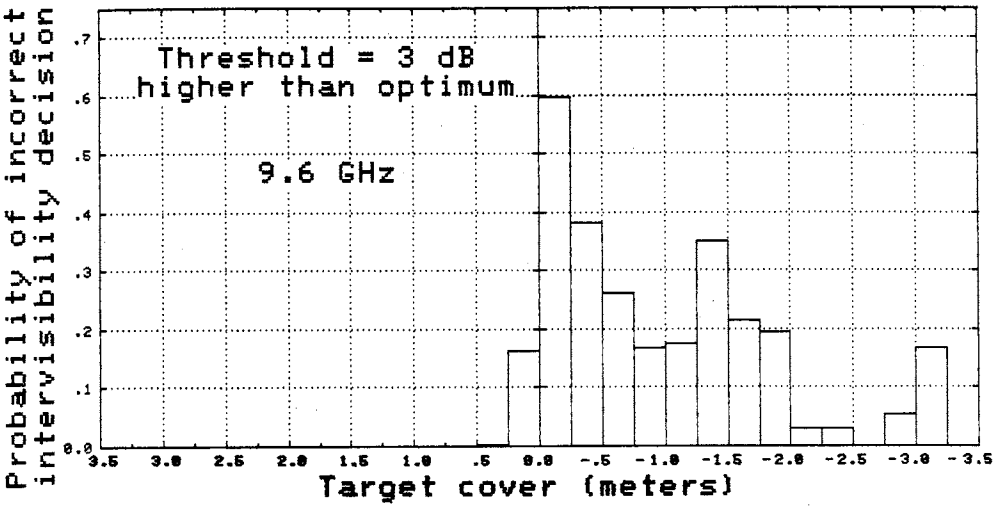

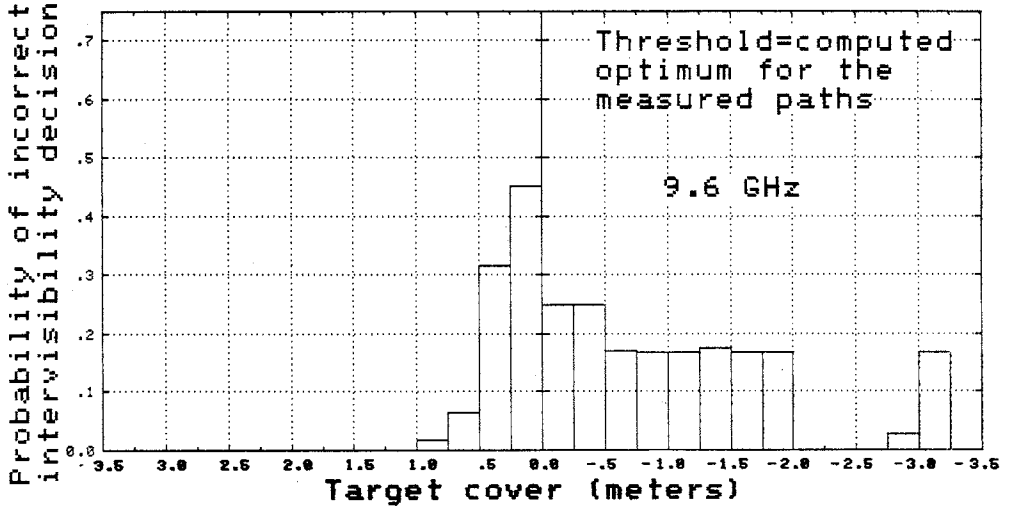

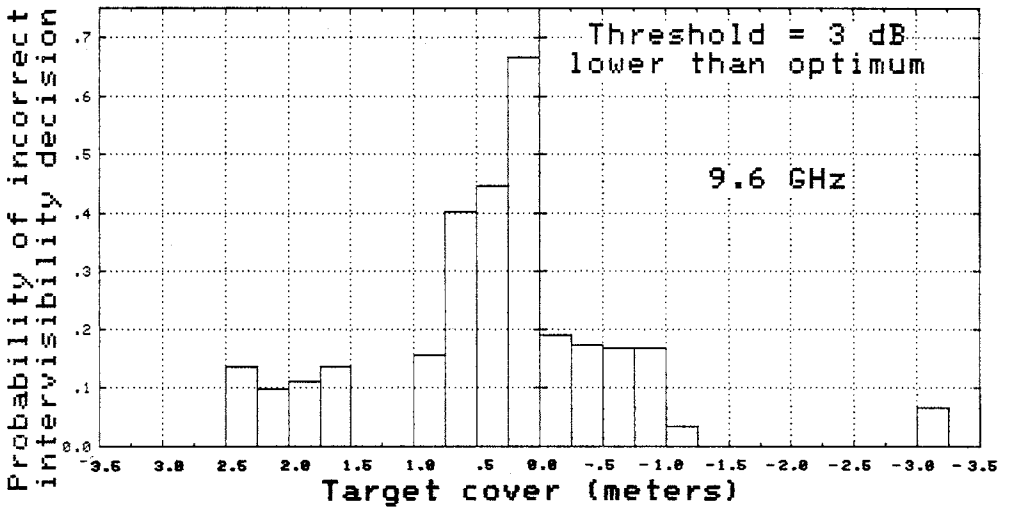

Figure 5-1. Probability of an error by the simulated MIS different thresholds at 9.6 GHz.

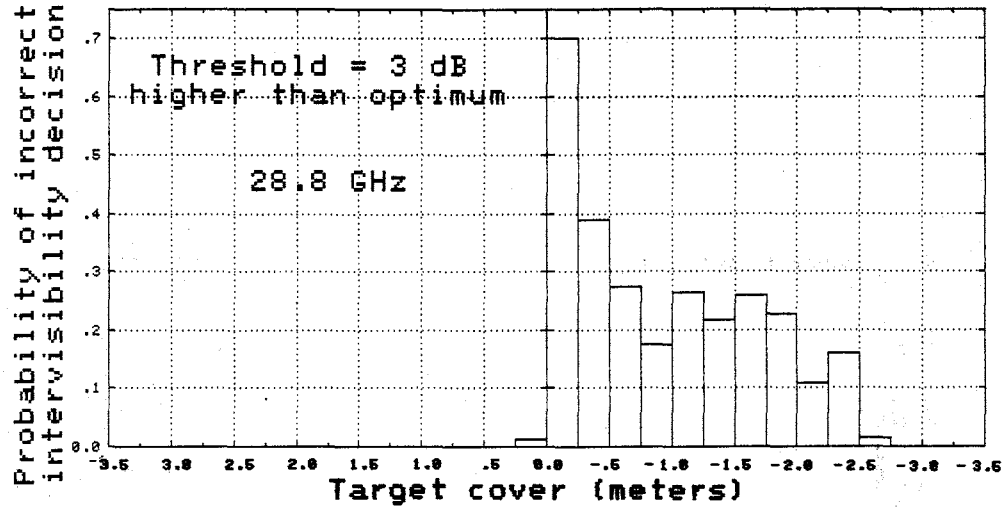

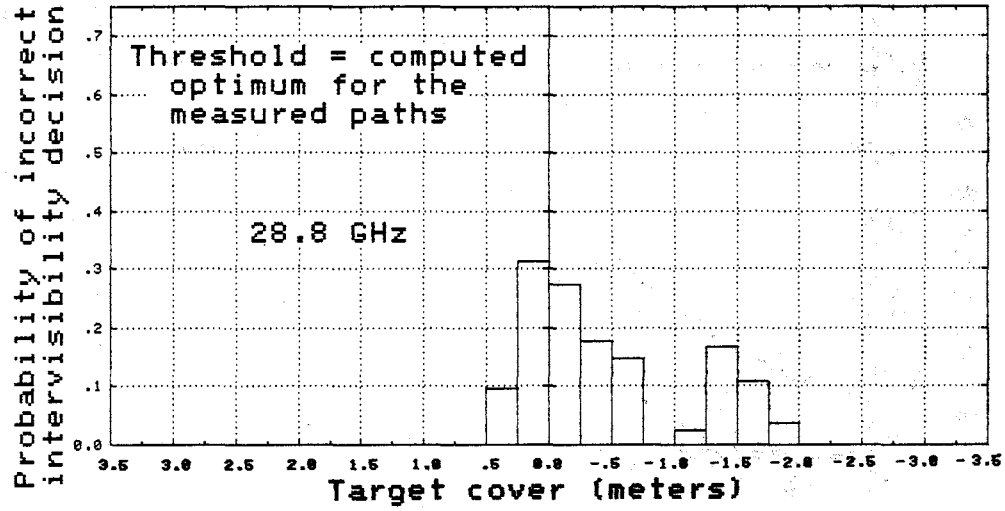

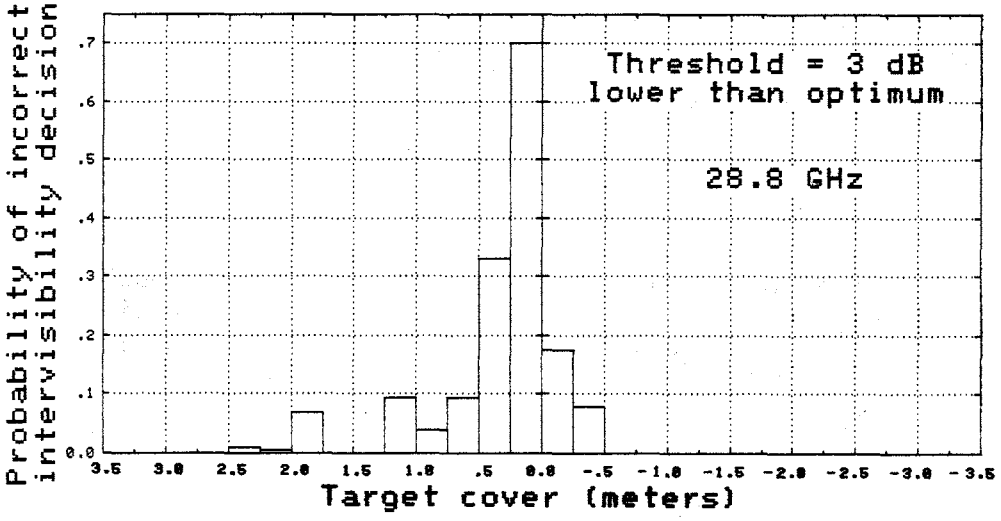

Figure 5-2. Probability of an error by the simulated MIS for three different thresholds at 28.8 GHz.

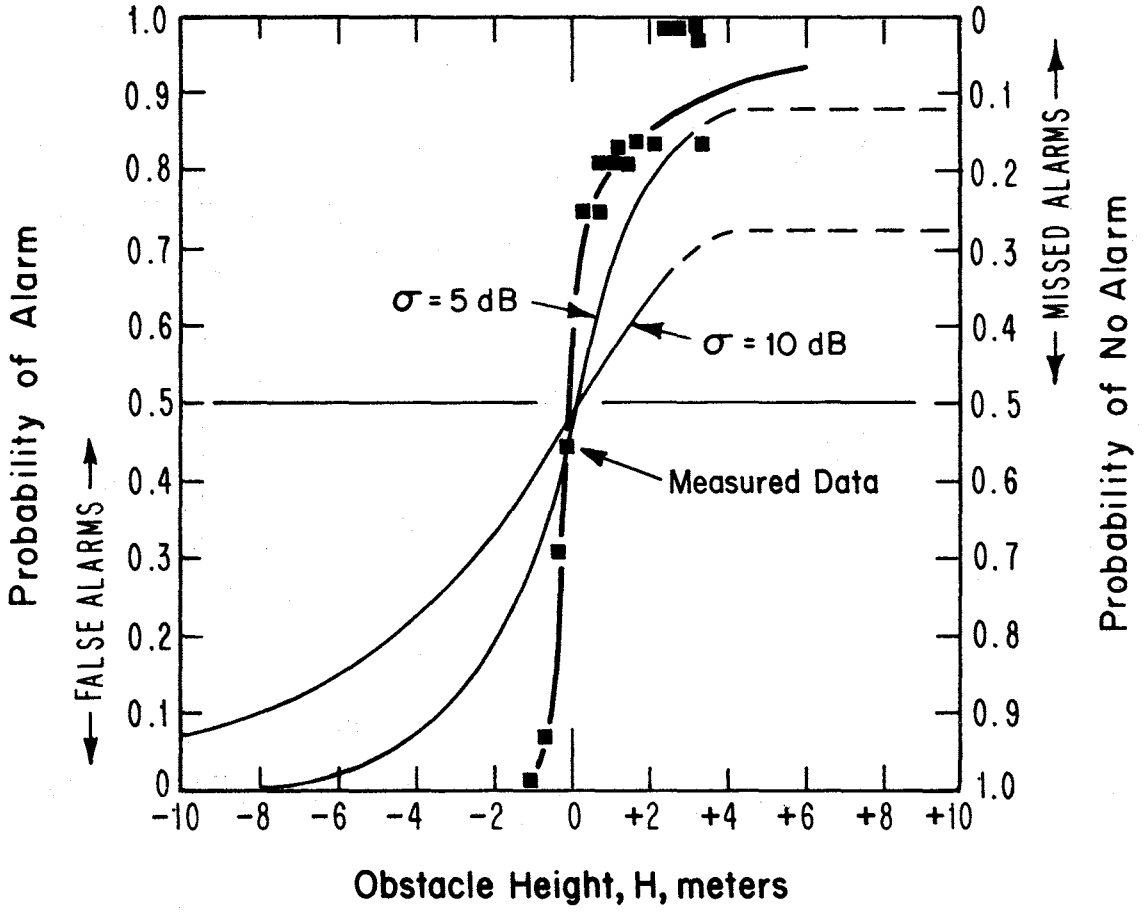

Figure 5-3. Comparison of measured alarm probability (9.6 GHz, decision threshold at optimum) with two theoretical alarm probabilities.

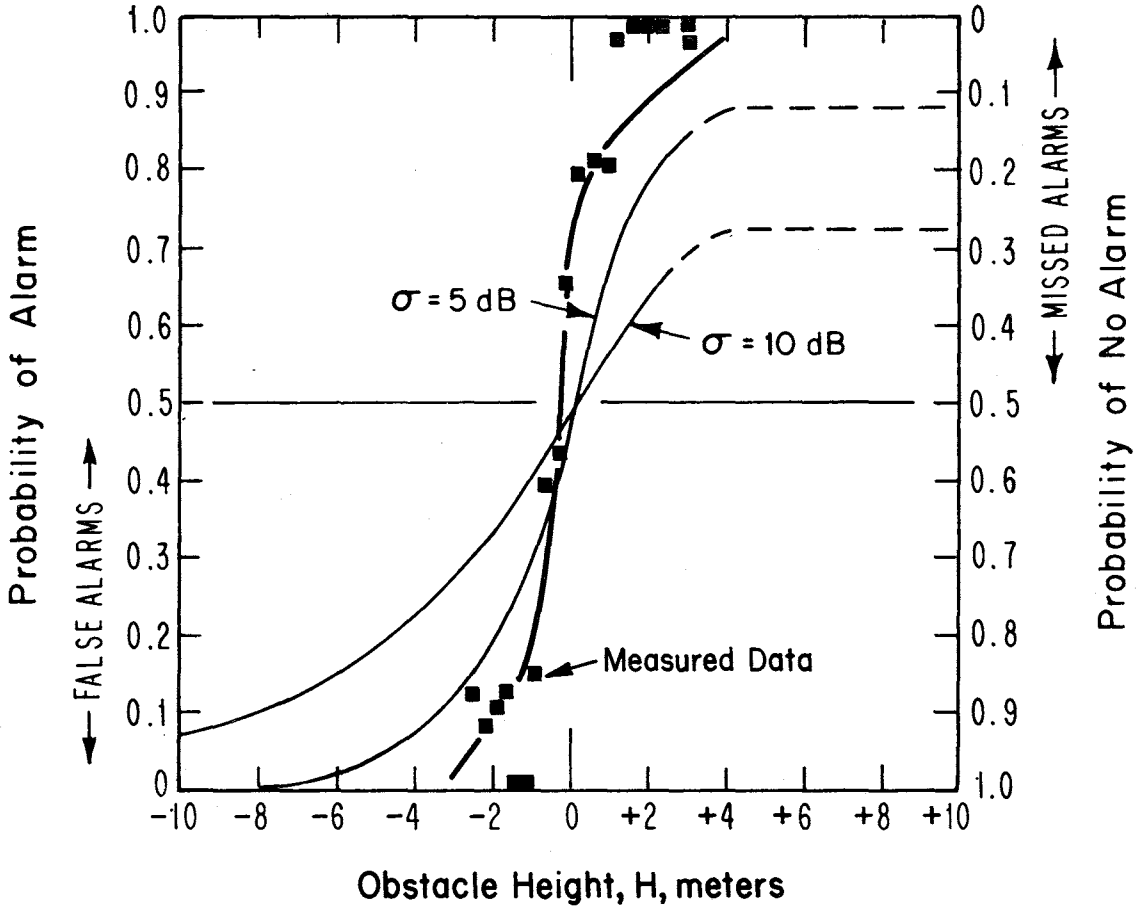

Figure 5-4. Comparison of measured alarm probability (9.6 GHz, decision threshold at 3 dB below optimum) with two theoretical alarm probabilities.

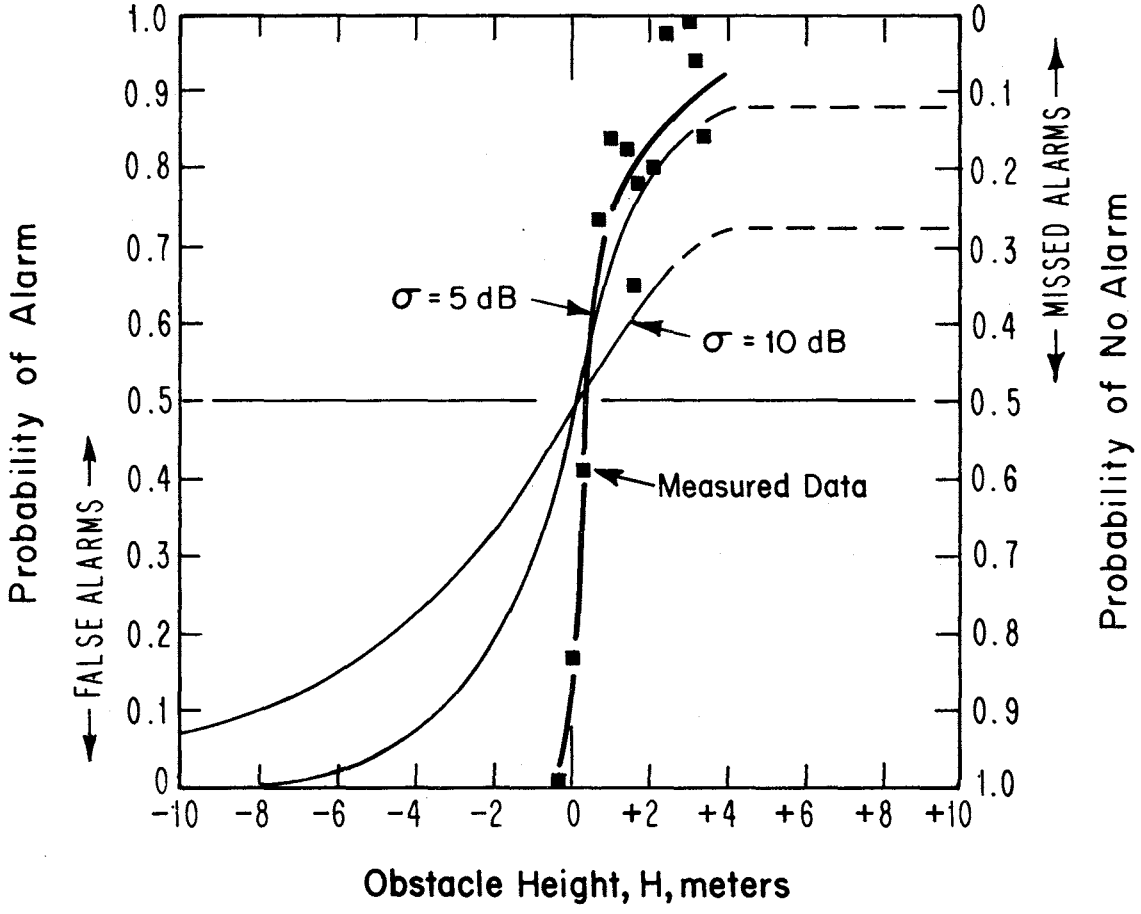

Figure 5-5. Comparison of measured alarm probability (9.6 GHz, decision threshold at 3 dB above optimum) with two theoretical alarm probabilities.

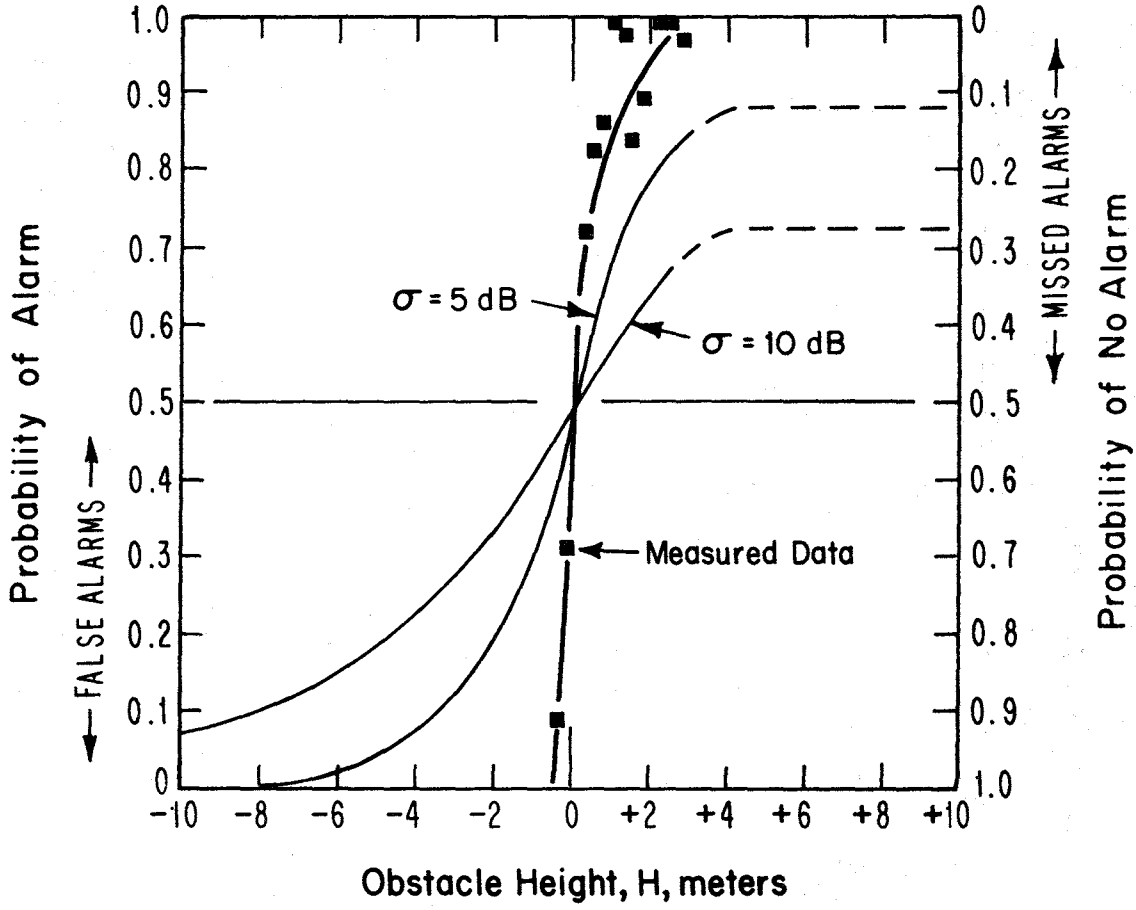

Figure 5-6. Comparison of measured alarm probability (28.8 GHz, decision threshold at optimum) with two theoretical alarm probabilities.

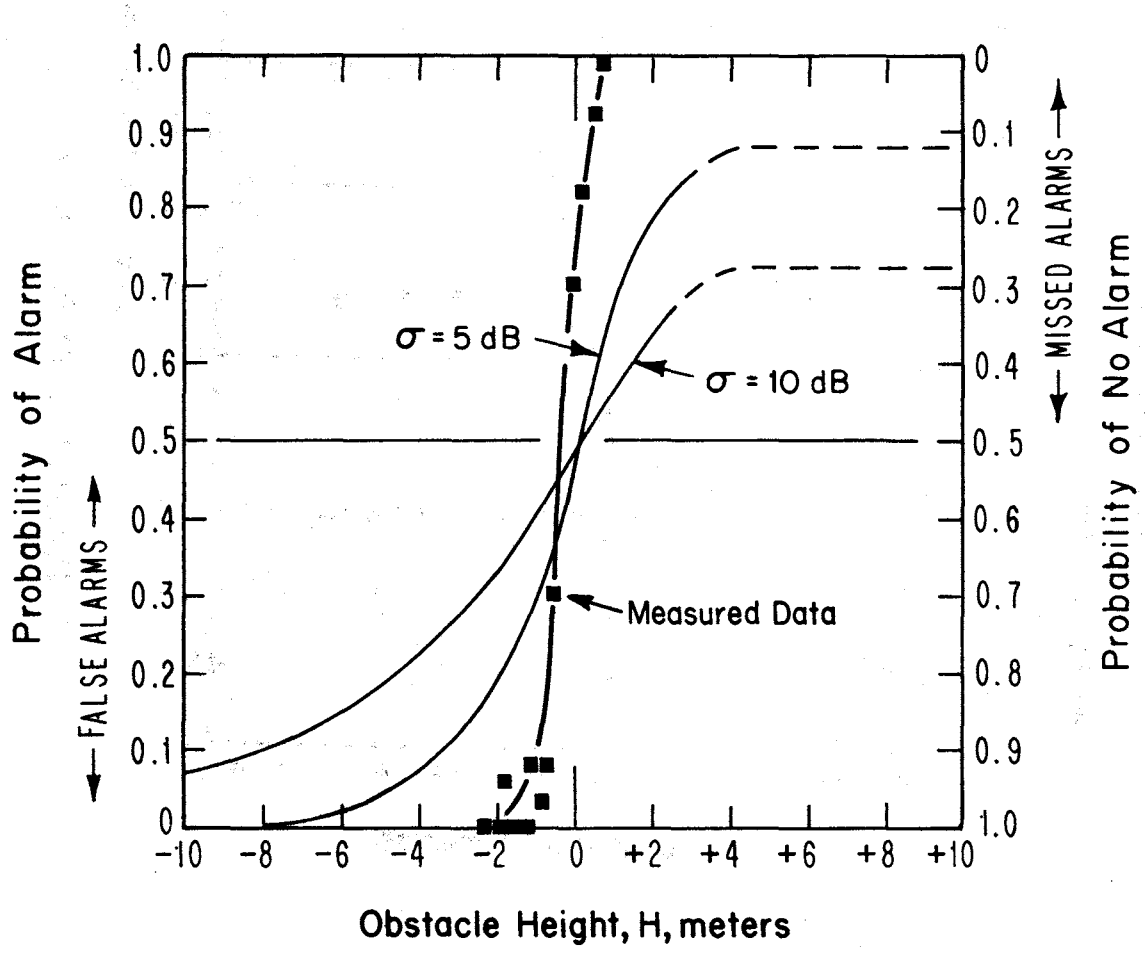

Figure 5-7. Comparison of measured alarm probability (28.8 GHz, decision threshold at 3 dB below optimum) with two theoretical alarm probabilities.

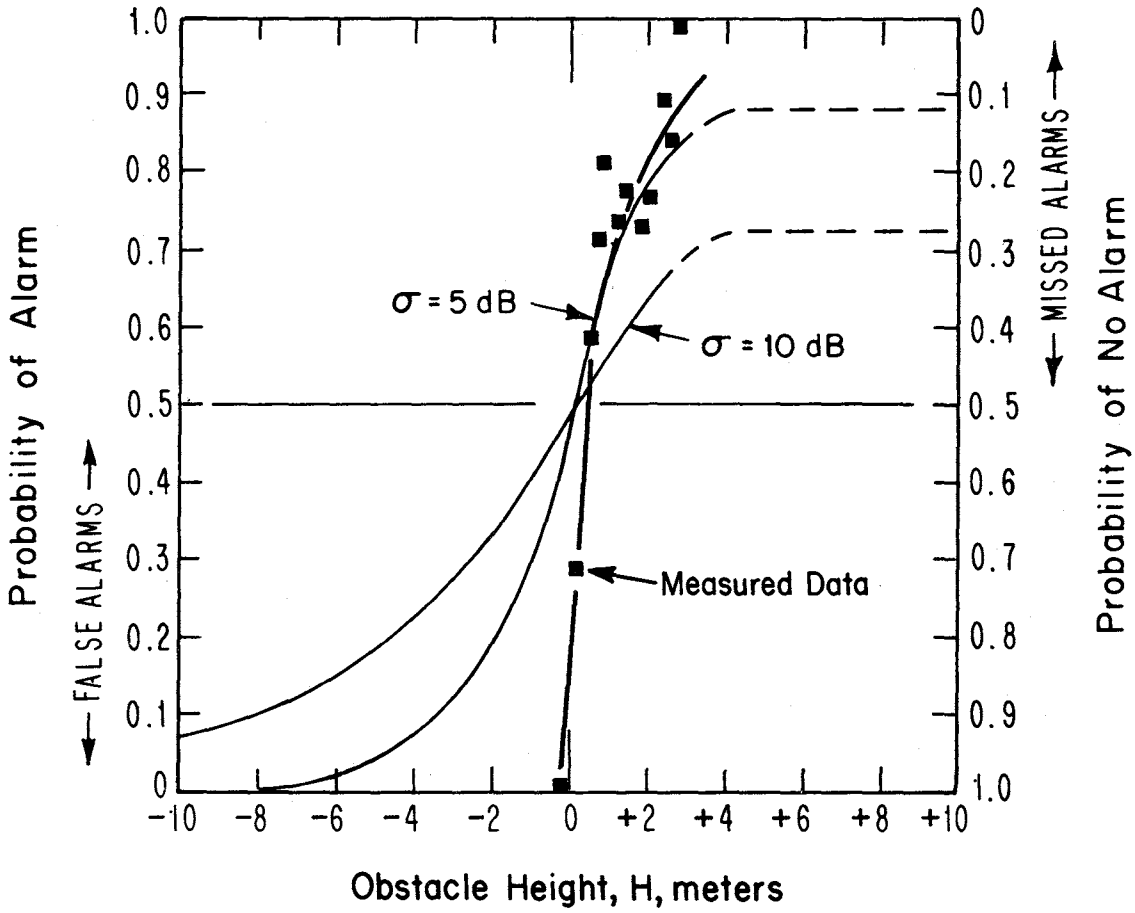

Figure 5-8. Comparison of measured alarm probability (28.8 GHz, decision threshold at 3 dB above optimum) with two theoretical alarm probabilities.

Figures 5-1 and 5-2 give the histograms of probability of an error based on the results listed in Appendix C. As an additional check of the simulated MIS's performance, Figure 2-2 can be presented now with data from Appendix C and Figures 5-1 and 5-2; this is given in Figures 5-3 through 5-8. For the optimum thresholds, the system σ is about 4 dB.

6. SUMMARY OF PROPAGATION EFFECTS ON AN INTERVISIBILITY MEASUREMENT SYSTEM OPERATING IN THE SHF BAND

The purpose of this study was to determine what limiting effects propagation may have on the performance of a microwave radio system that would be used to determine when two vehicles are optically visible to one another in irregular, obstructed terrain. When the antennas for the microwave intervisibility system as placed on the vehicles are within optical line-of-sight, we would like an alarm to be registered indicating that the two antennas are optically intervisible; similarly as soon as the antennas are optically hidden due to obstructions between the antennas, we would like the alarm to cease. Unfortunately, the microwave radio system is less perfect in judging intervisibility than an optical system so we will sometimes have no alarms (missed alarms) even when the antennas are optically intervisible and we will sometimes have alarms (false alarms) even when the antennas are optically hidden due to obstructions. The percentage of invalid alarms (false and missed alarms) relative to desired outcomes will be greatest when the two antennas are at their reference elevations, defined as the elevations such that an optical ray from one antenna to the other just grazes the intervening obstacle. As the antennas are moved above or below their reference elevations, the percentage of invalid alarms will tend to decrease (and usually quite rapidly). This report has shown that we can determine an "optimum threshold," computed from measured data, that can be used with a microwave intervisibility system to determine when its antennas are optically intervisible. Using the measured data as an input to a simulated microwave intervisibility system, Table 6-1 shows the percentage of invalid alarms whenever the antennas were at least one meter above or below their reference elevations. Note that as we raised the threshold by 3 dB, the percentage of missed alarms increased and when we lowered the threshold by 3 dB, the percentage of false alarms increased; both are expected results.

This report also has shown that signal variability has an effect, due to propagation, on the performance of a microwave intervisibility system. In Section 2, we listed the sources of the variability and estimated their magnitude. In Table 6-2, we compare the estimated magnitude with the observed values from the measurements. The interesting feature of the comparison is that the observed path-to-path variability was much less than predicted. Of course a lower standard deviation results in better performance by a microwave intervisibility system.

In summary, we have shown that a microwave intervisibility system is less perfect than a purely optical one, due to the variability of the received microwave radio signal. However, we have shown that we can predict the performance of the microwave intervisibility system based upon the magnitude of the signal's variability. We also have shown that through propagation measurements we can estimate an "optimum" microwave signal threshold and estimate the signal variability. Based on these results, a microwave intervisibility system should have a performance similar to that given in Table 6-1, the performance a computer-simulated microwave intervisibility system. Finally, we noted little difference in performance between the 9.6 GHz system and the 28.8 GHz system. The antenna system needs further investigation; we no not know how the performance would be affected if omni-directional antennas were used instead of the horns. Perhaps, circular polarization may improve the performance to that of the tested linear polarization.

Table 6-1. Performance of a Simulated Microwave Intervisiblity System

Threshold	Percent of Invalid Alarms Relative To Desired Outcomes	
	False Alarms (when the antenna positions were at least 1 meter below their reference elevations)	Missed Alarms (when the antenna positions were at least 1 meter above their reference elevations)
"optimum"	5%	20%
"optimum" + 3dB	5%	45%
"optimum" - 3dB	20%	10%

Table 6-2. Sources of Signal Variability

Source	Estimated Standard Deviation (dB)	Observed Standard Deviation (dB)
Time Variability	<1	<1 (over 20 minute periods)
Local Variability	<5.6	<7
Path-to-Path Variability	10 to 25	4 to 5
Region-to-Region Variability	3 to 5	N/A
Equipment Variability	2 to 3	N/A

7. REFERENCES

Dougherty, H.T. [1969], Radio wave propagation for irregular boundaries, Radio Science Vol. 4, No. 11, November, pp. 997-1004.

Dougherty, H.T. [1970], Diffraction by irregular aperatures, Radio Science, Vol 5, No. 1, January, pp. 55-60.

Dougherty, H.T. [1979], private correspondence.

Longley, A.G. [1976], Location variability of transmission loss--land mobile broadcast systems, OT Report 76-87 (NTIS Access. No. PB254472).

Longley, A.G., R.K. Reasoner, and V.L. Fuller [1971], Measured and predicted long-term distributions of tropospheric transmission loss, OT/TRER 16 (NTIS Access. No. COM 75-11205).

Ott, R.H. [1979], private correspondence.

Rice, P.L., A.G. Longley, K.A. Norton, and A.P. Barsis [1967], Transmission loss predictions for tropospheric communication circuits, Vol. 1, Technical Note 101 (NTIS Access. No. AD687820).

Vogler, L.E. [1979], private correspondence.

Wilkerson [1966], Approximation to the double knife-edge attenuation coefficient, Radio Science, Vol. 1 (new series, No. 12) December, pp. 1439-1443.

APPENDIX A

THE PROPAGATION MEASUREMENT SYSTEM AND CALIBRATION PROCEDURE

A.1 INTRODUCTION

A measurement system to provide reliable data relative to signal characteristics between two terminals which are at or near optical line of sight was designed and instrumented for this project. Previous system concepts and tests conducted for CDEC, in part, dictate the choice of frequencies. In general, the band of frequencies of interest for this application lies between 8 and 40 GHz because of small component size without using expensive state-of-the-art hardware. In addition, the availability of assignments is a major consideration. Because the wave lengths differ substantially over this range of frequencies, the propagation effects also may differ. For this reason a two frequency probing system was provided. Portable transmit and receive terminals were developed to adequately test the application in the actual battlefield environment. The receive terminal also includes the data recording, processing, and logging equipment. In order to obtain signal characteristics when the two terminals are separated by an obstacle, the transmitter source can be positioned several meters below to several meters above the optical grazing line at the obstacle.

A.2 TRANSMITTER AND RECEIVER

Two van type 4-wheel drive vehicles were obtained to contain each terminal (see Figure 3-4, etc.). A telescoping tower, attached to the transmitter van, provided a range of height positions from about 5 meters to 12 meters above the ground. The complete transmitting terminal was designed to be set atop the tower. Test frequencies of 9.6 and 28.8 GHz were selected partly because some components were available for these frequencies, but primarily because this set is representative of both ends of the usable range. The source for the 9.6 GHz was a phased-locked cavity-tuned times 96 multiplier which generates 34 mW. A Gunn source, held on frequency by injection locking, provided 84 mW at 28.8 GHz. Both source frequencies were referenced to a 100 MHz temperature compensated crystal oscillator. All sensitive components were attached to a temperature controlled heat sink

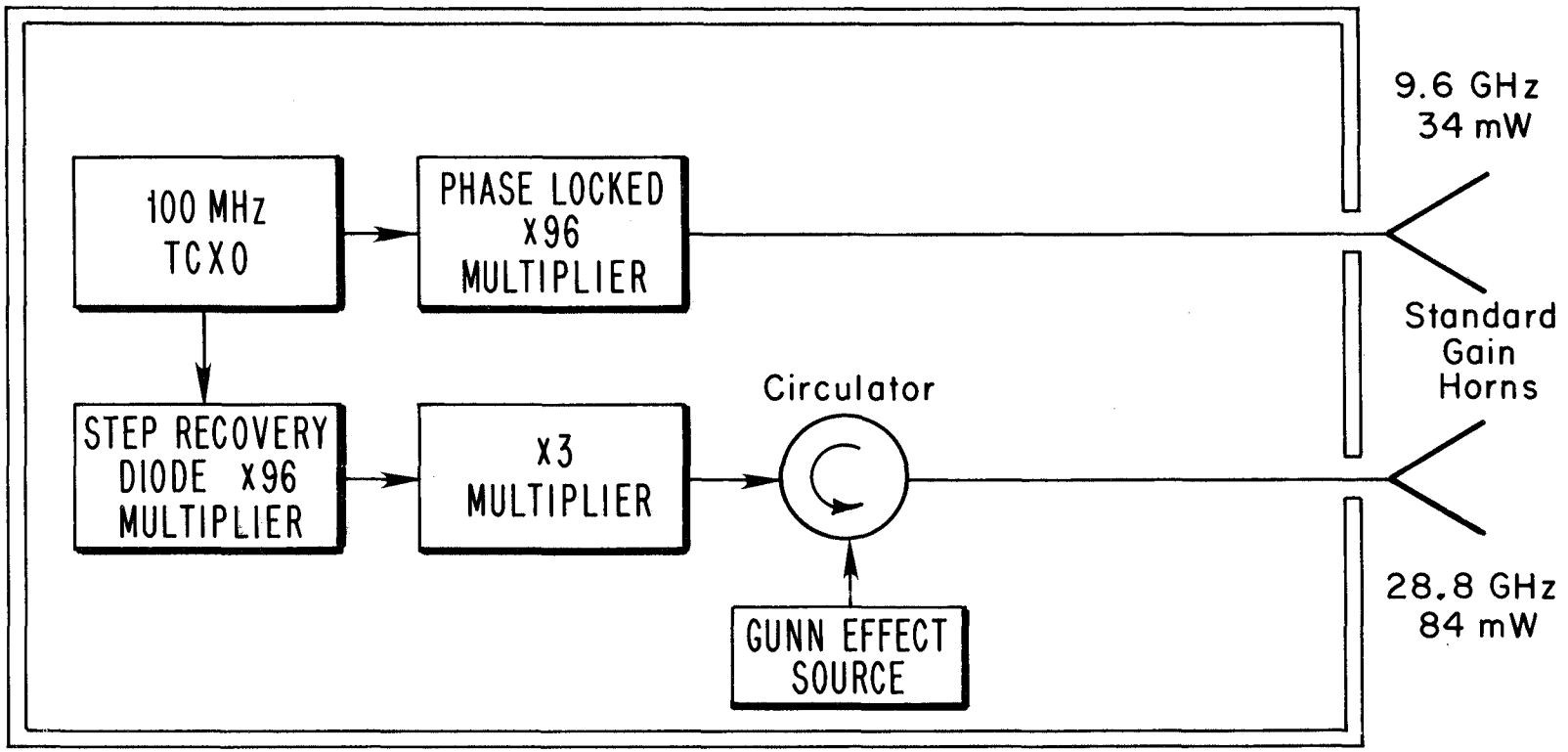

Figure A-1. Transmitter block diagram.

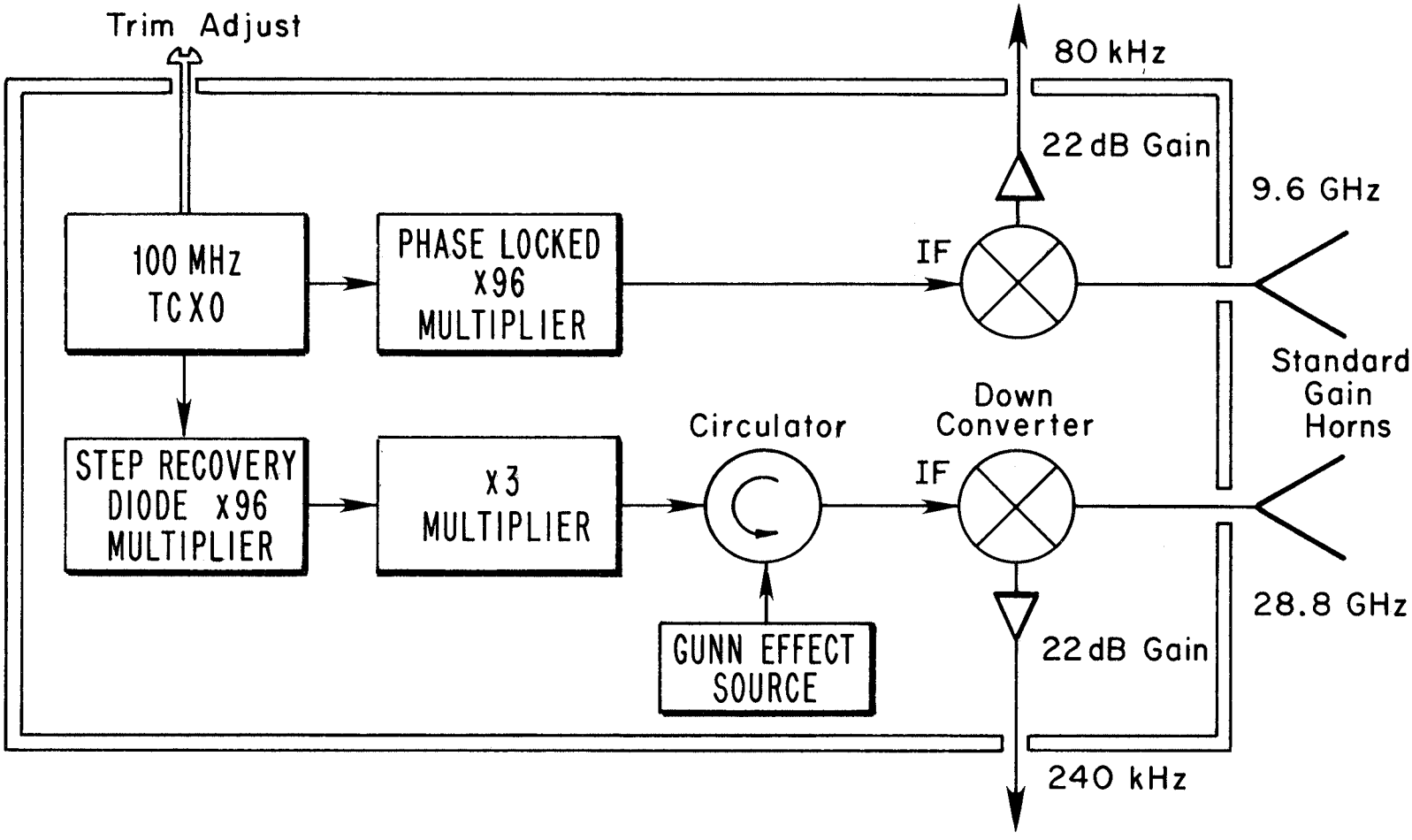

Figure A-2. Receiver block diagram.

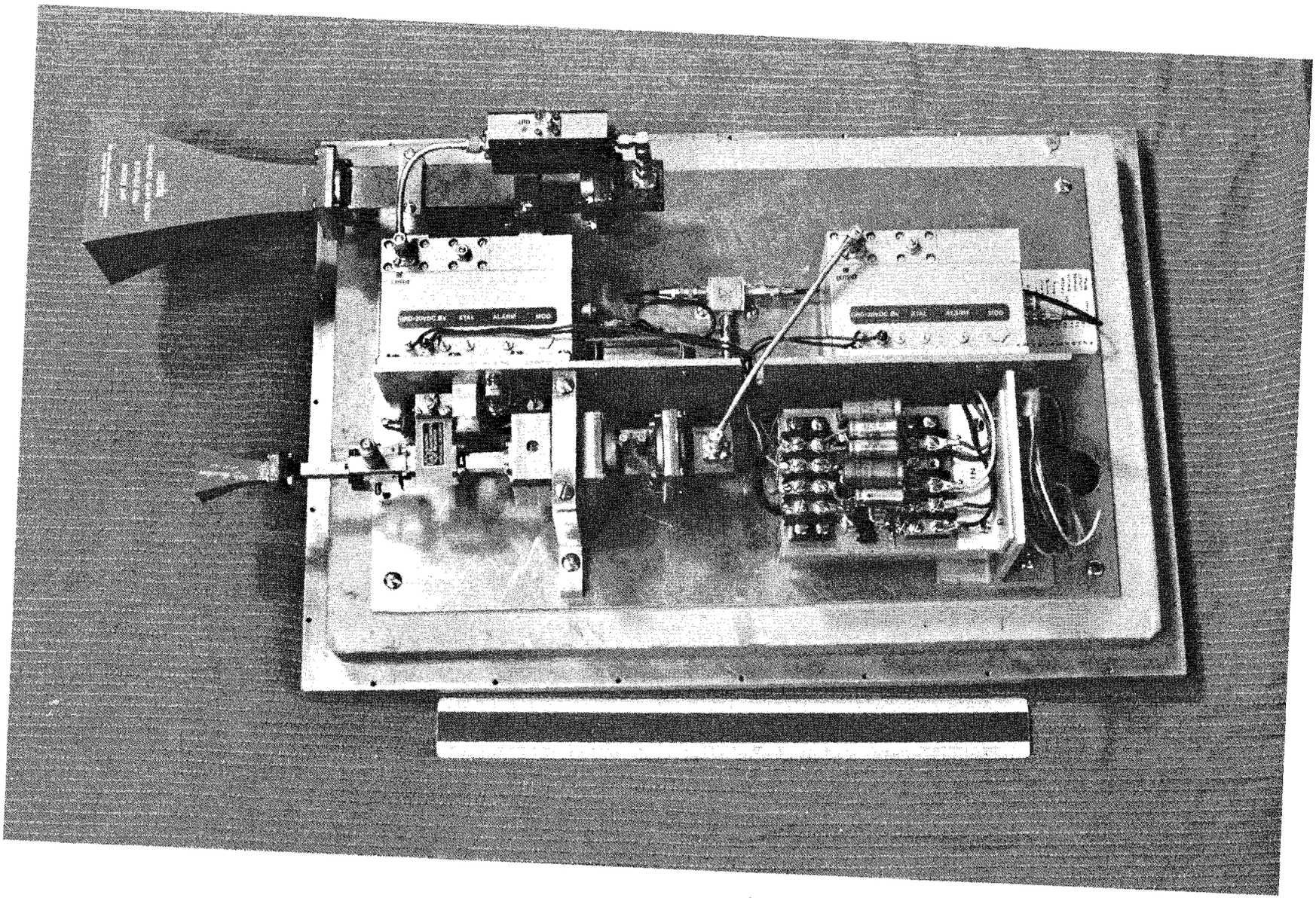

Figure A-3. Photograph of transmitter rf terminal.

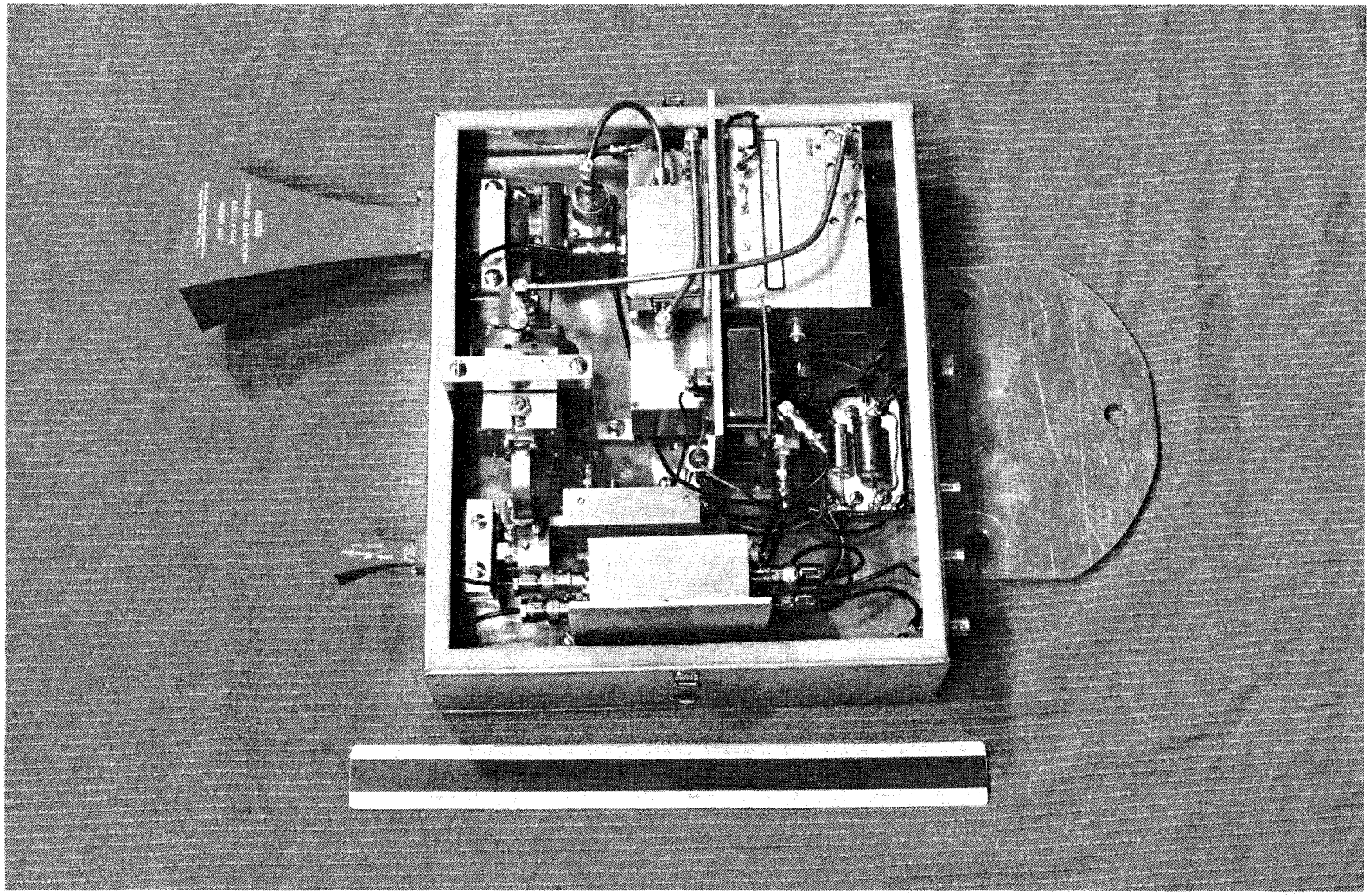

Figure A-4. Photograph of receiver rf terminal.

within the enclosure and held at $45^{\circ}C \pm 1^{\circ}C$ to reduce power variations to less than ± 0.2 dB. Each signal source drove a nominal 16 dB standard gain horn with a beamwidth of approximately 28 degrees at the half power points in both E and H planes.

The second van served as the receiving terminal and contained the data recording instrumentation. Both antennas, front end sections, and a low noise preamplifier for each channel were contained in an enclosure that could be adjusted in height above ground from 2 to 5 meters on vertical rails. In addition, the enclosure was mounted on a milling head assembly to allow the receiving terminal to travel about 13 cm in line with, or transverse to, the path. Each turn of the milling head crank moved the receiver about 2.5 mm so that signal variation could be plotted as the path length was changed by a fraction of its wave length. Standard gain horns identical to those on the transmitter were used on the receiver. The receiver enclosure was temperature controlled in the same manner as the transmitter. A pair of state-of-the-art low noise balanced mixers follow the horns to down convert the 9.6 GHz to 80 kHz and the 28.8 GHz to 240 kHz. Figures A-1 and A-2 show a functional diagram of the rf sections of the transmitter and receiver.

The IF signals were connected to a narrow band amplifier inside the van and fed to individual log amplifiers capable of 110 dB dynamic range. A frequency synthesizer with a stable reference (1 part in 10^9) and a 1 Hz frequency resolution was used in place of the TCXO in Figures A-1 and A-2 and was used to derive the local oscillator signal for the mixers. The exact synthesizer frequency was adjusted to compensate for minor changes in the transmitted frequency, centering the received signal in the IF bandpass to obtain absolute levels for path loss. Photographs of the transmitter and receiver rf sections are shown in Figures A-3 and A-4.

Each IF output signal from the receiver was passed through a log converter to provide a dc voltage level which is logarithmically related to the signal amplitude seen at the receiving antenna. Any one of three low pass filters with cut-off frequencies of 10, 100, and 1000 Hz could be selected at the output of the log converter. Only the 10 Hz filter was used in recording data for this project.

A.3 DATA COLLECTION SUBSYSTEM

The data collection subsystem was required to read and record the dc voltage from the log converters with sufficient resolution to reproduce all maximums and minimums of the received signal while the transmitter was continuously moved from below the grazing level of the obstacle to above the obstacle. Figure A-5 shows a block diagram of the data recording and test control equipment. The controller interfaced with 1) the operator for test information, 2) the analog-to-digital (A/D) converter to encode receiver output data, 3) the tape recorder for reading and writing the digital data, and 4) other peripherals such as the time-of-day clock, strip chart recorder, etc. The operator specified information such as the data, test site, test number, weather conditions, sampling rate, sampling period, etc. The controller formatted the input information and put it on the header record of the tape. After the operator had put the calibration data on the tape and initiated the test start, the controller read the A/D values at the sample rate selected by the operator. The data were stored in the controller's memory and transferred to the tape formatter by DMA.

For real-time judgment of the performance of the hardware and a quick look indicator of path characteristics, the controller was preprogrammed to print out mean signal level in dBm, standard deviation in dB, maximum instantaneous levels, and minimum instantaneous levels in dBm for each frequency. Each of the values printed out was taken from the selectable sampling rate, which was 10 per second for this experiment. The interval between printout and data blocks on tape was determined by the controller's buffered storage capacity, which was approximately 33 seconds.

All of the data (ten samples each second) were recorded and used in the analysis. For example, Figure 4-3 shows all of the recorded data points for path 6, 9.6 GHz.

A.4 SYSTEM CALIBRATION AND FREE SPACE SIGNAL CALCULATIONS

The complete system was assembled in the lab with the rf terminals of transmitter and receiver connected by waveguide through precision rf attenuators. A calibration curve was obtained over a 70 dB dynamic range and stored on magnetic tape. The calibration was repeated using precision attenuators in the IF line ahead of the narrow band amplifier to determine the

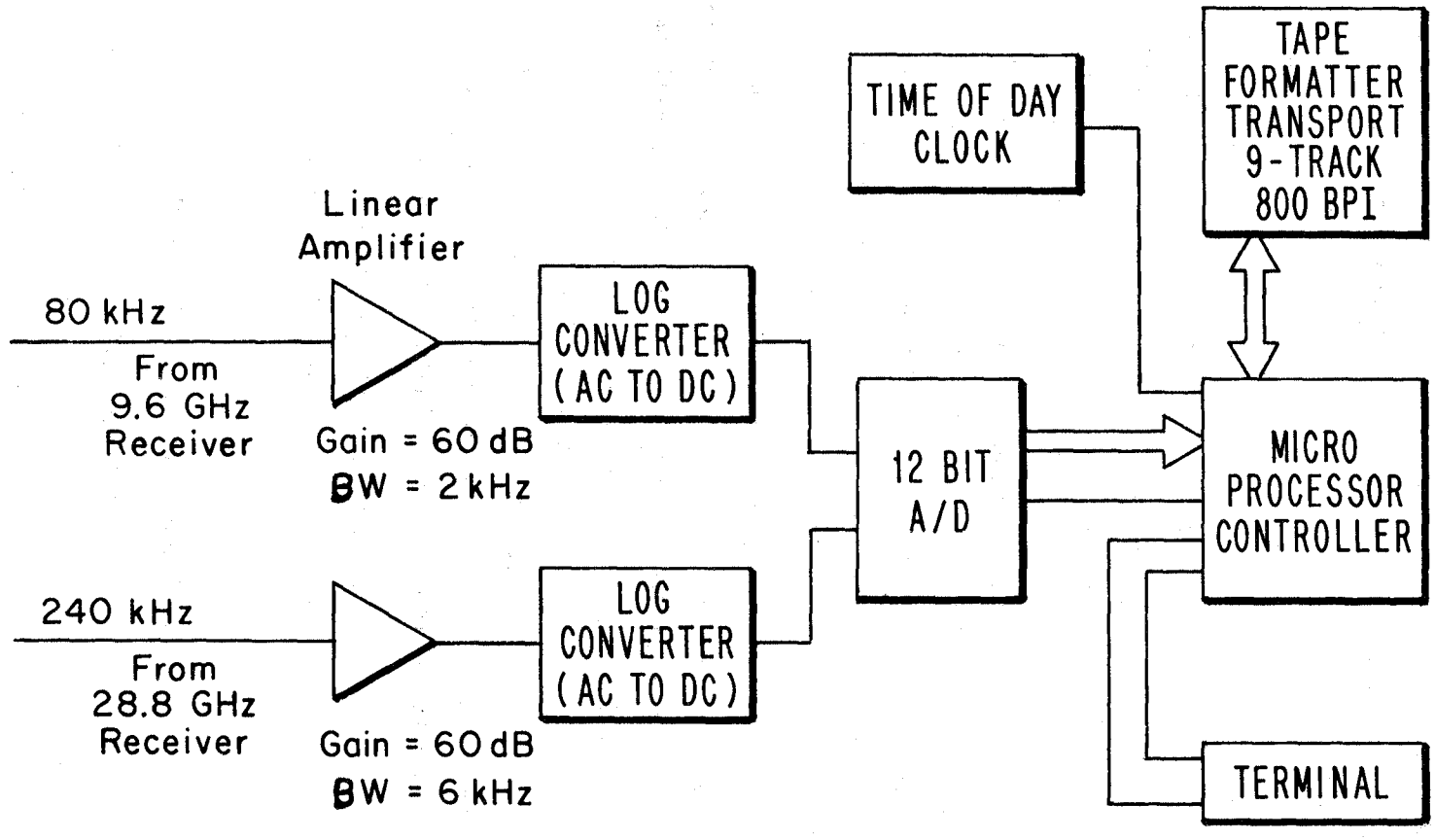

Figure A-5. Log video receiver and data collection equipment block diagram.

linearity of the rf sections. Both calibration curves matched to within less than $\pm$0.1 dB, verifying that the rf and preamplifier stages of the receivers were linear to within the tolerances indicated. Once the rf and IF linearities were confirmed, absolute signal calibration was obtained with considerably more ease because leakage from waveguide joints complicate the procedure when transmitter and receiver are co-located. More important, calibration in the field using the vans was straightforward, and the free space signal reference could be checked regularly in the field to compensate for decline in source power level or other component deteriorations during the course of the tests. While in the lab, during the month of November, the equipment was subjected to ambient temperature changes from 55°F to 90°F by controlling the room heating. During a four-day observing period, mean signal level for a 30-second measuring interval did not vary by more than $\pm$0.25 dB for the ambient temperature range indicated.

In order to obtain the value for mixer loss for the receiver configuration used, a calibrated signal generator was inserted at the output of the mixer and set to produce the same output level as the attenuated transmitter signal. This procedure yielded a mixer loss of 12.3 dB at 9.6 GHz and 10.5 dB at 28.8 GHz. The receiver sensitivity of -132 dBm for a 3 dB signal-to-noise ratio was measured at 9.6 GHz and -128 dBm at 28.8 GHz.

Because the application of microwave signals to determine intervisibility requires an accurate measure of the free space signal level, these levels must be computed and verified with the instrumentation. All parameters necessary in calculating the free space loss, in this case, are constants except for path length and atmospheric losses. If the atmospheric loss is assumed for a worst case clear air condition (no rain), it is so small for path lengths of interest (<4 km) that it can be neglected. For example, with 100 percent relative humidity at 0.3 km above sea level (for Hunter Liggett), an atmospheric loss of 0.016 dB/km at 9.6 GHz and 0.12 dB/km at 28.8 GHz would result.

The information discussed above permits a calculation of received power for a free space path using the following expression:

$$P_r = \frac{P_t\, G_t\, G_r\, \lambda^2}{(4\pi d)^2\, L_t\, L_r\, L_a}$$

where,

P_r = received power,
P_t = transmitter power,
G_t = transmitter antenna gain
G_r = receiver antenna gain,
λ = rf wave length (km),
πd = length of path (km),
L_t = transmitter lines loss,
L_r = receiver line loss, and
L_a = atmospheric loss (≈ 0 for short paths).

Expressed in decibels when $\lambda = \frac{c}{f}$, $c \approx 3 \times 10^8$ m/sec

$$P_r(\text{dBm}) = 10 \log P_t + G_t + G_r - 32.44 - 20 \log f(\text{MHz}) - 20 \log d(\text{km}) - L_t - L_r - L_a;$$

at 9.6 GHz

$P_t = 10 \log 34 \text{ mW} = +15.3 \text{ dBm}$,
$G_t = G_r = 16 \text{ dB}$,
$L_t = L_r = L_a \simeq 0$, and
$P_r = [-64.74 - 20 \log d(\text{km})] \text{ dBm}$;

at 28.8 GHz

$P_t = 10 \log 84 \text{ mW} = +19.24 \text{ dBm}$,
$G_t = G_r = 15.75 \text{ dB}$,
$L_t = L_r = L_a \simeq 0$, and
$P_r = [-70.85 - 20 \log d(\text{km})] \text{ dBm}$.

These equations for received power were used to establish the free space signal levels for all measured paths. Table A-1 gives the free space values for each path.

Table A-1. Received Signal Levels in Free Space for Each Path

Path No.	d(km)	Pr at 9.6 GHz (dBm)	Pr at 28.8 GHz (dBm)
1	0.199	-50.7	-56.8
2	0.492	-58.6	-64.6
3	0.472	57.7	-63.9
4	0.44	-57.6	-63.7
5	1.036	-65.05	-71.2
6	3.6	-75.9	-82.0
7	0.9	-63.8	-69.9
8	1.498	-68.25	-74.35
9	0.831	-63.1	-69.2

A.5 IN-FIELD SYSTEM CALIBRATION

In order to obtain an absolute system calibration and a reference of total system gain that could be readily checked in the field, a standard path was established. The main requirement for the standard path is that the separation between terminals be sufficient to place them in the far field, but not so far as to allow an additional path from a ground reflection. A conservative far field boundary is a distance of $2D^2/\lambda$, where D is the size of the antenna aperture. A separation of 86 feet (25.3 meters) met both requirements and fitted conveniently within the confines of the security compound. By use of a precision attenuator, an absolute calibration was placed on the magnetic tape for selected received power levels in dBm versus the voltage out of the log amplifier. A standard path check of the calibration curve was performed twice during the experiment with agreement to within +0.3 dB at received signal levels greater than -70 dBm and $\pm$0.6 dB at signal levels greater than -100 dBm.

A.6 MEASUREMENT UNCERTAINTY

A source of long-term drift was discovered in the field when primary power to the log convertors was supplied by the portable gasoline generator with interruption. In the lab, power remained on the log convertor or, at worst, warm-up was started from an ambient temperature of 70°F or more. In the field, power was applied after each new set-up of the terminals and starting temperatures were frequently near 40°F. All other gain determining

hardware stabilized within 15 minutes and, generally, collection of test data began very soon thereafter. Log convertor drift continued for up to an hour, depending on ambient temperature.

This drift was monitored and corrected as frequently as possible during the course of the experiment by observing the known noise level voltage and adjusting the dc offset level in the log convertor to the proper value. The log convertor drift was undoubtedly the largest measurement uncertainty. In the worst case (no correction made) a gradual level change over a period of about one measurement could result in about a 1 dB error at signal levels to -80 dBm, perhaps increasing to 2 dB down to -110 dBm.

Another source of error in the apparent received signal was a fluctuation in source frequency due to the temperature controller cycling resulting in a shift of the 100 MHz reference oscillator. This shift causes the IF frequency to move away from the center of the response of the narrow band amplifier. During a test run the IF signal is monitored and frequency adjustments of 1 to 3 Hz are required at 2 to 30 minute intervals depending on weather (temperature and wind primarily). A 1 Hz change at the 100 MHz reference results in a 96 Hz and 288 Hz change of the 9.6 and 28.8 GHz source, respectively. The IF bandpass was widened to 2 kHz at lowest frequency and 6 kHz at the highest frequency, so this variation seldom exceeded $\pm$0.2 dB even on short warm-up.

A third potential contribution to system gain error was change in output power due to temperature changes within the enclosure. The enclosed compartment has an adjustable air vent which was regulated at the start of the experiment to prevent the enclosure temperature from rising above that set by the controller (+45^{o}C). At times rain storms and strong winds producing lower temperatures occurred during the course of an experiment which prevented the enclosure from getting up to temperature with the heating element ON. This condition was indicated by a shift in the 100 MHz reference oscillator. When the source temperature drops by 10^{o}C the output power increases about 0.1 dB on 9.6 GHz source and about 0.08 dB on the 28.8 GHz Gunn oscillator. It is unlikely that a signal increase of more than two or three tenths of a dB occurred due to changes in temperature of the sources. This was deduced by observing the reference oscillator frequency.

The last known source of error is the pointing of the horns. For comparison with theoretical values, it must be assumed that the antennas of both terminals are essentially directed at that portion of the crest of the obstructing terrain feature that provides the minimum H value. In all but one case (path 5) the vertical positioning of the terminal did not change the angle between antenna boresight and the obstruction crest by more than ± 5 degrees; therefore, the variation within the 28 degree antenna beam would not exceed 1 dB in the deep shadow region. For path 5 the angle to the obstacle was about 26 degrees and could account for a 3 dB variation in the shadow regions, but not above the obstacle, because it was directed on the transmitter sources, However, when making the measurement transverse to the obstacle, an effort was made to track the antenna; an error of up to 6 dB along path 8 was known to have occurred due to a combination of azimuth and elevation pointing errors, caused by driving over irregular terrain.

APPENDIX B

RESULTS FOR PATHS 1 AND 2

The results for paths 1 and 2 were not reported in the main body of this report because of the way the data for those paths were taken. For paths 3 through 9, data were continuously recorded as the transmitter tower was moved from below to above the grazing LOS elevation. Unfortunately, for paths 1 and 2, data were recorded only at discrete heights below and above grazing. For example, if data had been recorded only at one-meter intervals for path 3, one would have been left with a much different interpretation of the behavior of the data than that gotten from Figure 4-16 where the data were recorded continuously as the height above grazing changed.

With the above as background (and as a warning about their interpretation), Figures B-1 through B-4 give the diffraction results for paths 1 and 2. Note that the measured data are indicated by dots in the figures. Lines connecting the measured points are there to assist in reading the figures and do not imply that additional data would lie on the interconnecting lines.

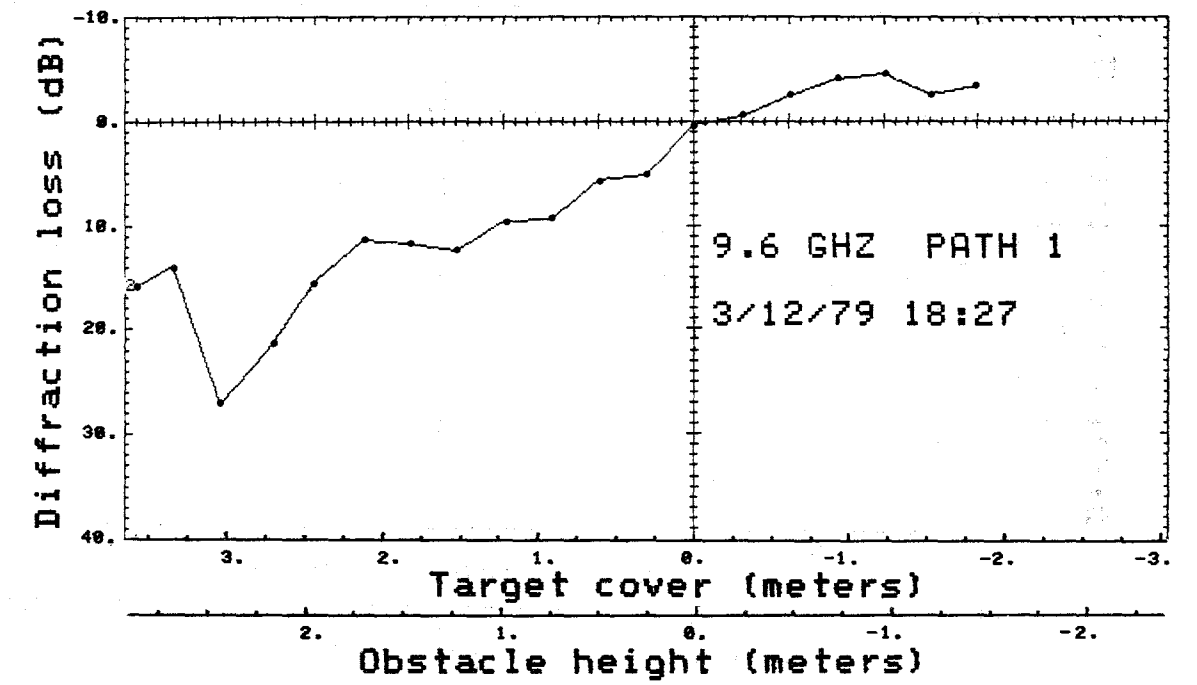

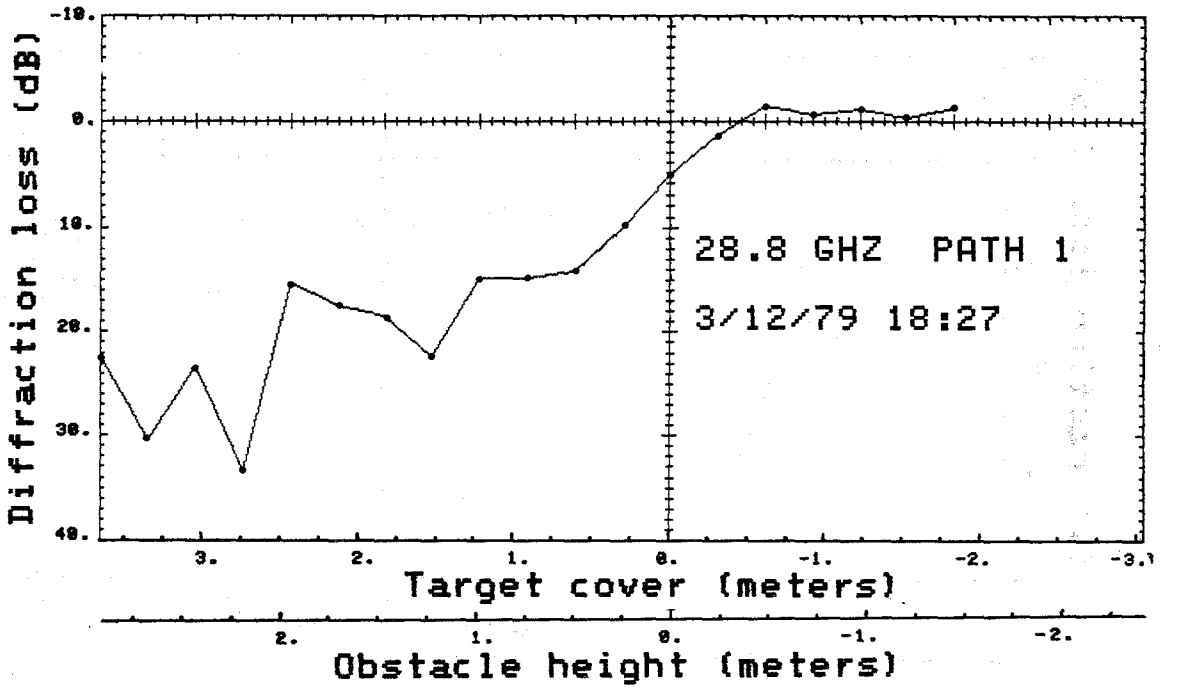

Figure B-1. Diffraction results for path 1.

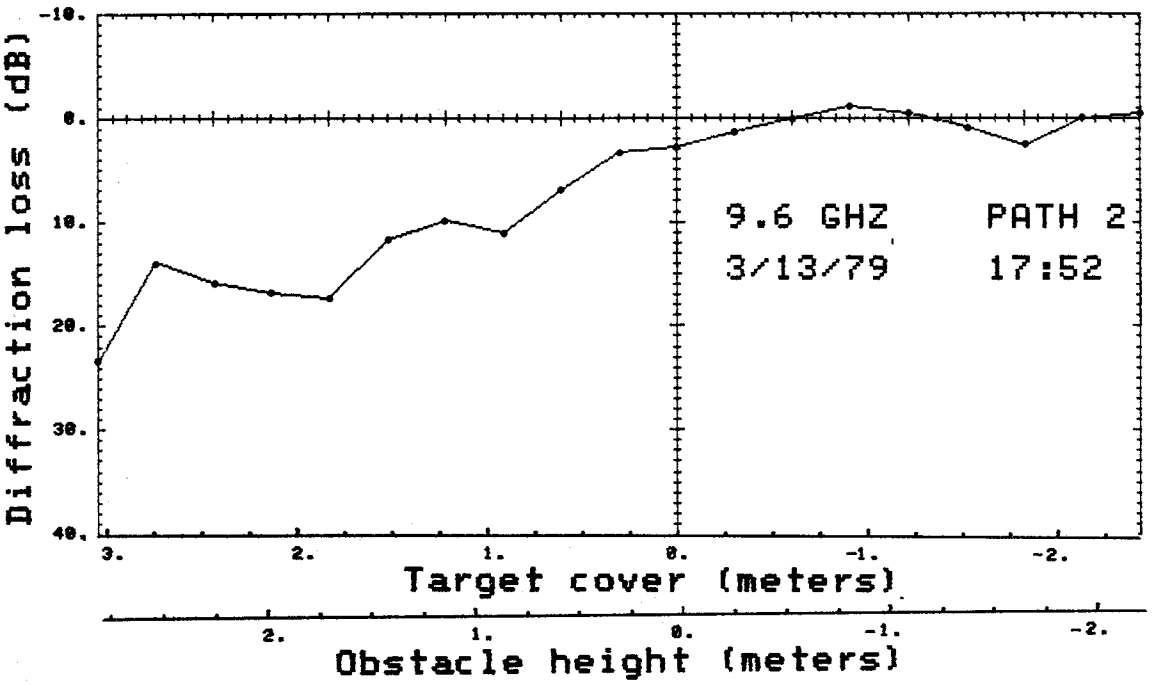

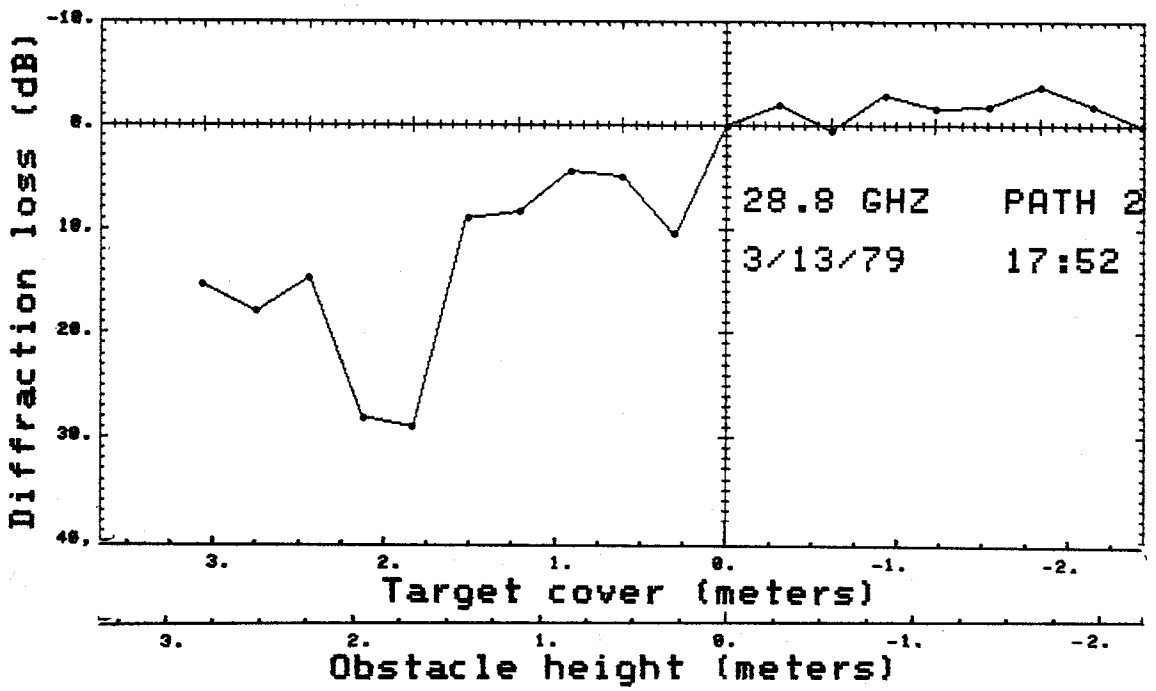

Figure B-2. Diffraction results for path 2.

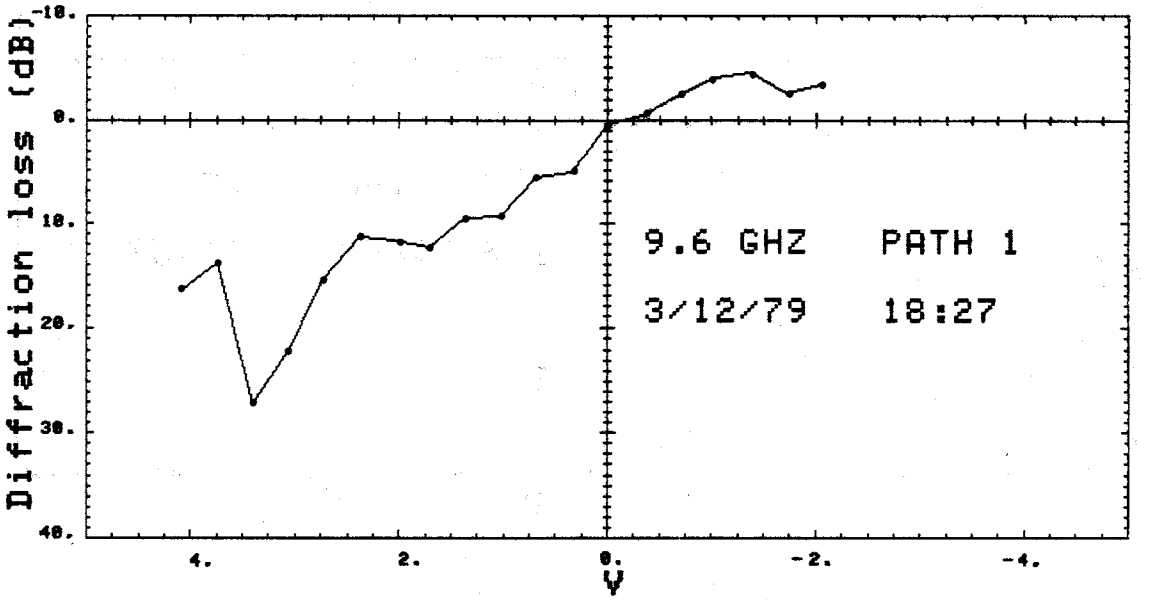

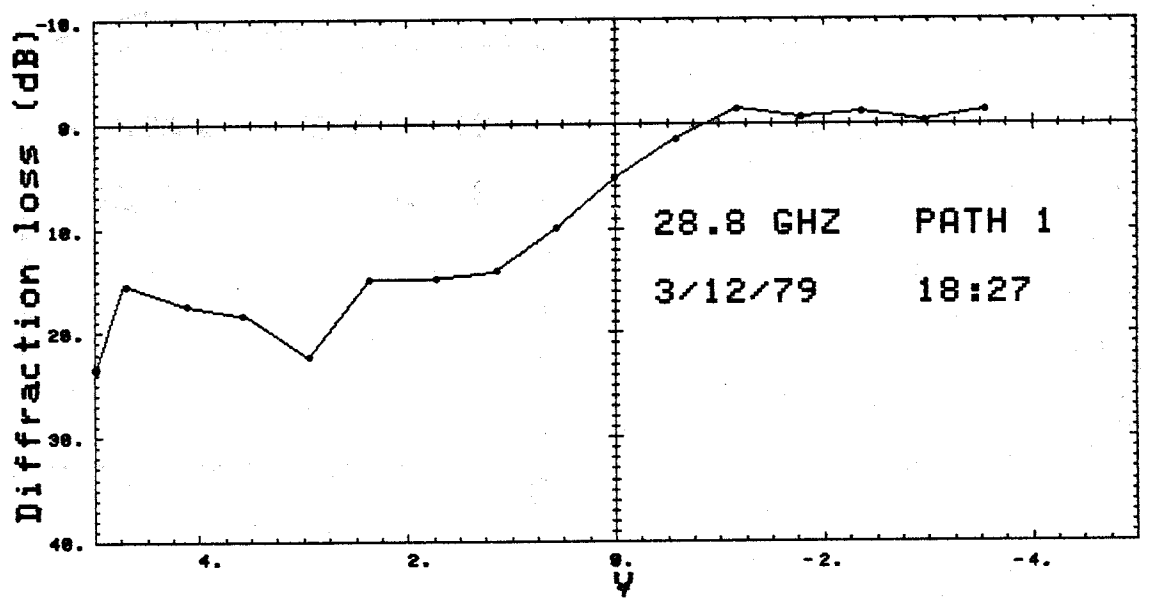

Figure B-3. Normalized results for path 1.

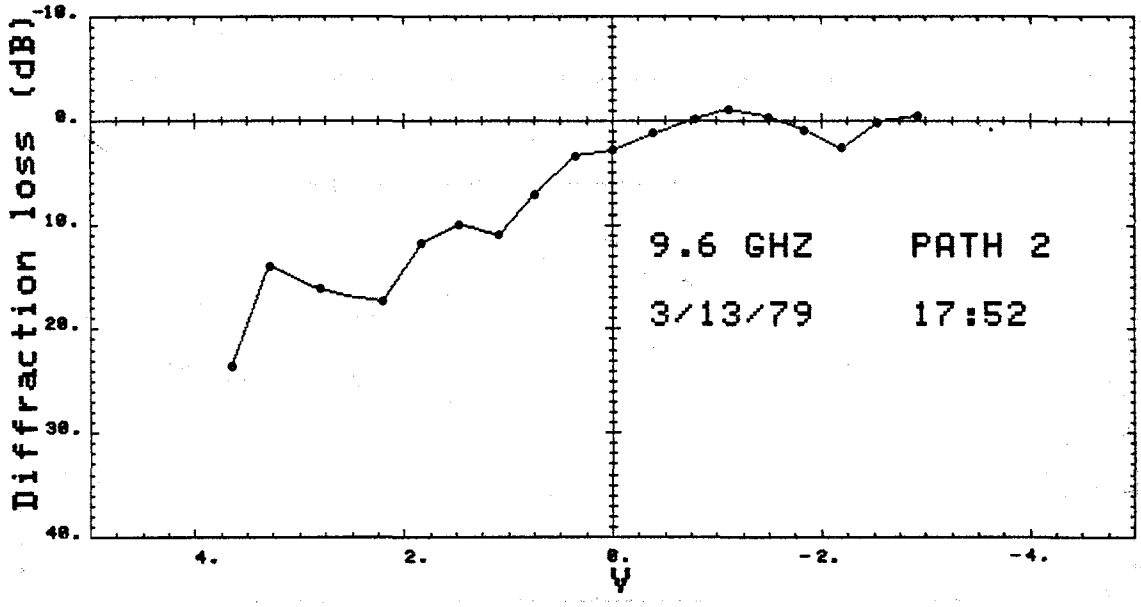

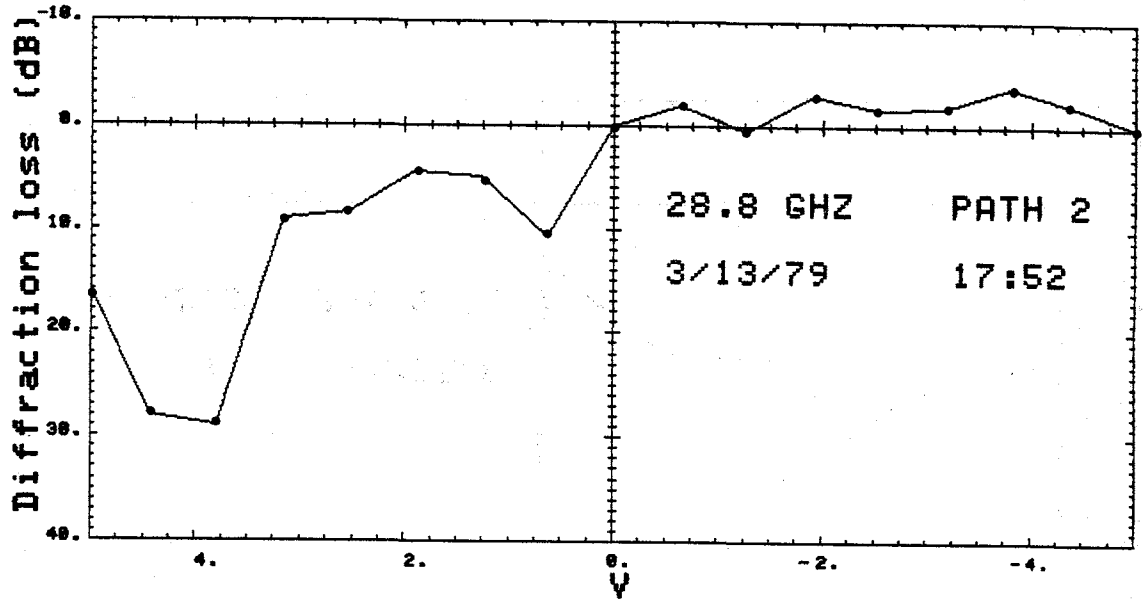

Figure B-4. Normalized results for path 2.

APPENDIX C

SIMULATED MICROWAVE INTERVISIBILITY SYSTEM RESULTS

Tables C-1 through C-21 present the results of simulated microwave intervisibility measurement system operating on the measured data. Three different decision thresholds were used in the intervisibility decision process. The first threshold was the computed optimum for the measured paths; the second threshold as 3 dB above the optimum; and the third was 3 dB below the optimum.

Table C-1. False Alarm and Missed Alarm Percentages for Path 3, Threshold at the Computed Optimum

9.6 GHZ THRESHOLD = +4.4 DB

28.8 GHZ THRESHOLD = +4.0 DB

TARGET COVER HT RANGE		9.6 GHZ NO. PTS	NO. FA	% FA	NO. MA	% MA	28.8 GHZ NO. PTS	NO. FA	% FA	NO. MA	% MA
3.50	3.25	43	0	0.0			43	0	0.0		
3.25	3.00	82	0	0.0			82	0	0.0		
3.00	2.75	110	0	0.0			110	0	0.0		
2.75	2.50	87	0	0.0			87	0	0.0		
2.50	2.25	91	0	0.0			91	0	0.0		
2.25	2.00	88	0	0.0			88	0	0.0		
2.00	1.75	122	0	0.0			122	0	0.0		
1.75	1.50	86	0	0.0			86	0	0.0		
1.50	1.25	62	0	0.0			62	0	0.0		
1.25	1.00	104	0	0.0			104	0	0.0		
1.00	.75	102	0	0.0			102	0	0.0		
.75	.50	89	0	0.0			89	0	0.0		
.50	.25	90	0	0.0			90	0	0.0		
.25	0.00	94	0	0.0			94	0	0.0		
0.00	-.25	107			107	100.0	107			59	55.1
-.25	-.50	80			80	100.0	80			0	0.0
-.50	-.75	563			27	4.8	563			0	0.0

Table C-2. False Alarm and Missed Alarm Percentages for Path 3, Threshold 3 dB Above the Optimum

9.6 GHZ THRESHOLD = +1.4 DB

28.8 GHZ THRESHOLD = +1.0 DB

TARGET COVER HT RANGE		9.6 GHZ NO. PTS	NO. FA	% FA	NO. MA	% MA	28.8 GHZ NO. PTS	NO. FA	% FA	NO. MA	% MA
3.50	3.25	43	0	0.0			43	0	0.0		
3.25	3.00	82	0	0.0			82	0	0.0		
3.00	2.75	110	0	0.0			110	0	0.0		
2.75	2.50	87	0	0.0			87	0	0.0		
2.50	2.25	91	0	0.0			91	0	0.0		
2.25	2.00	88	0	0.0			88	0	0.0		
2.00	1.75	122	0	0.0			122	0	0.0		
1.75	1.50	86	0	0.0			86	0	0.0		
1.50	1.25	62	0	0.0			62	0	0.0		
1.25	1.00	104	0	0.0			104	0	0.0		
1.00	.75	102	0	0.0			102	0	0.0		
.75	.50	89	0	0.0			89	0	0.0		
.50	.25	90	0	0.0			90	0	0.0		
.25	0.00	94	0	0.0			94	0	0.0		
0.00	-.25	107			107	100.0	107			107	100.0
-.25	-.50	80			80	100.0	80			12	15.0
-.50	-.75	563			563	100.0	563			0	0.0

Table C-3. False Alarm and Missed Alarm Percentages for Path 3, Threshold 3 dB Below the Optimum

9.6 GHZ THRESHOLD = +7.4 DB

28.8 GHZ THRESHOLD = +7.0 DB

TARGET COVER HT RANGE		9.6 GHZ NO. PTS	NO. FA	% FA	NO. MA	% MA	28.8 GHZ NO. PTS	NO. FA	% FA	NO. MA	% MA
3.50	3.25	43	0	0.0			43	0	0.0		
3.25	3.00	82	0	0.0			82	0	0.0		
3.00	2.75	110	0	0.0			110	0	0.0		
2.75	2.50	87	0	0.0			87	0	0.0		
2.50	2.25	91	0	0.0			91	0	0.0		
2.25	2.00	88	0	0.0			88	0	0.0		
2.00	1.75	122	0	0.0			122	0	0.0		
1.75	1.50	86	0	0.0			86	0	0.0		
1.50	1.25	62	0	0.0			62	0	0.0		
1.25	1.00	104	0	0.0			104	0	0.0		
1.00	.75	102	0	0.0			102	0	0.0		
.75	.50	89	0	0.0			89	0	0.0		
.50	.25	90	0	0.0			90	3	3.3		
.25	0.00	94	0	0.0			94	70	74.5		
0.00	-.25	107			29	27.1	107			10	9.3
-.25	-.50	80			5	6.3	80			0	0.0
-.50	-.75	563			0	0.0	563			0	0.0

Table C-4. False Alarm and Missed Alarm Percentages for Path 4, Threshold at the Computed Optimum

9.6 GHZ THRESHOLD = +4.4 DB

28.8 GHZ THRESHOLD = +4.0 DB

TARGET COVER HT RANGE		9.6 GHZ NO. PTS	NO. FA	% FA	NO. MA	% MA	28.8 GHZ NO. PTS	NO. FA	% FA	NO. MA	% MA
3.50	3.25	58	0	0.0			58	0	0.0		
3.25	3.00	208	0	0.0			208	0	0.0		
3.00	2.75	158	0	0.0			158	0	0.0		
2.75	2.50	163	0	0.0			163	0	0.0		
2.50	2.25	190	0	0.0			190	0	0.0		
2.25	2.00	220	0	0.0			220	0	0.0		
2.00	1.75	179	0	0.0			179	0	0.0		
1.75	1.50	149	0	0.0			149	0	0.0		
1.50	1.25	191	0	0.0			191	0	0.0		
1.25	1.00	224	0	0.0			224	0	0.0		
1.00	.75	170	17	10.0			170	0	0.0		
.75	.50	163	50	30.7			163	0	0.0		
.50	.25	193	193	100.0			193	111	57.5		
.25	0.00	197	189	48.9			197	144	73.1		
0.00	-.25	288			0	0.0	288			44	15.3
-.25	-.50	175			0	0.0	175			12	6.9
-.50	-.75	182			0	0.0	182			0	0.0
-.75	-1.00	221			0	0.0	221			0	0.0
-1.00	-1.25	159			0	0.0	159			0	0.0
-1.25	-1.50	155			0	0.0	155			0	0.0
-1.50	-1.75	203			0	0.0	203			0	0.0
-1.75	-2.00	191			0	0.0	191			0	0.0
-2.00	-2.25	104			0	0.0	104			0	0.0
-2.25	-2.50	91			0	0.0	91			0	0.0

Table C-5. False Alarm and Missed Alarm Percentages for Path 4, Threshold 3 dB Above the Computed Optimum

9.6 GHZ THRESHOLD = +1.4 DB

28.8 GHZ THRESHOLD = +1.0 DB

TARGET COVER HT RANGE		9.6 GHZ NO. PTS	NO. FA	% FA	NO. MA	% MA	28.8 GHZ NO. PTS	NO. FA	% FA	NO. MA	% MA
3.50	3.25	58	0	0.0			58	0	0.0		
3.25	3.00	208	0	0.0			208	0	0.0		
3.00	2.75	158	0	0.0			158	0	0.0		
2.75	2.50	163	0	0.0			163	0	0.0		
2.50	2.25	190	0	0.0			190	0	0.0		
2.25	2.00	220	0	0.0			220	0	0.0		
2.00	1.75	179	0	0.0			179	0	0.0		
1.75	1.50	149	0	0.0			149	0	0.0		
1.50	1.25	191	0	0.0			191	0	0.0		
1.25	1.00	224	0	0.0			224	0	0.0		
1.00	.75	170	0	0.0			170	0	0.0		
.75	.50	163	0	0.0			163	0	0.0		
.50	.25	193	3	1.6			193	0	0.0		
.25	0.00	197	0	0.0			197	1	0.5		
0.00	-.25	288			177	61.5	288			244	84.7
-.25	-.50	175			0	0.0	175			137	78.3
-.50	-.75	182			0	0.0	182			30	0.0
-.75	-1.00	221			0	0.0	221			0	0.0
-1.00	-1.25	159			0	0.0	159			0	0.0
-1.25	-1.50	155			0	0.0	155			0	0.0
-1.50	-1.75	203			29	14.3	203			0	0.0
-1.75	-2.00	191			36	18.8	191			0	0.0
-2.00	-2.25	104			11	10.6	104			8	7.7
-2.25	-2.50	91			34	37.4	91				

Table C-6. False Alarm and Missed Alarm Percentages for Path 4, Threshold 3 dB Below the Computed Optimum

9.6 GHZ THRESHOLD = +7.4 DB

28.8 GHZ THRESHOLD = +7.0 DB

TARGET COVER HT RANGE		9.6 GHZ NO. PTS	9.6 GHZ NO. FA	9.6 GHZ % FA	9.6 GHZ NO. MA	9.6 GHZ % MA	28.8 GHZ NO. PTS	28.8 GHZ NO. FA	28.8 GHZ % FA	28.8 GHZ NO. MA	28.8 GHZ % MA
3.50	3.25	58	0	0.0			58	0	0.0		
3.25	3.00	208	0	0.0			208	0	0.0		
3.00	2.75	158	0	0.0			158	0	0.0		
2.75	2.50	163	2	1.2			163	0	0.0		
2.50	2.25	190	158	83.2			190	14	7.4		
2.25	2.00	220	128	58.2			220	5	2.3		
2.00	1.75	179	118	65.9			179	76	42.5		
1.75	1.50	149	126	84.6			149	0	0.0		
1.50	1.25	191	0	0.0			191	0	0.0		
1.25	1.00	224	0	0.0			224	127	56.7		
1.00	.75	170	112	65.9			170	44	25.9		
.75	.50	163	163	100.0			163	93	57.1		
.50	.25	193	193	100.0			193	193	100.0		
.25	0.00	197	197	100.0			197	197	100.0		
0.00	-.25	288			0	0.0	288			0	0.0
-.25	-.50	175			0	0.0	175			0	0.0
-.50	-.75	182			0	0.0	182			0	0.0
-.75	-1.00	221			0	0.0	221			0	0.0
-1.00	-1.25	159			0	0.0	159			0	0.0
-1.25	-1.50	155			0	0.0	155			0	0.0
-1.50	-1.75	203			0	0.0	203			0	0.0
-1.75	-2.00	191			0	0.0	191			0	0.0
-2.00	-2.25	104			0	0.0	104			0	0.0
-2.25	-2.50	91			0	0.0	91			0	0.0

Table C-7. False Alarm and Missed Alarm Percentages for Path 5 (First Location), Threshold at the Computed Optimum

9.6 GHZ THRESHOLD = +4.4 DB

28.8 GHZ THRESHOLD = +4.0 DB

TARGET COVER HT RANGE	9.6 GHZ NO. PTS	NO. FA	% FA	NO. MA	% MA	28.8 GHZ NO. PTS	NO. FA	% FA	NO. MA	% MA
2.50 2.25	146	0	0.0			146	0	0.0		
2.25 2.00	188	0	0.0			188	0	0.0		
2.00 1.75	153	0	0.0			153	0	0.0		
1.75 1.50	171	0	0.0			171	0	0.0		
1.50 1.25	199	0	0.0			199	0	0.0		
1.25 1.00	146	0	0.0			146	0	0.0		
1.00 .75	173	0	0.0			173	0	0.0		
.75 .50	176	0	0.0			176	0	0.0		
.50 .25	147	0	0.0			147	0	0.0		
.25 0.00	163	0	57.7			163	4	2.5		
0.00 -.25	147			0	0.0	147			20	13.6
-.25 -.50	199			0	0.0	199			0	0.0
-.50 -.75	146			0	0.0	146			0	0.0
-.75 -1.00	167			0	0.0	167			0	0.0
-1.00 -1.25	157			0	0.0	157			0	0.0
-1.25 -1.50	174			17	9.8	174			0	0.0
-1.50 -1.75	170			0	0.0	170			0	0.0
-1.75 -2.00	142			0	0.0	142			0	0.0
-2.00 -2.25	179			0	0.0	179			0	0.0
-2.25 -2.50	179			0	0.0	179			23	12.8
-2.50 -2.75	167			0	0.0	167			0	0.0
-2.75 -3.00	181			29	1.6	181			0	0.0
-3.00 -3.25	84			84	100.0	84			0	0.0

Table C-8. False Alarm and Missed Alarm Percentages for Path 5 (First Location), Threshold 3 dB Above the Optimum

9.6 GHZ THRESHOLD = +1.4 DB

28.8 GHZ THRESHOLD = +1.0 DB

TARGET COVER HT RANGE	9.6 GHZ NO. PTS	NO. FA	% FA	NO. MA	% MA	28.8 GHZ NO. PTS	NO. FA	% FA	NO. MA	% MA
2.50 2.25	146	0	0.0			146	0	0.0		
2.25 2.00	188	0	0.0			188	0	0.0		
2.00 1.75	153	0	0.0			153	0	0.0		
1.75 1.50	171	0	0.0			171	0	0.0		
1.50 1.25	199	0	0.0			199	0	0.0		
1.25 1.00	146	0	0.0			146	0	0.0		
1.00 .75	173	0	0.0			173	0	0.0		
.75 .50	176	0	0.0			176	0	0.0		
.50 .25	147	0	0.0			147	0	0.0		
.25 0.00	163	6	3.7			163	0	0.0		
0.00 -.25	147			13	8.8	147			110	74.8
-.25 -.50	199			0	0.0	199			0	0.0
-.50 -.75	146			0	0.0	146			38	26.0
-.75 -1.00	167			0	0.0	167			0	0.0
-1.00 -1.25	157			8	5.1	157			3	2.1
-1.25 -1.50	174			101	58.0	174			44	25.3
-1.50 -1.75	170			18	10.6	170			0	0.0
-1.75 -2.00	142			0	0.0	142			42	29.6
-2.00 -2.25	179			0	0.0	179			0	0.0
-2.25 -2.50	179			0	0.0	179			0	52.0
-2.50 -2.75	167			0	0.0	167			15	9.0
-2.75 -3.00	181			59	32.6	181			0	0.0
-3.00 -3.25	84			84	100.0	84			0	0.0

Table C-9. False Alarm and Missed Alarm Percentages for Path 5 (First Location), Threshold 3 dB Below the Optimum

9.6 GHZ THRESHOLD = +7.4 DB

28.8 GHZ THRESHOLD = +7.0 DB

TARGET COVER HT RANGE	9.6 GHZ NO. PTS	9.6 GHZ NO. FA	9.6 GHZ % FA	9.6 GHZ NO. MA	9.6 GHZ % MA	28.8 GHZ NO. PTS	28.8 GHZ NO. FA	28.8 GHZ % FA	28.8 GHZ NO. MA	28.8 GHZ % MA
2.50 2.25	146	0	0.0			146	0	0.0		
2.25 2.00	188	0	0.0			188	0	0.0		
2.00 1.75	153	0	0.0			153	0	0.0		
1.75 1.50	171	0	0.0			171	0	0.0		
1.50 1.25	199	0	0.0			199	0	0.0		
1.25 1.00	146	0	0.0			146	0	0.0		
1.00 .75	173	0	0.0			173	0	0.0		
.75 .50	176	0	0.0			176	0	0.0		
.50 .25	147	18	12.2			147	0	0.0		
.25 0.00	163	163	100.0			163	65	39.9		
0.00 -.25	147			0	0.0	147			0	0.0
-.25 -.50	199			0	0.0	199			0	0.0
-.50 -.75	146			0	0.0	146			0	0.0
-.75 -1.00	167			0	0.0	167			0	0.0
-1.00 -1.25	157			0	0.0	157			0	0.0
-1.25 -1.50	174			0	0.0	174			0	0.0
-1.50 -1.75	170			0	0.0	170			0	0.0
-1.75 -2.00	142			0	0.0	142			0	0.0
-2.00 -2.25	179			0	0.0	179			0	0.0
-2.25 -2.50	179			0	0.0	179			0	0.0
-2.50 -2.75	167			0	0.0	167			0	0.0
-2.75 -3.00	181			0	0.0	181			0	0.0
-3.00 -3.25	84			48	78.7	84			0	0.0

Table C-10. False Alarm and Missed Alarm Percentages for Path 5 (Second Location), Threshold at the Computed Optimum

9.6 GHZ THRESHOLD = +4.4 DB

28.8 GHZ THRESHOLD = +4.0 DB

TARGET COVER HT RANGE	9.6 GHZ NO. PTS	9.6 GHZ NO. FA	9.6 GHZ % FA	9.6 GHZ NO. MA	9.6 GHZ % MA	28.8 GHZ NO. PTS	28.8 GHZ NO. FA	28.8 GHZ % FA	28.8 GHZ NO. MA	28.8 GHZ % MA
2.50 2.25	188	0	0.0			188	0	0.0		
2.25 2.00	202	0	0.0			202	0	0.0		
2.00 1.75	215	0	0.0			215	0	0.0		
1.75 1.50	179	0	0.0			179	0	0.0		
1.50 1.25	187	0	0.0			187	0	0.0		
1.25 1.00	180	0	0.0			180	0	0.0		
1.00 .75	199	0	0.0			199	0	0.0		
.75 .50	212	12	5.7			212	0	0.0		
.50 .25	221	200	90.5			221	0	0.0		
.25 0.00	196	196	100.0			196	60	30.6		
0.00 -.25	196			0	0.0	196			28	14.3
-.25 -.50	184			0	0.0	184			0	0.0
-.50 -.75	221			0	0.0	221			0	0.0
-.75 -1.00	188			0	0.0	188			0	0.0
-1.00 -1.25	201			0	0.0	201			0	0.0
-1.25 -1.50	201			8	4.0	201			0	0.0
-1.50 -1.75	220			0	0.0	220			0	0.0
-1.75 -2.00	193			0	0.0	193			0	0.0
-2.00 -2.25	195			0	0.0	195			0	0.0
-2.25 -2.50	179			0	0.0	179			19	10.6
-2.50 -2.75	94			0	0.0	94			0	0.0

Table C-11. False Alarm and Missed Alarm Percentages for Path 5 (Second Location), Threshold at 3 dB Above the Optimum

9.6 GHZ THRESHOLD = +1.4 DB

28.8 GHZ THRESHOLD = +1.0 DB

TARGET COVER HT RANGE		9.6 GHZ NO. PTS	NO. FA	% FA	NO. MA	% MA	28.8 GHZ NO. PTS	NO. FA	% FA	NO. MA	% MA
2.50	2.25	188	0	0.0			188	0	0.0		
2.25	2.00	202	0	0.0			202	0	0.0		
2.00	1.75	215	0	0.0			215	0	0.0		
1.75	1.50	179	0	0.0			179	0	0.0		
1.50	1.25	187	0	0.0			187	0	0.0		
1.25	1.00	180	0	0.0			180	0	0.0		
1.00	.75	199	0	0.0			199	0	0.0		
.75	.50	212	0	0.0			212	0	0.0		
.50	.25	221	0	0.0			221	0	0.0		
.25	0.00	196	184	93.9			196	0	0.0		
0.00	-.25	196			0	0.0	196			124	63.3
-.25	-.50	184			0	0.0	184			0	0.0
-.50	-.75	221			0	0.0	221			0	0.0
-.75	-1.00	188			0	0.0	188			11	5.9
-1.00	-1.25	201			0	0.0	201			125	62.2
-1.25	-1.50	201			99	49.3	201			1	0.5
-1.50	-1.75	220			8	3.6	220			121	55.0
-1.75	-2.00	193			0	0.0	193			20	10.4
-2.00	-2.25	195			0	0.0	195			46	23.6
-2.25	-2.50	179			0	0.0	179			80	44.7
-2.50	-2.75	94			0	0.0	94			0	0.0

Table C-12. False Alarm and Missed Alarm Percentages for Path 5 (Second Location), Threshold at 3 dB Below the Optimum

9.6 GHZ THRESHOLD = +7.4 DB

28.8 GHZ THRESHOLD = +7.0 DB

TARGET COVER HT RANGE	9.6 GHZ NO. PTS	9.6 GHZ NO. FA	9.6 GHZ % FA	9.6 GHZ NO. MA	9.6 GHZ % MA	28.8 GHZ NO. PTS	28.8 GHZ NO. FA	28.8 GHZ % FA	28.8 GHZ NO. MA	28.8 GHZ % MA
2.50 2.25	188	0	0.0			188	0	0.0		
2.25 2.00	202	0	0.0			202	0	0.0		
2.00 1.75	215	0	0.0			215	0	0.0		
1.75 1.50	179	0	0.0			179	0	0.0		
1.50 1.25	187	0	0.0			187	0	0.0		
1.25 1.00	180	0	0.0			180	0	0.0		
1.00 .75	199	21	10.6			199	0	0.0		
.75 .50	212	192	90.6			212	0	0.0		
.50 .25	221	221	100.0			221	37	16.7		
.25 0.00	196	196	100.0			196	184	93.9		
0.00 -.25	196			0	0.0	196			0	0.0
-.25 -.50	184			0	0.0	184			0	0.0
-.50 -.75	221			0	0.0	221			0	0.0
-.75 -1.00	188			0	0.0	188			0	0.0
-1.00 -1.25	201			0	0.0	201			0	0.0
-1.25 -1.50	201			0	0.0	201			0	0.0
-1.50 -1.75	220			0	0.0	220			0	0.0
-1.75 -2.00	193			0	0.0	193			0	0.0
-2.00 -2.25	195			0	0.0	195			0	0.0
-2.25 -2.50	179			0	0.0	179			0	0.0

Table C-13. False Alarm and Missed Alarm Percentages for Path 6, Threshold at the Computed Optimum

9.6 GHZ THRESHOLD = +4.4 DB

28.8 GHZ THRESHOLD = +4.0 DB

TARGET COVER HT RANGE		9.6 GHZ NO. PTS	NO. FA	% FA	NO. MA	% MA	28.8 GHZ NO. PTS	NO. FA	% FA	NO. MA	% MA
3.25	3.00	8	0	0.0			8	0	0.0		
3.00	2.75	128	0	0.0			128	0	0.0		
2.75	2.50	192	0	0.0			192	0	0.0		
2.50	2.25	228	0	0.0			228	0	0.0		
2.25	2.00	200	0	0.0			200	0	0.0		
2.00	1.75	211	0	0.0			211	0	0.0		
1.75	1.50	205	0	0.0			205	0	0.0		
1.50	1.25	212	0	0.0			212	0	0.0		
1.25	1.00	181	0	0.0			181	0	0.0		
1.00	.75	221	0	0.0			221	0	0.0		
.75	.50	196	0	0.0			196	0	0.0		
.50	.25	199	0	0.0			199	0	0.0		
.25	0.00	208	16	7.7			208	0	72.1		
0.00	-.25	195			0	0.0	195			0	0.0
-.25	-.50	198			0	0.0	198			0	0.0
-.50	-.75	180			0	0.0	180			0	0.0
-.75	-1.00	215			0	0.0	215			0	0.0
-1.00	-1.25	186			0	0.0	186			0	0.0
-1.25	-1.50	191			0	0.0	191			0	0.0
-1.50	-1.75	206			0	0.0	206			0	0.0
-1.75	-2.00	210			0	0.0	210			0	0.0
-2.00	-2.25	215			0	0.0	215			0	0.0
-2.25	-2.50	206			0	0.0	206			0	0.0

Table C-14. False Alarm and Missed Alarm Percentages for Path 6, Threshold 3 dB Above the Optimum

9.6 GHZ THRESHOLD = +1.4 DB

28.8 GHZ THRESHOLD = +1.0 DB

TARGET COVER HT RANGE	9.6 GHZ NO. PTS	NO. FA	% FA	NO. MA	% MA	28.8 GHZ NO. PTS	NO. FA	% FA	NO. MA	% MA
3.25 3.00	8	0	0.0			8	0	0.0		
3.00 2.75	128	0	0.0			128	0	0.0		
2.75 2.50	192	0	0.0			192	0	0.0		
2.50 2.25	228	0	0.0			228	0	0.0		
2.25 2.00	200	0	0.0			200	0	0.0		
2.00 1.75	211	0	0.0			211	0	0.0		
1.75 1.50	205	0	0.0			205	0	0.0		
1.50 1.25	212	0	0.0			212	0	0.0		
1.25 1.00	181	0	0.0			181	0	0.0		
1.00 .75	221	0	0.0			221	0	0.0		
.75 .50	196	0	0.0			196	0	0.0		
.50 .25	199	0	0.0			199	0	0.0		
.25 0.00	208	0	0.0			208	12	5.8		
0.00 -.25	195			195	100.0	195			0	0.0
-.25 -.50	198			12	26.8	198			0	0.0
-.50 -.75	180			0	0.0	180			0	0.0
-.75 -1.00	215			0	0.0	215			0	0.0
-1.00 -1.25	186			0	0.0	186			0	0.0
-1.25 -1.50	191			0	0.0	191			0	0.0
-1.50 -1.75	206			0	0.0	206			0	0.0
-1.75 -2.00	210			0	0.0	210			0	0.0
-2.00 -2.25	215			0	0.0	215			0	0.0
-2.25 -2.50	206			0	0.0	206			0	0.0

Table C-15. False Alarm and Missed Alarm Percentages for Path 6, Threshold 3 dB Below the Optimum

9.6 GHZ THRESHOLD = +7.4 DB

28.8 GHZ THRESHOLD = +7.0 DB

TARGET COVER HT RANGE		9.6 GHZ NO. PTS	NO. FA	% FA	NO. MA	% MA	28.8 GHZ NO. PTS	NO. FA	% FA	NO. MA	% MA
3.25	3.00	8	0	0.0			8	0	0.0		
3.00	2.75	128	0	0.0			128	0	0.0		
2.75	2.50	192	0	0.0			192	0	0.0		
2.50	2.25	228	0	0.0			228	0	0.0		
2.25	2.00	200	0	0.0			200	0	0.0		
2.00	1.75	211	0	0.0			211	0	0.0		
1.75	1.50	205	0	0.0			205	0	0.0		
1.50	1.25	212	0	0.0			212	0	0.0		
1.25	1.00	181	0	0.0			181	0	0.0		
1.00	.75	221	0	0.0			221	0	0.0		
.75	.50	196	0	0.0			196	0	0.0		
.50	.25	199	14	7.0			199	96	48.2		
.25	0.00	208	208	100.0			208	208	100.0		
0.00	-.25	195			0	0.0	195			0	0.0
-.25	-.50	198			0	0.0	198			0	0.0
-.50	-.75	180			0	0.0	180			0	0.0
-.75	-1.00	215			0	0.0	215			0	0.0
-1.00	-1.25	186			0	0.0	186			0	0.0
-1.25	-1.50	191			0	0.0	191			0	0.0
-1.50	-1.75	206			0	0.0	206			0	0.0
-1.75	-2.00	210			0	0.0	210			0	0.0
-2.00	-2.25	215			0	0.0	215			0	0.0
-2.25	-2.50	206			0	0.0	206			0	0.0

Table C-16. False Alarm and Missed Alarm Percentages for Path 7, Threshold at Computed Optimum

9.6 GHZ THRESHOLD = +4.4 DB

28.8 GHZ THRESHOLD = +4.0 DB

TARGET COVER HT RANGE	9.6 GHZ NO. PTS	NO. FA	% FA	NO. MA	% MA	28.8 GHZ NO. PTS	NO. FA	% FA	NO. MA	% MA
2.75 2.50	125	0	0.0			125	0	0.0		
2.50 2.25	101	0	0.0			101	0	0.0		
2.25 2.00	87	0	0.0			87	0	0.0		
2.00 1.75	82	0	0.0			82	0	0.0		
1.75 1.50	105	0	0.0			105	0	0.0		
1.50 1.25	117	0	0.0			117	0	0.0		
1.25 1.00	88	0	0.0			88	0	0.0		
1.00 .75	85	0	0.0			85	0	0.0		
.75 .50	85	0	0.0			85	0	0.0		
.50 .25	102	0	0.0			102	0	0.0		
.25 0.00	92	19	20.7			92	0	0.0		
0.00 -.25	96			0	0.0	96			7	7.3
-.25 -.50	95			0	0.0	95			0	0.0
-.50 -.75	115			0	0.0	115			0	0.0
-.75 -1.00	99			0	0.0	99			0	0.0
-1.00 -1.25	95			0	0.0	95			0	0.0
-1.25 -1.50	88			0	0.0	88			0	0.0
-1.50 -1.75	93			0	0.0	93			0	0.0
-1.75 -2.00	121			0	0.0	121			0	0.0
-2.00 -2.25	99			0	0.0	99			0	0.0
-2.25 -2.50	100			0	0.0	100			0	0.0
-2.50 -2.75	88			0	0.0	88			0	0.0

Table C-17. False Alarm and Missed Alarm Percentages for Path 7, Threshold 3 dB Above the Optimum

9.6 GHZ THRESHOLD = +1.4 DB

28.8 GHZ THRESHOLD = +1.0 DB

TARGET COVER HT RANGE	9.6 GHZ NO. PTS	9.6 GHZ NO. FA	9.6 GHZ % FA	9.6 GHZ NO. MA	9.6 GHZ % MA	28.8 GHZ NO. PTS	28.8 GHZ NO. FA	28.8 GHZ % FA	28.8 GHZ NO. MA	28.8 GHZ % MA
2.75 2.50	125	0	0.0			125	0	0.0		
2.50 2.25	101	0	0.0			101	0	0.0		
2.25 2.00	87	0	0.0			87	0	0.0		
2.00 1.75	82	0	0.0			82	0	0.0		
1.75 1.50	105	0	0.0			105	0	0.0		
1.50 1.25	117	0	0.0			117	0	0.0		
1.25 1.00	88	0	0.0			88	0	0.0		
1.00 .75	85	0	0.0			85	0	0.0		
.75 .50	85	0	0.0			85	0	0.0		
.50 .25	102	0	0.0			102	0	0.0		
.25 0.00	92	0	0.0			92	0	0.0		
0.00 -.25	96			96	100.0	96			96	100.0
-.25 -.50	95			95	100.0	95			95	100.0
-.50 -.75	115			17	14.8	115			61	53.0
-.75 -1.00	99			0	0.0	99			0	0.0
-1.00 -1.25	95			0	0.0	95			0	0.0
-1.25 -1.50	88			0	0.0	88			0	0.0
-1.50 -1.75	93			0	0.0	93			0	0.0
-1.75 -2.00	121			0	0.0	121			0	0.0
-2.00 -2.25	99			0	0.0	99			0	0.0
-2.25 -2.50	100			0	0.0	100			0	0.0
-2.50 -2.75	88			0	0.0	88			0	0.0

Table C-18. False Alarm and Missed Alarm Percentages for Path 7, Threshold 3 dB Below the Optimum

9.6 GHZ THRESHOLD = +7.4 28.8 GHZ THRESHOLD = +7.0

TARGET COVER HT RANGE		9.6 GHZ NO. PTS	NO. FA	% FA	NO. MA	% MA	28.8 GHZ NO. PTS	NO. FA	% FA	NO. MA	% MA
2.75	2.50	125	0	0.0			125	0	0.0		
2.50	2.25	101	0	0.0			101	0	0.0		
2.25	2.00	87	0	0.0			87	0	0.0		
2.00	1.75	82	0	0.0			82	0	0.0		
1.75	1.50	105	0	0.0			105	0	0.0		
1.50	1.25	117	0	0.0			117	0	0.0		
1.25	1.00	88	0	0.0			88	0	0.0		
1.00	.75	85	27	31.8			85	0	0.0		
.75	.50	85	85	100.0			85	0	0.0		
.50	.25	102	102	100.0			102	60	58.8		
.25	0.00	92	92	100.0			92	92	100.0		
0.00	-.25	96			0	0.0	96			0	0.0
-.25	-.50	95			0	0.0	95			0	0.0
-.50	-.75	115			0	0.0	115			0	0.0
-.75	-1.00	99			0	0.0	99			0	0.0
-1.00	-1.25	95			0	0.0	95			0	0.0
-1.25	-1.50	88			0	0.0	88			0	0.0
-1.50	-1.75	93			0	0.0	93			0	0.0
-1.75	-2.00	121			0	0.0	121			0	0.0
-2.00	-2.25	99			0	0.0	99			0	0.0
-2.25	-2.50	100			0	0.0	100			0	0.0
-2.50	-2.75	88			0	0.0	88			0	0.0

Table C-19. False Alarm and Missed Alarm Percentages for Path 9, Threshold at the Computed Optimum

9.6 GHZ THRESHOLD = +4.4 DB

28.8 GHZ THRESHOLD = +4.0 DB

TARGET COVER HT RANGE		9.6 GHZ NO. PTS	NO. FA	% FA	NO. MA	% MA	28.8 GHZ NO. PTS	NO. FA	% FA	NO. MA	% MA
3.75	3.50	94	0	0.0			94	0	0.0		
3.50	3.25	110	0	0.0			110	0	0.0		
3.25	3.00	107	0	0.0			107	0	0.0		
3.00	2.75	104	0	0.0			104	0	0.0		
2.75	2.50	87	0	0.0			87	0	0.0		
2.50	2.25	123	0	0.0			123	0	0.0		
2.25	2.00	150	0	0.0			150	0	0.0		
2.00	1.75	167	0	0.0			167	0	0.0		
1.75	1.50	168	0	0.0			168	0	0.0		
1.50	1.25	224	0	0.0			224	0	0.0		
1.25	1.00	207	0	0.0			207	0	0.0		
1.00	.75	183	0	0.0			183	0	0.0		
.75	.50	176	0	0.0			176	0	0.0		
.50	.25	184	0	0.0			184	0	0.0		
.25	0.00	232	0	0.0			232	0	0.0		
0.00	-.25	182			182	100.0	182			182	100.0
-.25	-.50	182			182	100.0	182			182	100.0
-.50	-.75	188			188	100.0	188			169	89.9
-.75	-1.00	216			216	100.0	216			0	0.0
-1.00	-1.25	229			229	100.0	229			36	15.7
-1.25	-1.50	290			290	100.0	290			290	100.0
-1.50	-1.75	125			125	100.0	125			81	64.8
-1.75	-2.00	206			206	100.0	206			0	0.0

Table C-20. False Alarm and Missed Alarm Percentages for Path 9, Threshold 3 dB Above the Optimum

9.6 GHZ THRESHOLD = +1.4DB

28.8 GHZ THRESHOLD = +1.0 DB

TARGET COVER HT RANGE		9.6 GHZ NO. PTS	NO. FA	% FA	NO. MA	% MA	28.8 GHZ NO. PTS	NO. FA	% FA	NO. MA	% MA
3.75	3.50	94	0	0.0			94	0	0.0		
3.50	3.25	110	0	0.0			110	0	0.0		
3.25	3.00	107	0	0.0			107	0	0.0		
3.00	2.75	104	0	0.0			104	0	0.0		
2.75	2.50	87	0	0.0			87	0	0.0		
2.50	2.25	123	0	0.0			123	0	0.0		
2.25	2.00	150	0	0.0			150	0	0.0		
2.00	1.75	167	0	0.0			167	0	0.0		
1.75	1.50	168	0	0.0			168	0	0.0		
1.50	1.25	224	0	0.0			224	0	0.0		
1.25	1.00	207	0	0.0			207	0	0.0		
1.00	.75	183	0	0.0			183	0	0.0		
.75	.50	176	0	0.0			176	0	0.0		
.50	.25	184	0	0.0			184	0	0.0		
.25	0.00	232	0	0.0			232	0	0.0		
0.00	-.25	182			182	100.0	182			182	100.0
-.25	-.50	182			182	100.0	182			182	100.0
-.50	-.75	188			188	100.0	188			188	100.0
-.75	-1.00	216			216	100.0	216			216	100.0
-1.00	-1.25	229			229	100.0	229			229	100.0
-1.25	-1.50	290			290	100.0	290			290	100.0
-1.50	-1.75	125			125	100.0	125			125	100.0
-1.75	-2.00	206			206	100.0	206			206	100.0

Table C-21. False Alarm and Missed Alarm Percentages for Path 9, Threshold 3 dB Below the Optimum

9.6 GHZ THRESHOLD = +7.4 DB

28.8 GHZ THRESHOLD = +7.0 DB

TARGET COVER HT RANGE	9.6 GHZ NO. PTS	NO. FA	% FA	NO. MA	% MA	28.8 GHZ NO. PTS	NO. FA	% FA	NO. MA	% MA
3.75 3.50	94	0	0.0			94	0	0.0		
3.50 3.25	110	0	0.0			110	0	0.0		
3.25 3.00	107	0	0.0			107	0	0.0		
3.00 2.75	104	0	0.0			104	0	0.0		
2.75 2.50	87	0	0.0			87	0	0.0		
2.50 2.25	123	0	0.0			123	0	0.0		
2.25 2.00	150	0	0.0			150	0	0.0		
2.00 1.75	167	0	0.0			167	0	0.0		
1.75 1.50	168	0	0.0			168	0	0.0		
1.50 1.25	224	0	0.0			224	0	0.0		
1.25 1.00	207	0	0.0			207	0	0.0		
1.00 .75	183	0	0.0			183	0	0.0		
.75 .50	176	0	0.0			176	0	0.0		
.50 .25	184	0	0.0			184	0	0.0		
.25 0.00	232	0	0.0			232	0	0.0		
0.00 -.25	182			182	100.0	182			182	100.0
-.25 -.50	182			182	100.0	182			86	47.3
-.50 -.75	188			188	100.0	188			0	0.0
-.75 -1.00	216			216	100.0	216			0	0.0
-1.00 -1.25	229			53	23.1	229			0	0.0
-1.25 -1.50	290			0	0.0	290			0	0.0
-1.50 -1.75	125			0	0.0	125			0	0.0
-1.75 -2.00	206			0	0.0	206			0	0.0

FORM OT-29
(3-73)

U.S. DEPARTMENT OF COMMERCE
OFFICE OF TELECOMMUNICATIONS

BIBLIOGRAPHIC DATA SHEET

1. PUBLICATION OR REPORT NO.	2. Gov't Accession No.	3. Recipient's Accession No.
NTIA Report 80-35		

4. TITLE AND SUBTITLE

PROPAGATION EFFECTS ON AN INTERVISIBILITY MEASUREMENT SYSTEM OPERATING IN THE SHF BAND

5. Publication Date
February 1980

6. Performing Organization Code
910.01

7. AUTHOR(S)
E.J. Haakinson, E.J. Violette and G.H. Hufford

8. PERFORMING ORGANIZATION NAME AND ADDRESS
U.S. Department of Commerce
National Telecommunications and Information Admin.
Institute for Telecommunication Sciences
Boulder, CO 80303

9. Project/Task/Work Unit No.
9101900

10. Contract/Grant No.
ATEC 40-78

11. Sponsoring Organization Name and Address
USACDEC
Ft. Ord, CA 93941

12. Type of Report and Period Covered
Technical Report

13.

14. SUPPLEMENTARY NOTES

15. ABSTRACT *(A 200-word or less factual summary of most significant information. If document includes a significant bibliography or literature survey, mention it here.)*

A study was conducted to determine the limiting propagation effects on the performance of a microwave system that could be used to detect the optical visibility to one another of two vehicles, separated by up to 10 km, in irregular, obstructed terrain. The study had four objectives: 1) to demonstrate what effects signal variability has on the intervisibility decision process, 2) to identify the possible sources of the signal variability and to estimate the magnitude of each source's contribution to the total variability, 3) to obtain propagation loss data, over various types of terrain and obstructed paths, which could be used to predict received signal variability due to propagation over similar paths, and 4) to use the measured data to determine the performance of simulated intervisibility measurement system. A measurement system was prepared and sent to Ft. Hunter Liggett, CA, where propagation path loss was measured over several selected paths of varying lengths, varying path geometrics, and varying amounts of vegetation and rock outcroppings.

16. Key words *(Alphabetical order, separated by semicolons)*

Intervisibility measurement systems; propagation measurements; SHF

17. AVAILABILITY STATEMENT

[X] UNLIMITED.

[ ] FOR OFFICIAL DISTRIBUTION.

18. Security Class *(This report)*
UNCLASSIFIED

19. Security Class *(This page)*
UNCLASSIFIED

20. Number of pages
128

21. Price:

USCOMM-DC 29716-P73
USCOMM - ERL